The Effects of Arrhythmogenic Right Ventricular Cardiomyopathy-Causing Proteins on the Mechanical and Signaling Properties of Cardiac Myocytes

Venkatesh Hariharan

Submitted in partial fulfillment of the
requirements for the degree
of Doctor of Philosophy
in the Graduate School of Arts and Sciences

COLUMBIA UNIVERSITY

2014

ABSTRACT

The Effects of Arrhythmogenic Right Ventricular Cardiomyopathy-Causing Proteins on the Mechanical and Signaling Properties of Cardiac Myocytes

Venkatesh Hariharan

Arrhythmogenic right ventricular cardiomyopathy (ARVC) is characterized by a high incidence of lethal ventricular arrhythmias, fibrofatty replacement of myocardium, and can account for up to 20% of sudden cardiac death (SCD) cases in the young. Typically involving autosomal dominant transmission, germline mutations in genes encoding desmosomal proteins have been identified as a cause of ARVC, although the pathogenesis of the disease is still unclear. While early detection and treatment can provide a normal life expectancy for the majority of patients, with less than 10% progressing to overt right ventricular failure, low genetic penetrance and epigenetic modifiers (such as endurance exercise) can make the condition difficult to diagnose. Addressing this clinical challenge requires a better understanding of the defective molecular mechanisms that underlie the disease. To that end, the goal of this dissertation is to provide insight into the effects of ARVC-causing mutant proteins on the mechanical and signaling properties of cardiac myocytes.

Using elastography and histological techniques, we begin by characterizing the structural and mechanical properties of the native right ventricular myocardium, particularly the right ventricular apex (RVA). Because the RVA is a key site for development of arrhythmias and a potential pacing target, a careful characterization of its structure and mechanical properties are essential for understanding its role in cardiac physiology. In the first section of this dissertation, we perform a systematic analysis of the structural features and mechanical strains in the heart, focusing on the RVA region.

More than half of ARVC patients exhibit one or more mutations in genes encoding desmosomal proteins. This has led many investigators to suggest that ARVC is a "disease of the desmosome" in which defective cell-cell adhesion plays a critical pathogenic role, although direct evidence for this hypothesis is lacking. To gain greater insights into potential mechanisms by which desmosomal mutations cause ARVC, we next characterize biomechanical properties and responses to shear stress (motivated by our results in the previous section) in neonatal rat ventricular myocytes expressing two distinct mutant forms of the desmosomal protein plakoglobin which have been linked to ARVC in patients. We show that ARVC-causing mutations in plakoglobin lead to altered cellular distribution of plakoglobin, without alterations in cell mechanical properties or certain early signaling pathways.

The identification of defective molecular mechanisms that are common across ARVC-patients remains a strategic area of research. Specifically, recent studies have investigated the mechanistic basis for different ARVC-causing mutations in hopes of identifying common defects in a signaling pathway – information that could be used to develop diagnostic tests or identify therapeutic targets. In the last section of this dissertation, we investigate the effects of mutant plakophilin-2 expression, and repeat key experiments performed in the previous section to identify common defects in mechanical and signaling properties. We identify a common, underlying defect in ARVC pathogenesis. Specifically, we show that disease-causing mutations across different desmosomal proteins can cause the cell to respond abnormally to mechanical shear stress with respect to plakoglobin trafficking.

TABLE OF CONTENTS

LIST OF TABLES

LIST OF FIGURES

column) shows a localization of vertical fibers (white) near the RVA region apposing fibers with a horizontal orientation (black), in contrast with the left-ventricular section. (A-B) Scale bar = 500 μm; (C) Quantification of angle mapping in left-ventricular (LV) and right-ventricular canine heart sections showing the percentage of cells where $\cos(\theta) < 0.3$. * $p \leq 0.05$; ** $p \leq 0.01$

Figure 2.3: Diminished plakoglobin expression occurs at the right ventricular apex in the mouse heart - (A) Left-ventricular, (B) right-ventricular, and (C) septal myocardial samples immunostained against pan-cadherin. The localization of expression is predominantly at the end-to-end junctions of the myocytes. Scale bar = 100 μm. (D) Cadherin stained region of cardiac tissue including the RVA and some tissue peripheral to the RVA. (E) Plakoglobin stained region of cardiac tissue including the RVA and some tissue peripheral to the RVA. The upper-middle region, representing the RVA, exhibits weaker staining and less organization of intercalated disks. Scale bar = 250 μm. (F) Quantification of plakoglobin (JUP) and pan-cadherin (PC) signal intensity in non-apical (N) and apical (A) regions of the right ventricle. ** $p \leq 0.01$

Figure 2.4: Elevated incremental strains occur at the right ventricle during systole - Spatial distribution of incremental radial strains, superimposed on echocardiogram, across canine ventricular walls at different time points in one complete ECG cycle (denoted by red dots). The left ventricular wall (LVW) is shown at the top of the image, followed by the septum (SEP) in the middle and the right ventricular wall (RVW) at the bottom. Incremental strains are superimposed against the acquired echocardiography data.

Figure 2.5: Elevated cumulative strains occur at the right ventricle during systole - Spatial distribution of cumulative radial strains, superimposed on echocardiogram, across canine ventricular walls at different time points in one complete ECG cycle (denoted by red dots). The left ventricular wall (LVW) is shown at the top of the image, followed by the septum (SEP) in the middle and the right ventricular wall (RVW) at the bottom. Cumulative strains are superimposed against the acquired echocardiography data.

Figure 2.6: Heterogeneous strain distributions occur at the right ventricular apex - Spatial distribution of (A) incremental strains during systole and (B) cumulative radial strains near the beginning of diastole, showing a transition in strain magnitude near the RVA (circled in red), over a short distance compared to a similar transition over the cardiac apex. Black outlines (A) are used to identify regions used for whole-wall strain analysis. Black squares (B) are used to identify regions used for mid-wall strain analysis.

Figure 2.7: Quantification of incremental and cumulative strains in the canine Heart 1 - Incremental (A) and cumulative (B) strains within canine Heart 1 during systole (S, 0-310 ms) and diastole (D, 310-595 ms). Sustained, elevated strains are observed within the right ventricle (RV) as compared to the left ventricle (LV) during systole. Mid-wall incremental strains (C) and end-systolic mid-wall cumulative strains (D) show elevated RV strains compared to LV strains. ** $p \leq 0.01$

Figure 2.8: Quantification of incremental and cumulative strains in the canine Heart 2 - Incremental (A) and cumulative (B) strains within canine Heart 2 during systole (S, 0-290 ms)

and diastole (D, 290-645 ms). Sustained, elevated strains are observed within the right ventricle (RV) as compared to the left ventricle (LV) during systole. Mid-wall incremental strains (C) and end-systolic mid-wall cumulative strains (D) show elevated RV strains compared to LV strains. ** $p \leq 0.01$

Figure 2.7: Healthy bovine hearts exhibit fatty deposits along the triangle of dysplasia - Intact bovine heart. Note the significant fatty deposit around the superior circumference of the heart, some mild fatty streaks following the left-anterior descending coronary artery, and notably, the right-ventricular apical region (red circle), but not the primary cardiac apex.

Figure 3.1 – Diagram of shear flow device and force balance: (Left) Diagram showing the dimensions of the shear flow chamber, where 'H' represents the vertical distance between the two parallel plates and 'D' represents the depth of the chamber normal to the direction of flow. (Right) Force balance on an incremental block of fluid used to derive the relationship between shear stress, parallel plate chamber dimensions, and fluid flow rate.

Figure 3.2 – Media flow rate is directly proportional to applied shear stress: As derived in section 3.2.5, the derived expression to calculate applied shear stress is directly proportional to the flow rate of media through the shear chamber. As determined above using Matlab, to achieve a physiologically relevant shear stress level of 0.06 pascals, we flow media in the chamber at a rate of 0.12 mL/sec.

Figure 3.3 – ARVC models express transgenic plakoglobin at endogenous levels: **(A)** V5 immunostaining of control (non-transfected) myocytes (C) and myocytes transfected to express wild-type plakoglobin (WT PG), S39_K40insS (InsS PG), or 2057del2 PG. No signal is seen in non-transfected control cells (thus demonstrating absence of non-specific binding). Normal junctional localization of V5 labeled protein is seen in cells transfected to express WT PG, InsS PG and 2057del2 PG mutants. Cells transfected with 2057del2 PG also show nuclear localization of truncated 2057del2 plakoglobin. **(B)** Immunostaining with an anti-plakoglobin antibody against an N-terminal epitope (which recognizes both endogenous and transfected forms of WT PG, InsS PG and 2057del2 PG) shows a similar pattern. **(C)** Immunoblot (left) using an N-terminal anti-plakoglobin antibody, with quantification (right) showing roughly equivalent amounts of endogenous plakoglobin and transgene plakoglobin in WT PG, InsS PG and 2057del2 PG cells (n=4). While the control lane shows a single band corresponding to endogenous plakoglobin, the WT PG, InsS PG, and 2057del2 PG lanes exhibit a second band, corresponding to the transgenic plakoglobin. The larger molecular weight of transgenic plakoglobin observed in the WT PG and InsS PG lanes is explained by the addition of a C-terminal V5 tag, connected using a linker peptide. The lower molecular weight transgenic plakoglobin band observed in the 2057del2 PG lane is explained by the truncation of the C-terminal end of plakoglobin – a result of the premature stop codon generated by the frame-shift 2057del2 mutation. **(D)** Quantification of cells transfected with a GFP virus to confirm 98.9 ± 1.1% transfection efficiency (n=5). Scale bars = 20 μm.

Figure 3.4 - Cell-cell adhesion strength and cell stiffness are unaffected by mutant plakoglobin: **(A)** Quantification of control and mutant plakoglobin-transfected cardiac myocyte monolayer

fragmentation in dispase assays before and after 1 or 3 minutes of agitation. Cardiac myocytes expressing mutant plakoglobin show no differences in cell-cell adhesion relative to WT PG (n=5). **(B)** Quantification of cluster sizes in control and transfected cardiac myocytes in cell aggregate assays (n=3). Cardiac myocyte aggregates expressing mutant plakoglobin show no differences in aggregate fragmentation relative to WT PG. **(C)** Dispase assays in normal (non-transfected) cardiac myocytes showing significant reduction in cell-cell adhesion in cells exposed to 1uM cytochalasin-D (n=5). **(D)** Dispase assays in normal (non-transfected) cardiac myocytes showing significant reduction in cell-cell adhesion in cells following siRNA knock-down of endogenous plakoglobin (n=5). Plakoglobin knock-down was confirmed by immunoblotting (inset), and quantified (right). **(E)** Quantification of apoptosis (percent TUNEL-positive nuclei) in control (C) cells transfected with non-targeting siRNA, or siRNA targeting plakoglobin (n=6). Mechanical shear caused cells to shear off the glass slide, preventing quantification. **(F)** Dispase assays in normal (non-transfected) cardiac myocytes showing significant reduction in cell-cell adhesion in cells following siRNA knock-down of endogenous N-cadherin (Nc) (n=6). N-cadherin knock-down was confirmed by immunoblotting (inset), and quantified (right). *$p < 0.05$; **$p < 0.01$

Figure 3.5 – Shear-induced plakoglobin remodeling is reversibly altered in ARVC: **(A)** Immuno-fluorescence images showing the distribution of plakoglobin (N-terminal antibody) in control (C) and transfected cardiac myocytes before (top) and after (middle) exposure to shear, and after treatment with SB216763 (SB2; bottom). Control and WT PG cells show increased immunoreactive signal with junctional localization after shear, whereas cells expressing InsS PG or 2057del2 PG show no apparent increase in junctional signal after shear. Treatment with the

drug restored the normal shear-induced increase in junctional signal in cells expressing mutant plakoglobin or plakophilin. **(B)** Quantification of junctional plakoglobin signal before and after shear in cells transfected to express mutant plakoglobin (n=5). **(C)** Quantification of junctional plakoglobin signal before and after shear in cells transfected to express mutant plakoglobin and treated with SB216763 (n=6). **(D)** Immunoblot using a N-terminal anti-plakoglobin antibody showing no overt changes in plakoglobin levels in cells expressing WT or 2057del2 PG (n=5) in response to shear or treatment with SB216763. Scale bars = 20 μm. *$p< 0.05$; ** $p< 0.01$

Figure 3.6 - Shear-induced N-cadherin remodeling is reversibly altered in ARVC: **(A)** N-cadherin immunofluorescence images showing the distribution of N-cadherin in control (C) and transfected cardiac myocytes before (top) and after (middle) exposure to shear, and after treatment with SB216763 (bottom). As seen in Figure 3, control (non-transfected) cells and cells transfected to express wild-type plakoglobin (WT PG) show increased junctional signal for N-cadherin after shear, whereas no shear-induced increase was seen in cells expressing mutant forms of plakoglobin. Treatment with the drug restored the normal shear-induced increase in junctional signal in cells expressing mutant plakoglobin. **(B)** Quantification of junctional N-cadherin signal before and after shear (n=5). **(C)** Quantification of junctional N-cadherin signal before and after shear in cardiac myocytes treated with SB216763 (n=5). SB216763 restored the normal shear-induced increase in junctional N-cadherin signal. **(D)** Dispase assay measurements in control cells (C) and cells expressing transgenic plakoglobin after exposure to mechanical shear stress (n=5). Cardiac myocytes expressing mutant plakoglobin show no differences in cell-cell adhesion as compared to control cells. **(E)** Cell stiffness measurements in control cells (C) and cells expressing wild type or mutant plakoglobin before and after exposure to mechanical

shear stress (n=4). Cardiac myocytes expressing mutant plakoglobin show no differences in cell stiffness compared to control cells. *p<0.05; **p<0.01

Figure 3.7 - Cell viability, but not ERK phosphorylation, is altered by mutant plakoglobin expression: **(A)** Quantification of apoptosis (percent TUNEL-positive nuclei) in control (C) cells and cells transfected to express wild-type or mutant forms of plakoglobin before and after exposure to shear (n=4). Mechanical shear stress caused an increase in apoptosis in cells expressing 2057del2 PG. **(B)** Quantification of apoptosis (percent TUNEL-positive nuclei) in cells treated with SB216763 (SB2) before and after shear (n=3). SB216763 prevented the shear-induced increase in apoptosis in cells expressing 2057del2 PG. **(C)** Representative immunoblot and quantitative data showing equivalent levels of phospho-ERK activation (P-ERK), with total ERK (T-ERK) as a loading control, in control cells (C) or cells transfected to express wild-type or mutant forms of plakoglobin (n=3). *p<0.05

Figure 3.8 - GSK3 Suppression Does Not Mimic the Effects of SB216763: **(A-B)** Quantification of junctional plakoglobin signal before and after shear in cells treated with **(A)** non-targeting (n=3) or **(B)** GSK3 siRNA (n=3). Knockdown of GSK3 did not restore the normal shear-induced increase in junctional signal in cells expressing InsS or NX plakoglobin. **(C)** Scatter plots from microarray data analysis showing differential gene expression when comparing NX cells exposed to shear stress, treated with SB216763, or both (n=3). **(D)** Immunoblots using anti-Rnd1 (top), anti-Isg15 (middle) or anti-GAPDH (bottom) antibodies in WT and NX cells exposed to shear stress, treated with SB216763, or both. Isg15 and Rnd1 were targets identified using microarray analysis. *p< 0.05

Figure 4.1 – ARVC models express transgenic plakophilin: **(A)** V5 Stain on control (C), wild-type plakophilin (WT PKP), and mutant plakophilin (1851del123 PKP) transfected myocytes. Normal junctional localization is seen in WT PKP transfected cells. No junctional signal is observed in cells expressing 1851del123 PKP. **(B)** Immunostaining with an anti-plakophilin-2 antibody against a C-terminal epitope (which recognizes both endogenous and transfected forms of WT PKP and 1851del123 PKP. **(C)** Immunoblots using anti-V5 (top), anti-C-terminal plakophilin (middle) and anti-GAPDH (bottom) antibodies. V5 bands in the WT PKP and 1851del123 PKP lysates confirm successful transfection. The relatively similar size between exogenous and endogenous plakophilin prevented detection of discrete bands using the anti-C-terminal plakophilin antibody. **(D)** Quantification of cells transfected with a GFP virus to confirm 97.9 ± 0.2% transfection efficiency (n=3). Scale bars = 20 μm.

Figure 4.2 - Cell-cell adhesion strength and stiffness are unaffected by mutant plakophilin expression: **(A)** Quantification of control and mutant plakophilin transfected cardiac myocyte monolayer fragmentation in dispase assays before and after 1 or 3 minutes of agitation. Similar to myocytes expressing mutant plakoglobin, cardiac myocytes expressing mutant plakophilin-2 (n=6) also show no differences in cell-cell adhesion relative to WT PKP (n=4), suggesting the effect does not depend on which desmosomal protein is being mutated. **(B)** Dispase assays in normal (non-transfected) cardiac myocytes showing significant reduction in cell-cell adhesion in cells following siRNA knock-down of endogenous plakophilin-2 (n=5). Plakophilin-2 knock-down was confirmed by immunoblotting (inset), and quantified (right). **(C)** Quantification of apoptosis (percent TUNEL-positive nuclei) in control cells transfected with non-targeting

siRNA, or siRNA targeting plakophilin (n=6). **(D)** Cell stiffness measurements in control cells (C) and cells expressing wild type or mutant plakophilin before and after exposure to mechanical shear stress (n=3). Cardiac myocytes expressing mutant plakophilin show no differences in cell stiffness compared to control cells. *p<0.05; **p<0.01

Figure 4.3 – Shear-induced plakoglobin and plakophilin localization are reversibly altered in pkp-model ARVC cells: **(A)** Immunofluorescence images showing the distribution of plakophilin (C-terminal antibody) in control (C) and transfected cardiac myocytes before (top) and after (middle) exposure to shear, and after treatment with SB216763 (SB2; bottom). Control and WT PKP cells show increased immunoreactive signal with junctional localization after shear, whereas cells expressing 1851del123 PKP show no apparent increase in junctional signal after shear. Treatment with the drug restored the normal shear-induced increase of in junctional signal in cells expressing mutant plakophilin. **(B-C)** Quantification of junctional plakophilin signal before and after shear in **(B)** untreated (n=3) or **(C)** SB216763 treated (n=3) cells transfected with wild-type or mutant plakophilin. **(D-E)** Quantification of junctional plakoglobin signal before and after shear in **(D)** untreated (n=4) or **(E)** SB216763 treated (n=4) cells transfected with wild-type or mutant plakophilin. **(F-G)** Quantification of junctional plakophilin signal before and after shear in **(F)** untreated (n=3) or **(G)** SB216763 treated (n=3) cells transfected with wild-type or mutant plakophilin.*p< 0.05; **p<0.01

Figure 4.4 – Plakophilin Knockdown Alters Plakoglobin Remodeling, But Not Vice Versa: **(A-B)** Quantification of junctional plakophilin signal before and after shear in **(B)** untreated (n=3) or **(C)** SB216763 treated (n=3) cells where plakoglobin has been suppressed. **(C-D)** Quantification

of junctional plakoglobin signal before and after shear in **(B)** untreated (n=3) or **(C)** SB216763 treated (n=3) cells where plakophilin has been suppressed.

Figure 4.5 - SB216763 treatment, but not GSK3 suppression, rescues wild-type phenotype: Quantification of junctional plakoglobin signal before and after shear in non-targeting siRNA treated (n=3) or GSK3 siRNA treated (n=3) cells transfected with wild-type or mutant plakophilin. Suppression of GSK3 siRNA did not mimic the effects of SB216763. Suppression of GSK3 did not recover junctional remodeling in cells expressing mutant plakoglobin. *$p < 0.05$

ACKNOWLEDGEMENTS

This dissertation would not have been possible without the love and support of many people, to whom I dedicate this work.

First and foremost, I would like to thank my family – Aylur V. Hariharan, Lalitha Hariharan, Nithya Hariharan, Vivek Jayaraman, Arun Jayaraman, Dharam Vir Singh, Sarita Singh, Kiran Guthikonda, Anita Guthikonda, Leena Guthikonda, Karthik Eticala, and Sapna Eticala – whose steadfast convictions have steered my own. Their encouragement serves as a foundation for my success, and I can not thank them enough.

To my advisor, Dr. Hayden Huang – I could not have asked for a better mentor. Unyielding in your support, regardless of the circumstances; you taught me how to ask the questions that matter most, and my career will be defined by it.

I would also like to thank my peers in the Cardiac Biomechanics and Mechanotransduction Lab – Dr. Jarett Michaelson, Dr. Qi Wei, Benjamin Childs, Sahil Shah, Brandan Walters. Your groundwork and insight are critical to the findings in this dissertation.

To my committee members, Dr. Gordana Vunjak-Novakovic, Dr. Christopher R. Jacobs, Dr. Jonathan Lu, and Dr. Leonardo Liberman – your insight into my thesis work is invaluable. Thank you for helping me refine this dissertation work.

My friends have been a driving force throughout the years, with who I could always discuss the ‘perks’ of being a graduate student. In particular, I would like to thank Keith Yeager, Woo Hyeun ‘Andrew’ Kang, Michael Lamprecht, Tushar Patel, Kevin Dooley, Matthew Downs, Jared Roseman, Kyle Fricker, Edward Swanson, Matthew Bouchard, Kacey Ronaldson, Michael Khalil, and Nikul Ukani.

Most importantly, I could not have achieved this feat without my fiancée Deepika Singh. The best part of my time at Columbia was finding you. Thank you for everything!

1 Overview

1.1 – Arrhythmogenic Right Ventricular Cardiomyopathy (ARVC)

1.1.1 – Clinical Presentation, Prevalence and Pathogenesis

Arrhythmogenic right ventricular cardiomyopathy (ARVC) is a disease affecting roughly 1 in 5000 people worldwide, and is exhibited morphologically as fibro-adipocytic replacement of the ventricular myocardium.[1, 2] Specifically, ARVC usually originates in the right ventricular epicardium between the conus arteriosus and ventricular apex, referred to as the 'triangle of dysplasia,' yet reasons for this localization remain unknown.[1, 3, 4] The gradual replacement of myocardium with fibrous, fatty tissue can cause hypokinesis of the affected tissue, causing early stage palpitations, ventricular tachycardia or syncope, prior to sudden cardiac death (particularly following exertion). Without treatment, life expectancy can be highly variable from patient to patient, depending on phenotypic expression, although normal life expectancy can be restored with early detection and the right treatment. Unfortunately, the clinical diagnosis of ARVC can be difficult, even with recently proposed amendments to the 1994 International ARVC Task Force Criteria. Patients can be diagnosed with the condition by satisfying 2 (out of 10) major criteria, or 1 major and 2 (out of 15) minor criteria.[5] One commonly satisfied criteria is the identification of a pathogenic mutation associated with ARVC.

Typically involving autosomal dominant transmission, multiple studies have identified ARVC-causing mutations in genes encoding proteins that localize at the desmosome, a highly ordered junctional protein complex that enhances cell-cell adhesion, stabilizes gap junctions, and participates in signaling roles (Figure 1).[6-15] Mutations have also been identified in the genes

encoding the cardiac ryanodine receptor (RYR2) and transmembrane protein 43 (TMEM43), although the frequency of these mutations in patients diagnosed with ARVC is rare.[16, 17] Because desmosomes contribute to tissue integrity by linking the intermediate filament networks of adjacent cells, the expression of mutant ARVC-causing desmosomal proteins have led many investigators to hypothesize that defective cell-cell adhesion plays a critical pathogenic role. Interestingly, there is no direct evidence of weakened cell-cell adhesion in the hearts of patients with ARVC.

One hypothesis for ARVC etiology suggests desmosomal disruption can cause nuclear translocation of plakoglobin, and can recapitulate the ARVC phenotype by suppressing the canonical Wnt/beta-catenin signaling pathway, and resulting in a transcriptional switch to adipogenesis.[18, 19] Another hypothesis suggests that the gap-junctional remodeling resulting from cell-cell adhesion defects may affect signal conduction across the myocardium, producing the hallmark arrhythmogenic phenotype associated with ARVC.[20]

While inconsistent phenotypic presentation and variable genetic penetrance can make the condition difficult to diagnose, certain features of ARVC present consistently. For example, strenuous exercise increases age-related penetrance, risk of arrhythmia and sudden cardiac death, particularly in athletes.[21-23] Interestingly, little investigation has been done into the effects of mechanical stresses on disease progression.

1.1.2 – *In Vivo* and *In Vitro* Models of ARVC

Despite the fact that ARVC Task Force criteria have yet to be developed for animal models, it is widely accepted that rodent, feline, canine, bovine and primate species can all develop an ARVC phenotype similar to the human condition (canine and bovine species can

present with an ARVC-like phenotype independent of genetically manipulated animal models).[24-27] Murine models have been primarily used to study ARVC progression, as they provide the most convenient way to study the condition *in vivo*. While these models recapitulate the human phenotype well in terms of arrhythmogenicity and fibrosis, none exhibit the fatty infiltration observed in humans.[28] Larger animal models (feline, canine, bovine and primate) are difficult to house and maintain, but tend to exhibit the fatty tissue deposition observed in humans. Furthermore, the similarity in cardiac structure between these larger animals and humans offers an opportunity to study the mechanical properties of the heart, using electromechanical wave or diffusion tensor imaging techniques.

Several mouse models have been developed to study the molecular mechanisms underlying ARVC pathogenesis, and they focus on 4 major desmosomal proteins – plakoglobin, plakophilin-2, desmoplakin and desmoglein-2 (Table 1).[6, 29-34] Earlier models attempted to recapitulate the ARVC phenotype by deleting whole or partial genes. While the models expressing homozygous deletions generally resulted in embryonic lethality, analysis of embryos at different developmental stages provided valuable insight in to the role of desmosomal gene regulation on cardiac structure and function during development. The first investigations into the effects of targeted deletion of the plakoglobin gene were conducted by Bierkamp, *et al.* and Ruiz, *et al.*[29, 30] Independently, both groups observed that homozygous deletion of the plakoglobin gene resulted in embryonic lethality as early as 10 days into gestation. Interestingly, heterozygous models, expressing one mutated allele and one wild-type allele, exhibited much higher viability and more accurately recapitulated the ARVC phenotype (arrhythmia, enlarged right ventricles, etc). This effect was also observed in mice expressing desmoplakin deletions.[33] Furthermore, Kirchhof, *et al*. was able to link endurance training to an aggravation of the ARVC

phenotype. While exercise can induce changes independent of the increased mechanical stress, this data supports the hypothesis that susceptibility to mechanical forces may contribute to ARVC pathogenesis in heterozygous plakoglobin deficient mice.[31]

Although more ARVC-causing mutations have been identified within the plakophilin-2 gene than any other gene encoding a desmosomal protein, few models have been developed to study the role of mutant plakophilin in disease progression. One such model was developed by Grossman, *et al*. Similar to previous plakoglobin studies, their results showed that mice with homozygous deletions of the plakophilin-2 gene were embryonically lethal, while heterozygous mice carrying one functional plakophilin-2 allele were completely viable, with no observable cardiac phenotype. These data suggest that the cause of ARVC may not be due to a complete loss of desmosomal protein function, but rather from the expression of a mutant protein, with a possible gene dosage effect.

More recently, groups have begun studying the effects of transgene expression, as opposed to whole or partial gene deletion, in order to more accurately recapitulate the ARVC phenotype.[6, 34, 35] For example, Yang *et al.* created several transgenic mice with a cardiac overexpression of either C-terminal (Q90R and V30M) or N-terminal (R2834H) mutant desmoplakin. Interestingly, mice expressing C-terminal desmoplakin mutations exhibited embryonic lethality similar to mice developed by Gallicano, *et al*, which expressed a cardiac specific C-terminal desmoplakin deletion (Δ281-473).[33, 34] In contrast, mice that expressed the R2834H mutation were successfully generated, and exhibited increased apoptosis / fibrosis, and reduced ventricular function relative to wild-type litter mates. These data suggest that C-terminal mutations may have an adverse effect on embryonic development, and that gene deletions may not accurately recapitulate a disease phenotype caused by the expression of a mutant protein.

In vivo studies are often presumed to be the 'gold standard' for studying disease pathogenesis, but *in vitro* models have also been successfully exploited to study ARVC. Despite the progress made in understanding ARVC etiology through *in vivo* studies, mouse models fail to recapitulate the fatty infiltrations observed in humans. The mechanism by which fatty tissue infiltrated the myocardium remained a mystery until Garcia-Gras, *et al.* used the HL-1 cell line (immortalized atrial myocytes) to show that siRNA knockdown of desmoplakin resulted in a transcriptional switch to adipogenesis, as determined by semi-quantitative RT-PCR.[18] *In vitro* studies have also been able to shed light on how mutant desmosomal protein expression can alter the intracellular distribution of connexin-43. Because desmosomes play a supporting role in structural integrity of gap junctions, desmosmal defects could cause destabilization of gap junctions, and contribute to arrhythmogenesis by altering the normal electrical coupling between cardiac myocytes. Other studies have attempted to use patient-specific induced pluripotent stem cells to better characterize the disease in humans. For example, in 2013 Kim, *et al.* demonstrated that induced pluripotent stem cells expressing mutant plakophilin 2 exhibited some characteristics found in mouse models, such as nuclear translocation of plakoglobin.[36] They were also the first to report that the induction of an adult-like metabolism may underlie the pathogenesis of ARVC, which supports the clinical finding that ARVC symptoms usually present after puberty.[37] These studies show the development of *in vitro* models of ARVC may provide insight into the molecular mechanisms underlying patient-specific disease pathogenesis.

1.1.3 – Treatment Options for ARVC Patients

ARVC is a degenerative condition for which the underlying defective molecular mechanisms are not well defined, and no treatments exist to completely cure ARVC. Recent

studies have provided a wealth of information regarding the link between exercise and disease progression, supporting the most widely implemented disease management strategy of limiting physical exercise.[21-23] However, treatment options are available to mitigate the symptoms associated with ARVC, which include anti-arrhythmic medications, implantable cardioverter defibrillator (ICD) therapy, and catheter ablation.[38] If diagnosed early enough (i.e. – early adulthood), treatment with anti-arrhythmic medication and / or ICD therapy can alter the course of ARVC progression.

The current way clinicians interpret the typically non-specific clinical features of the disease, and arrive at a diagnosis, is to refer to ARVC Task Force criteria.[5] Unfortunately, these criteria tend to focus on features, such as overt changes in cardiac structure, fibrofatty infiltration of the myocardium, and conduction alterations, that tend to occur in patients that have progressed past the concealed stage. Early detection and treatment can provide a normal life-expectancy for patients, with less than 10% of patients progressing to overt right ventricular failure, and the need for heart transplant.[39-41] While each treatment option aims to fix the characteristic arrhythmia associated with the condition, disease management strategies are often individualized, with diagnoses depending on continued monitoring and symptom improvement. The clinical challenges that remain are identifying the condition at an early stage, and improving risk stratification by determining which combination of disease management strategies work best for a particular patient.[42] Addressing either of these challenges requires further investigation into the defective molecular mechanisms underlying the condition.

1.2 – Mechanotransduction in Cardiac Myocytes

External stimuli play an important role in cardiac tissue remodeling through the regulation of key intercellular adhesion proteins such as N-cadherin, plakoglobin, and connexin-43.[43-47] While previous studies of mechanotransduction in cardiac myocytes have characterized responses of monolayers of cultured myocytes to stretch,[48] responses to shear stress may also be particularly pertinent. For example, recent studies by Boycott, *et al.* demonstrated that shear stress was able to induce voltage-gated potassium channel remodeling in atrial myocytes.[49] It remains to be seen if shear stress plays a role in cardiac myocytes expressing ARVC-causing mutant proteins.

Interestingly, patients expressing the 2057del2 ARVC-causing plakoglobin mutation present with keratoderma in regions of the skin (i.e. – palms and soles) that specifically experience shear stress. Similarly, the effects of shear stress may be amplified in structurally weak regions of the heart, and may explain why ARVC preferentially affects the triangle of dysplasia, which represents thinner regions of the right ventricle.[50]

In vivo, cardiac myocytes are organized into a laminar, sheet-like architecture with loose collagenous coupling between sheets. Relative movement of these laminar sheets during the cardiac cycle may cause direct shearing between adjacent sheets or shear from interstitial fluid motion.[51, 52] Canine studies, for example, have identified myocardial shear as a significant factor in wall thickening.[53, 54] Additionally, short-term fluid shear stresses of 90 to 600 mdyn/ cm^2 regulate expression of a wide variety of cardiac markers in rat cardiac myocytes, including the contractile proteins α-sarcomeric actin and troponin-T, the gap junction protein connexin43 (Cx43), and the cell-cell adhesion protein N-cadherin without affecting phosphorylation of p38, an established marker of cell apoptosis.[55, 56] For cardiomyopathies affecting anchoring cell-cell

junctions, such as ARVC, the regulation of these proteins can alter tissue cohesion, intercellular signaling, and even regulate cell viability.

1.3 – Motivation, Specific Aims and Organization

1.3.1 – Motivation

There is increasing evidence that suggests mechanical stress plays a critical role in promoting the cardiac phenotype, which may be altered in ARVC. To that end, the goal of this work is to determine how ARVC-causing mutant desmosomal proteins alter the mechanical and signaling properties of cardiac myocytes, and their ability to respond to mechanical stimuli. Previous studies of mechanotransduction in cardiac myocytes have characterized responses of monolayers of wild-type myocytes, but how individual mutant desmosomal proteins might affect the cell's ability to respond to mechanical stimuli has yet to be determined.

In order to better understand the role of ARVC-causing mutant proteins on the mechanical and structural properties of the heart and its role in ARVC pathogenesis, we first start by studying the native right ventricular myocardium. Next, we aim to determine the role of ARVC-causing mutant plakoglobin on the mechanical properties of cardiac myocytes and their response to mechanical stress. Finally, in order to improve risk stratification for ARVC patients, there exists a critical need to first determine if mutations in different desmosomal proteins result in common mechanical and signaling defects. Accordingly, we aim to assess whether the observed changes in cardiac myocytes expressing ARVC-causing mutant plakoglobin are similar to those observed in myocytes expressing a more frequently mutated protein (i.e. – plakophilin).

1.3.2 – Specific Aims

We propose to address the following specific aims:

Aim 1. Characterize the mechanical strains and structural properties of the native right ventricular myocardium

Hypothesis: The right ventricular apex experiences altered fiber orientation and heterogeneous strain distributions

Aim 2. Assess changes in the mechanical and signaling properties of cardiac myocytes expressing ARVC-causing mutant plakoglobin

Hypothesis: The expression of ARVC-causing mutant plakoglobin alters the mechanical properties of cardiac myocytes (i.e. cell-cell adhesion and cell stiffness), and their ability to respond to mechanical stimuli (i.e. – junctional protein remodeling).

Aim 3. Determine if ARVC-causing mutations in different genes encoding desmosomal proteins result in similar alterations in mechanical and signaling properties

Hypothesis: Cardiac myocytes expressing ARVC-causing mutant plakophilin exhibit altered mechanical and signaling properties similar to those observed in cells expressing mutant plakoglobin.

1.3.3 – Organization

This work is organized into three major sections, focused on elucidating how mechanical forces affect the structural and mechanical properties of cardiac myocytes expressing ARVC-causing mutations. To this end, we first need to understand the structural and mechanical

properties of the native right ventricular myocardium. In Chapter 2, we use histology and immunofluorescence to characterize the structural properties of left ventricular, septal, and right ventricular healthy heart walls. Furthermore, we employ elastography techniques to investigate the mechanical forces throughout the heart. Generally, we focus our attention on the right ventricular apex, owing to the fact that this region is a point of origin for the fibrofatty tissue infiltration associated with ARVC.

In Chapters 3 and 4, we transition to *in vitro* models of ARVC. Using adenoviral infection, we express either mutant ARVC-causing plakoglobin (Chapter 3) or plakophilin (Chapter 4) in neonatal rat ventricular myocytes, and use an array of techniques to investigate the mechanical and signaling properties of these cell models. Plakoglobin was chosen for investigation for its proposed central role in ARVC pathogenesis. We investigate mutant plakophilin-2 because of its prevalence among the ARVC patient population. We develop and use dispase and aggregate assays to measure cell-cell adhesion properties, atomic force microscopy to measure cell stiffness, and quantitative confocal microscopy to measure changes in junctional protein localization. We repeated key assays in the presence of shear stress, to determine how ARVC-causing mutant proteins affect myocyte behavior under physiologically relevant mechanical stress. Finally, in order to learn more about common underlying defects across different ARVC-causing mutations, we compare the response of native plakoglobin and plakophilin in myocytes expressing ARVC-causing mutant plakophilin or plakoglobin, respectively.

In Chapter 5, we conclude by summarizing the results of this thesis work. Furthermore, we discuss the overall impact this work has had in the field, and the potential for future studies based on these results.

1.4 – Tables

Protein	Gene	Mutation	Mutation Type	Reference
Plakoglobin	JUP	**Exons 3-5**	**Deletion (Homozygous)**	**Bierkamp (1996)**
		Exons 3-5	Deletion (Heterozygous)	Bierkamp (1996)
		Exon 3-4	**Deletion (Homozygous)**	**Ruiz (1996)**
		Exon 3-4	Deletion (Heterozygous)	Ruiz (1996)
Plakophilin	PKP2	**Exon 1**	**Deletion (Homozygous)**	**Grossman (2004)**
		Exon 1	Deletion (Heterozygous)	Grossman (2004)
Desmoplakin	Dsp	**Δ281-473**	**Deletion**	**Gallicano (1998)**
		Wild-type	Transgene	Yang (2006)
		R2834H	Transgene	Yang (2006)
		Q90R	Transgene	Yang (2006)
		V30M	Transgene	Yang (2006)
Desmoglein	Dsg2	Wild-type	Transgene	Pilichou (2006)
		N271S	Transgene	Pilichou (2006)

*** Mutations resulting in embryonic lethality**

Table 1.1: Summary of ARVC mouse models used to study disease pathogenesis - From left to right, the columns identify the protein being affected, the gene being mutated, the exact mutation being investigated, the type of mutation, and the associated reference. These models focus on 4 out of 5 major desmosomal proteins thought to cause ARVC when mutated; no mouse models have been developed to study ARVC-causing desmocollin mutations.

1.5 – Figures

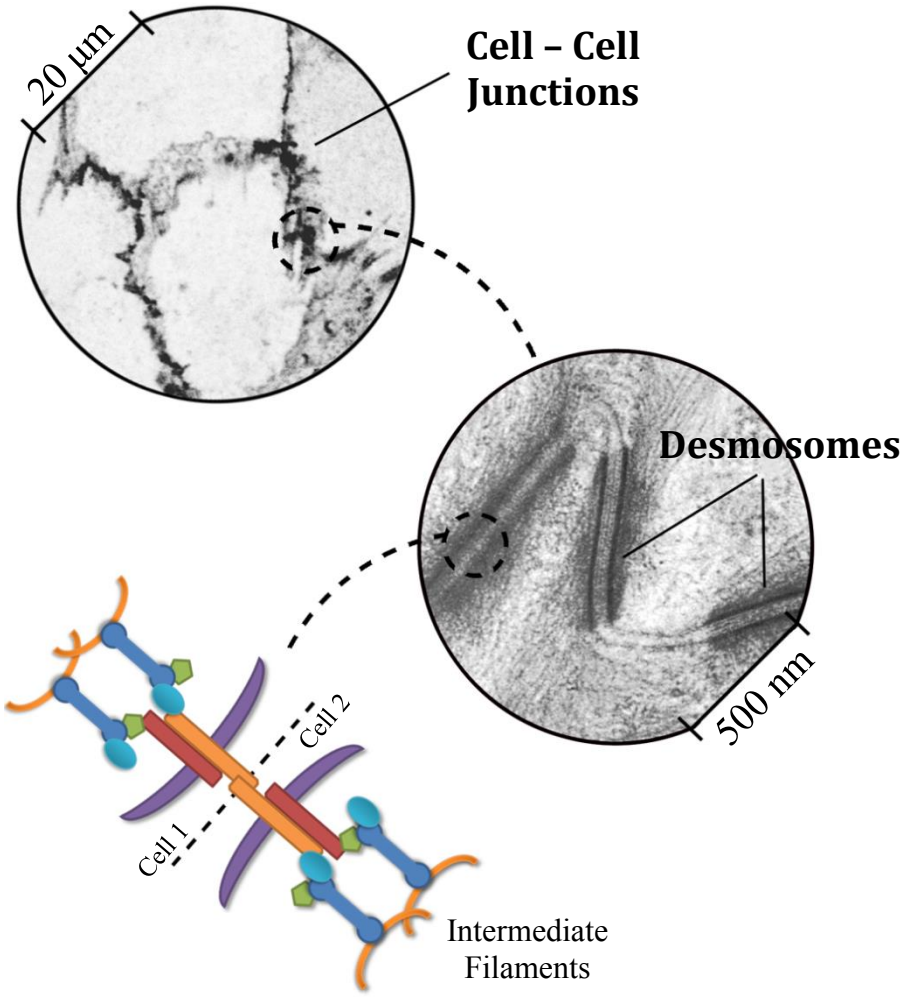

Scanning Electron Micrograph Adapted From: Fawcett DW, The Cell: An Atlas of Fine Structure, p. 371

Figure 1.1: Hierarchy of desmosomal architecture – (Top) Neonatal rat ventricular myocytes immunostained for the desmosomal protein plakoglobin. (Middle) Scanning electron micrograph of a desmosomal junction, showing why desmosomes are described as 'cellular spot welds'. (Bottom) A graphic showing how the desmosomal proteins plakoglobin (green), plakophilin (blue oval), desmoplakin (blue dumbbell), desmoglein (red) and desmocollin (orange) may organize at cell-cell junctions in order to link the intermediate filament networks of adjacent cells, allowing for force transduction through tissues.

1.6 – References

1. Marcus FI, Fontaine GH, Guiraudon G, Frank R, Laurenceau JL, Malergue C, Grosgogeat Y. Right ventricular dysplasia - a report of 24 adult cases. *Circulation*. 1982;65:384-398
2. Mckenna WJ, Thiene G, Nava A, Fontaliran F, Blomstromlundqvist C, Fontaine G, Camerini F. Diagnosis of arrhythmogenic right-ventricular dysplasia/cardiomyopathy. *Brit Heart J*. 1994;71:215-218
3. Lobo FV, Heggtveit HA, Butany J, Silver MD, Edwards JE. Right ventricular dysplasia: Morphological findings in 13 cases. *Can J Cardiol*. 1992;8:261-268
4. Thiene G, Nava A, Corrado D, Rossi L, Pennelli N. Right ventricular cardiomyopathy and sudden death in young people. *N Engl J Med*. 1988;318:129-133
5. Marcus FI, McKenna WJ, Sherrill D, Basso C, Bauce B, Bluemke DA, Calkins H, Corrado D, Cox MGPJ, Daubert JP, Fontaine G, Gear K, Hauer R, Nava A, Picard MH, Protonotarios N, Saffitz JE, Sanborn DMY, Steinberg JS, Tandri H, Thiene G, Towbin JA, Tsatsopoulou A, Wichter T, Zareba W. Diagnosis of arrhythmogenic right ventricular cardiomyopathy/dysplasia proposed modification of the task force criteria. *Circulation*. 2010;121:1533-U1118
6. Pilichou K, Nava A, Basso C, Beffagna G, Bauce B, Lorenzon A, Frigo G, Vettori A, Valente M, Towbin J, Thiene G, Danieli GA, Rampazzo A. Mutations in desmoglein-2 gene are associated with arrhythmogenic right ventricular cardiomyopathy. *Circulation*. 2006;113:1171-1179
7. Rampazzo A, Nava A, Malacrida S, Beffagna G, Bauce B, Rossi V, Zimbello R, Simionati B, Basso C, Thiene G, Towbin JA, Danieli GA. Mutation in human

desmoplakin domain binding to plakoglobin causes a dominant form of arrhythmogenic right ventricular cardiomyopathy. *Am J Hum Genet*. 2002;71:1200-1206

8. Sen-Chowdhry S, Syrris P, McKenna WJ. Role of genetic analysis in the management of patients with arrhythmogenic right ventricular ysplasia/ardiomyopathy. *J Am Coll Cardiol*. 2007;50:1813-1821

9. Awad MM, Calkins H, Judge DP. Mechanisms of disease: Molecular genetics of arrhythmogenic right ventricular dysplasia/cardiomyopathy. *Nature Clinical Practice Cardiovascular Medicine*. 2008;5:258-267

10. McKoy G, Protonotarios N, Crosby A, Tsatsopoulou A, Anastasakis A, Coonar A, Norman M, Baboonian C, Jeffery S, McKenna WJ. Identification of a deletion in plakoglobin in arrhythmogenic right ventricular cardiomyopathy with palmoplantar keratoderma and woolly hair (naxos disease). *Lancet*. 2000;355:2119-2124

11. Norgett EE, Hatsell SJ, Carvajal-Huerta L, Cabezas JCR, Common J, Purkis PE, Whittock N, Leigh IM, Stevens HP, Kelsell DP. Recessive mutation in desmoplakin disrupts desmoplakin-intermediate filament interactions and causes dilated cardiomyopathy, woolly hair and keratoderma. *Hum Mol Genet*. 2000;9:2761-2766

12. Gerull B, Heuser A, Wichter T, Paul M, Basson CT, McDermott DA, Lerman BB, Markowitz SM, Ellinor PT, MacRae CA, Peters S, Grossmann KS, Drenckhahn J, Michely B, Sasse-Klaassen S, Birchmeier W, Dietz R, Breithardt G, Schulze-Bahr E, Thierfelder L. Mutations in the desmosomal protein plakophilin-2 are common in arrhythmogenic right ventricular cardiomyopathy. *Nat Genet*. 2004;36:1162-1164

13. Syrris P, Ward D, Evans A, Asimaki A, Gandjbakhch E, Sen-Chowdhry S, McKenna WJ. Arrhythmogenic right ventricular dysplasia/cardiomyopathy associated with mutations in the desmosomal gene desmocollin-2. *Am J Hum Genet*. 2006;79:978-984

14. Awad MM, Dalal D, Cho E, Amat-Alarcon N, James C, Tichnell C, Tucker A, Russell SD, Bluemke DA, Dietz HC, Calkins H, Judge DP. Dsg2 mutations contribute to arrhythmogenic right ventricular dysplasia/cardiomyopathy. *Am J Hum Genet*. 2006;79:136-142

15. Heuser A, Plovie ER, Ellinor PT, Grossmann KS, Sasse-Klaassen S, Thierfelder L, MacRae CA, Gerull B. Mutant desmocollin-2 causes arrhythmogenic right ventricular cardiomyopathy. *Circulation*. 2006;114:193-193

16. Merner ND, Hodgkinson KA, Haywood AFM, Connors S, French VM, Drenckhahn JD, Kupprion C, Ramadanova K, Thierfelder L, McKenna W, Gallagher B, Morris-Larkin L, Bassett AS, Parfrey PS, Young TL. Arrhythmogenic right ventricular cardiomyopathy type 5 is a fully penetrant, lethal arrhythmic disorder caused by a missense mutation in the tmem43 gene. *Am J Hum Genet*. 2008;82:809-821

17. Tiso N, Stephan DA, Nava A, Bagattin A, Devaney JM, Stanchi F, Larderet G, Brahmbhatt B, Brown K, Bauce B, Muriago M, Basso C, Thiene G, Danieli GA, Rampazzo A. Identification of mutations in the cardiac ryanodine receptor gene in families affected with arrhythmogenic right ventricular cardiomyopathy type 2 (arvd2). *Hum Mol Genet*. 2001;10:189-194

18. Garcia-Gras E, Lombardi R, Giocondo MJ, Willerson JT, Schneider MD, Khoury DS, Marian AJ. Suppression of canonical wnt/beta-catenin signaling by nuclear plakoglobin

recapitulates phenotype of arrhythmogenic right ventricular cardiomyopathy. *J Clin Invest*. 2006;116:2012-2021

19. Lombardi R, Dong JJ, Rodriguez G, Bell A, Leung TK, Schwartz RJ, Willerson JT, Brugada R, Marian AJ. Genetic fate mapping identifies second heart field progenitor cells as a source of adipocytes in arrhythmogenic right ventricular cardiomyopathy. *Circ Res*. 2009;104:1076-U1120
20. Saffitz JE. Dependence of electrical coupling on mechanical coupling in cardiac myocytes - insights gained from cardiomyopathies caused by defects in cell-cell connections. *Ann Ny Acad Sci*. 2005;1047:336-344
21. Corrado D, Basso C, Pavei A, Michieli P, Schiavon M, Thiene G. Trends in sudden cardiovascular death in young competitive athletes after implementation of a preparticipation screening program. *Jama-J Am Med Assoc*. 2006;296:1593-1601
22. James CA, Bhonsale A, Tichnell C, Murray B, Russell SD, Tandri H, Tedford RJ, Judge DP, Calkins H. Exercise increases age-related penetrance and arrhythmic risk in arrhythmogenic right ventricular dysplasia/cardiomyopathy-associated desmosomal mutation carriers. *J Am Coll Cardiol*. 2013;62:1290-1297
23. Corrado D, Thiene G, Nava A, Rossi L, Pennelli N. Sudden-death in young competitive athletes - clinicopathological correlations in 22 cases. *Am J Med*. 1990;89:588-596
24. Fox PR, Maron BJ, Basso C, Liu SK, Thiene G. Spontaneously occurring arrhythmogenic right ventricular cardiomyopathy in the domestic cat - a new animal model similar to the human disease. *Circulation*. 2000;102:1863-1870

25. Basso C, Fox PR, Meurs KM, Towbin JA, Spier AW, Calabrese F, Maron BJ, Thiene G. Arrhythmogenic right ventricular cardiomyopathy causing sudden cardiac death in boxer dogs - a new animal model of human disease. *Circulation*. 2004;109:1180-1185

26. Dalal D, Molin LH, Piccini J, Tichnell C, James C, Bomma C, Prakasa K, Towbin JA, Marcus FI, Spevak PJ, Bluemke DA, Abraham T, Russell SD, Calkins H, Judge DP. Clinical features of arrhythmogenic right ventricular dysplasia/cardiomyopathy associated with mutations in plakophilin-2. *Circulation*. 2006;113:1641-1649

27. Tong LJ, Flach EJ, Sheppard MN, Pocknell A, Banerjee AA, Boswood A, Bouts T, Routh A, Feltrer Y. Fatal arrhythmogenic right ventricular cardiomyopathy in 2 related subadult chimpanzees (pan troglodytes). *Veterinary Pathology*. 2013

28. Lodder EM, Rizzo S. Mouse models in arrhythmogenic right ventricular cardiomyopathy. *Frontiers in Physiology*. 2012;3

29. Bierkamp C, McLaughlin KJ, Schwarz H, Huber O, Kemler R. Embryonic heart and skin defects in mice lacking plakoglobin. *Dev Biol*. 1996;180:780-785

30. Ruiz P, Brinkmann V, Ledermann B, Behrend M, Grund C, Thalhammer C, Vogel F, Birchmeier C, Gunthert U, Franke WW, Birchmeier W. Targeted mutation of plakoglobin in mice reveals essential functions of desmosomes in the embryonic heart. *J Cell Biol*. 1996;135:215-225

31. Kirchhof P, Fabritz L, Zwiener M, Witt H, Schafers M, Zellerhoff S, Paul M, Athai T, Hiller KH, Baba HA, Breithardt G, Ruiz P, Wichter T, Levkau B. Age- and training-dependent development of arrhythmogenic right ventricular cardiomyopathy in heterozygous plakoglobin-deficient mice. *Circulation*. 2006;114:1799-1806

32. Grossmann KS, Grund C, Huelsken J, Behrend M, Erdmann B, Franke WW, Birchmeier W. Requirement of plakophilin 2 for heart morphogenesis and cardiac junction formation. *J Cell Biol*. 2004;167:149-160

33. Gallicano GI, Kouklis P, Bauer C, Yin M, Vasioukhin V, Degenstein L, Fuchs E. Desmoplakin is required early in development for assembly of desmosomes and cytoskeletal linkage. *J Cell Biol*. 1998;143:2009-2022

34. Yang Z, Bowles NE, Scherer SE, Taylor MD, Kearney DL, Ge SP, Nadvoretskiy VV, DeFreitas G, Carabello B, Brandon LI, Godsel LM, Green KJ, Saffitz JE, Li H, Danieli GA, Calkins H, Marcus F, Towbin JA. Desmosomal dysfunction due to mutations in desmoplakin causes arrhythmogenic right ventricular dysplasia/cardiomyopathy. *Circ Res*. 2006;99:646-655

35. Lombardi R, Cabreira-Hansen MD, Bell A, Fromm RR, Willerson JT, Marian AJ. Nuclear plakoglobin is essential for differentiation of cardiac progenitor cells to adipocytes in arrhythmogenic right ventricular cardiomyopathy. *Circ Res*. 2011;109:1342-U1386

36. Kim C, Wong J, Wen JY, Wang SR, Wang C, Spiering S, Kan NG, Forcales S, Puri PL, Leone TC, Marine JE, Calkins H, Kelly DP, Judge DP, Chen HSV. Studying arrhythmogenic right ventricular dysplasia with patient-specific ipscs. *Nature*. 2013;494:105-110

37. Bauce B, Rampazzo A, Basso C, Mazzotti E, Rigato I, Steriotis A, Beffagna G, Lorenzon A, De Bortoli M, Pilichou K, Marra MP, Corbetti F, Daliento L, Iliceto S, Corrado D, Thiene G, Nava A. Clinical phenotype and diagnosis of arrhythmogenic right ventricular

cardiomyopathy in pediatric patients carrying desmosomal gene mutations. *Heart Rhythm*. 2011;8:1686-1695

38. Corrado D, Basso C, Thiene G. Arrhythmogenic right ventricular cardiomyopathy: Diagnosis, prognosis, and treatment. *Heart*. 2000;83:588-595

39. Dalal D, Nasir K, Bomma C, Prakasa K, Tandri H, Piccini J, Roguin A, Tichnell C, James C, Russell SD, Judge DP, Abraham T, Spevak PJ, Bluemke DA, Calkins H. Arrhythmogenic right ventricular dysplasia - a united states experience. *Circulation*. 2005;112:3823-3832

40. Hulot JS, Jouven X, Empana JP, Frank R, Fontaine G. Natural history and risk stratification of arrhythmogenic right ventricular dysplasia/cardiomyopathy. *Circulation*. 2004;110:1879-1884

41. Corrado D, Leoni L, Link MS, Della Bella P, Gaita F, Uriarte JS, Buja G, Thiene G. Implantable cardioverter-defibrillator therapy for primary and secondary prevention of sudden death in patients with arrhythmogenic right-ventricular cardiomyopathy/dysplasia. *Eur Heart J*. 2003;24:278-278

42. Basso C, Corrado D, Marcus FI, Nava A, Thiene G. Arrhythmogenic right ventricular cardiomyopathy. *Lancet*. 2009;373:1289-1300

43. Zhuang JP, Yamada KA, Saffitz JE, Kleber AG. Pulsatile stretch remodels cell-to-cell communication in cultured myocytes. *Circ Res*. 2000;87:316-322

44. Pimentel RC, Yamada KA, Kleber AG, Saffitz JE. Autocrine regulation of myocyte ca3 expression by vegf. *Circ Res*. 2002;90:671-677

45. Yamada K, Green KG, Samarel AM, Saffitz JE. Distinct pathways regulate expression of cardiac electrical and mechanical junction proteins in response to stretch. *Circ Res*. 2005;97:346-353

46. Radisic M, Park H, Shing H, Consi T, Schoen FJ, Langer R, Freed LE, Vunjak-Novakovic G. Functional assembly of engineered myocardium by electrical stimulation of cardiac myocytes cultured on scaffolds. *P Natl Acad Sci USA*. 2004;101:18129-18134

47. Xia Y, McMillin JB, Lewis A, Moore M, Zhu WG, Williams RS, Kellems RE. Electrical stimulation of neonatal cardiac myocytes activates the nfat3 and gata4 pathways and up-regulates the adenylosuccinate synthetase 1 gene. *J Biol Chem*. 2000;275:1855-1863

48. Asimaki A, Kapoor S, Plovie E, Arndt AK, Adams E, Liu Z, James CA, Judge DP, Calkins H, Churko J, Wu JC, MacRae CA, Kleber AG, Saffitz JE. Identification of a new modulator of the intercalated disc in a zebrafish model of arrhythmogenic cardiomyopathy. *Science Translational Medicine*. 2014;6:240ra274

49. Boycott HE, Barbier CSM, Eichel CA, Costa KD, Martins RP, Louault F, Dilanian G, Coulombe A, Hatem SN, Balse E. Shear stress triggers insertion of voltage-gated potassium channels from intracellular compartments in atrial myocytes. *P Natl Acad Sci USA*. 2013;110:E3955-E3964

50. Sen-Chowdhry S, Lowe MD, Sporton SC, McKenna WJ. Arrhythmogenic right ventricular cardiomyopathy: Clinical presentation, diagnosis, and management. *Am J Med*. 2004;117:685-695

51. Caulfield JB, Borg TK. Collagen network of the heart. *Lab Invest*. 1979;40:364-372

52. Dou JG, Tseng WYI, Reese TG, Wedeen VJ. Combined diffusion and strain mri reveals structure and function of human myocardial laminar sheets in vivo. *Magnet Reson Med*. 2003;50:107-113

53. Legrice IJ, Takayama Y, Covell JW. Transverse-shear along myocardial cleavage planes provides a mechanism for normal systolic wall thickening. *Circ Res*. 1995;77:182-193

54. Costa KD, Takayama Y, McCulloch AD, Covell JW. Laminar fiber architecture and three-dimensional systolic mechanics in canine ventricular myocardium. *Am J Physiol-Heart C*. 1999;276:H595-H607

55. Dvir T, Levy O, Shachar M, Granot Y, Cohen S. Activation of the erk1/2 cascade via pulsatile interstitial fluid flow promotes cardiac tissue assembly. *Tissue Eng*. 2007;13:2185-2193

56. Lorenzen-Schmidt I, Schmid-Schonbein GW, Giles WR, McCulloch AD, Chien S, Omens JH. Chronotropic response of cultured neonatal rat ventricular myocytes to short term fluid shear. *Cell Biochem Biophys*. 2006;46:113-122

2 Characterizing the Structural and Mechanical Properties of the Native Heart

2.1 – Introduction

The right ventricle of the heart is a secondary chamber whose structure is morphologically distinct from the left ventricle. In particular, the right ventricle 'wraps' around part of the left ventricle, so that the right ventricular chamber is more crescent-shaped than circular. Because the right ventricle is similar to an 'added' wall of the heart, cardiac structure can exhibit discontinuitie[1]s and experience altered mechanical stresses where the right ventricular lateral wall meets the septum, and in particular at the right ventricular apex (RVA), which must merge with the septum in multiple directions. Because myocytes typically form adhesion complexes end-to-end, discontinuous or juxtaposed myofibers could result in diminished junctional protein expression (i.e. – desmosomes, gap junctions, etc.), affecting electrical conduction across the myocardium. In fact, the RVA is a key site for development of arrhythmias and a potential pacing target, although recent large, randomized clinical trials have begun to correlate pacing at the RVA with a worse clinical outcome in patients with various arrhythmia diseases (i.e. - arrhythmogenic cardiomyopathy, Brugada Syndrome, etc.).[2-5] It has been proposed that the detrimental effects of pacing at the right ventricular apex can be attributed to an abnormal electrical activation pattern in the ventricles (i.e – conduction of the electrical wavefront through the myocardium instead of the His-Purkinje fiber system).[6] A careful characterization of the structure of the RVA is essential for understanding its role in cardiac physiology.

Further, the tendency for arrhythmia development may depend in part on the physical forces being experienced by the RVA region. However, a detailed characterization of the

structural and mechanical properties of the RVA, expanding on earlier studies that primarily focus on general fiber orientation within the ventricle itself, may yield new information on the influence of RVA anatomy on the progression of some diseases.[7, 8] For example, Arrhythmogenic Right Ventricular Cardiomyopathy (ARVC) preferentially affects the right ventricular epicardium between the conus arteriosus and ventricular apex, referred to as the 'triangle of dysplasia,' yet reasons for this localization remain unknown.[9-11] One study notes the triangle of dysplasia likely represents thinner regions of the right ventricle, but without definitive data.[12] While many conditions have underlying causes (genetic, molecular, etc.) exacerbating their symptoms, the hearts are typically structurally normal when the patient is young. Thus, it is worthwhile examining healthy hearts to determine whether there is any reason underlying the RVA's tendency to be involved in pacing and structural alterations.

Two methods for examining the structural properties of myocardial tissue are histology and diffusion tensor imaging, both having their own advantages and disadvantages. Histological analysis involves embedding tissue in paraffin wax, and taking planar sections of tissue, which can then be analyzed further (i.e. – immunofluorescence staining). Of the two, histology is the only technique that provides direct evidence of cardiac fiber orientation, as it requires sectioning the actual tissue, but limits the data acquisition to two dimensions, and can result in minor aberrations at the tissue periphery. Furthermore, histology requires fully infiltrating a tissue sample with embedding media (such as paraffin wax), limiting the size of the tissue construct that can be studied without tissue reconstruction. Diffusion tensor imaging, on the other hand, is a technique that uses magnetic resonance imaging to track the diffusion of water through tissue. In cardiac tissue, water generally moves through the myocardial fibers (the path of least resistance), which allows for the 3-dimensional mapping of cardiac fibers throughout the heart.

While this technique is less invasive than histology, the data cannot be used to draw conclusions at the molecular level (which requires immunostaining of histological sections). In order to study both the cardiac fiber orientation as well as the junctional localization of key cell-cell adhesion proteins (i.e. – plakoglobin and N-cadherin), we chose to use histological analysis. To measure the mechanical properties of the heart, we collaborated with the Ultrasound Elasticity Imaging Laboratory at Columbia University to use elastography – a non-invasive, ultrasound-based imaging technique that can be used to determine local tissue strain by cross-correlating RF segments throughout the cardiac cycle to calculate the arrival time-shift of an echo in a deformed region of tissue.[13, 14] While other motion-estimation techniques are also available for the study of myocardial strains (i.e. – Doppler myocardial imaging or Strain rate imaging), they are phase-shift based methods that require autocorrelation, which can limit the signal bandwidth that can be used (i.e. – resulting in low axial resolution).[15-17] Elastography is a time-shift based technique (proven to overcome the limitation of low axial resolution faced by phase-shift based techniques) that has been validated in myocardial tissue, and can be used to calculate the incremental axial displacements and strains.[15-18]

Because of a potential interplay between structure and mechanical stresses at the RVA, we propose a biomechanical hypothesis: regions of structural disarray, coupled with altered (elevated or heterogeneous) mechanical strains, may contribute to development of arrhythmias and altered tissue responses, and that these effects are exacerbated in certain disease processes. To test this hypothesis in the context of the RVA, we performed a systematic analysis of the structural features and mechanical strains in the heart, focusing on the RVA region. We examined healthy hearts from canines (suitable for elastography measurements and histological analysis) and rats (suitable for large-scale histological and immunofluorescence analysis) and

show that the RVA exhibits persistent elevation and significant gradients in mechanical strains, and diminished organization of a key junctional protein. These results support the 'biomechanical' hypothesis, and explain why the RVA may be predisposed to initiation of pathological tissue development and represents a hot spot for conduction abnormalities, independently of specific disease processes.

2.2 - Methods

2.2.1 – Histology

Whole rat hearts were extracted via cardiectomy from sacrificed (1-day) post-partum adult rats and fixed for 24 hours in 4% paraformaldehyde. Septal, left and right ventricular (S, LV and RV, respectively) sections were dissected along the long-axis planes of the heart. Right ventricular sections included myocardium inferior to the apex of the right ventricle, but not extending to the apex of the heart, while left ventricular samples consisted of tissue extending to the apex of the left ventricle, and myocardium from the right ventricular uptract. Septal sections did not include epicardial tissue. Samples were dehydrated with ethanol, cleared with xylene, and embedded in paraffin, taking care to preserve orientation and landmarks to ensure the right ventricular apex could be located. Epicardial sections were sectioned into 5 μm thick samples and mounted on glass slides. Left and right ventricular sections were taken along the epicardial wall, while septal sections were taken from myocardium lining the right ventricle. Sections were subsequently stained using the Chromaview Masson Trichrome Kit (Sigma, St. Louis, MO) according to the manufacturer's protocol, and mounted with Permount Mounting Medium (Fisher Scientific, Waltham, MA). Canine samples were obtained from formalin fixed whole hearts. Epicardial LV and RVA samples were dissected from the LV wall (toward the apex) and

where the RV lateral wall meets the septum, respectively. Samples were processed identically to rat heart samples. All animal work was performed in accordance with the Institute of Comparative Medicine at Columbia University.

2.2.2 – Structural Analysis

Rat and canine heart histological sections were imaged under bright field microscopy using a 4x, NA 0.13 objective on an Olympus IX-81 microscope (Center Valley, PA). Individual images were assembled using the FIJI plug-in for ImageJ to produce a single high-resolution image of the entire ventricular or septal wall, orienting the apex-base axis vertically with the apex toward the bottom. Line plots were hand-drawn by tracing local fiber orientation, as assessed visually. Lines were omitted at fiber bifurcations and regions where fiber orientation was visually ambiguous. Fiber direction was quantified in septal, left and right ventricular samples with color mapping using Matlab (Natick, MA); a 20 x 20 grid was used to discretize each image into cells where the fiber orientation was determined using a line segment parallel to the local fiber direction (Appendix 2.6). The cosine of each angle was determined in the range of 0 to 180 degrees, and scaled to a gray-scale map, where horizontal and vertical fibers correspond to black and white, respectively. This map provides a visualization of changes in fiber orientation within a single wall; the greater the changes in fiber orientation, the larger the amount of variance in grayscale. Analysis of fiber direction was performed by determining the percentage of cells within each 20 x 20 grid (Rat n=4; Canine n=2 for each wall) where the cosine of the angle was greater than 0.3, corresponding to cells with vertically oriented fibers.

2.2.3 – Immunofluorescence

Rat myocardial samples were immunostained using established protocol.[19] Paraffin-embedded samples were re-hydrated and boiled in citrate buffer (pH 6.0) for 11 minutes. After cooling to room temperature, tissue sections were concurrently blocked and permeabilized for 45 minutes (3% normal goat serum, 1% w/v BSA, and 0.15% Triton X-100 in PBS). Samples were then incubated with either mouse-monoclonal anti-plakoglobin (Sigma; 1:400 in blocking buffer) or anti-pan cadherin (Sigma; 1:400) antibody overnight at 4 ^{o}C, followed by a two-hour incubation with the secondary antibody (diluted 1:1000) on day two at 25 ^{o}C. Fluorescently labeled samples were then mounted with Permount Mounting Medium and imaged using an Olympus IX-81 fluorescence microscope and analyzed using Metamorph and ImageJ. Quantitative microscopy was used to determine JUP and PC signal intensity in regions of fiber disarray relative to regions with uniform fiber orientation. ImageJ was used to threshold fluorescence images to isolate junctional JUP or PC signal, and determine the fraction of pixels above threshold over pixels in the image space.

2.2.4 – Elastography

Elastography data was acquired following established protocol.[20] Two mongrel dogs were anesthetized with injection of thiopental and fitted with standard limb leads for electrocardiogram monitoring. Morphine (0.15 mg/kg, epidural) was administered before surgery, and lidocaine (50 µg/kg/hr, intravenous) was used throughout the procedure. A 0.9% saline solution was supplied intravenously (5 mL/kg/hr) to maintain blood volume. Echocardiography was performed using an Ultrasonix RP system with a 3.3 MHz phased array to acquire RF frames between 390 and 480 frames/sec via an automated composite technique.[21] Radial incremental (strain in one frame using the previous frame as reference) and cumulative

(change in strain relative to end-diastole) strains in the Eulerian description (motion relative to fixed spatial coordinates) were estimated by applying a least-squares estimator [22] on incremental and cumulative displacements, respectively. For example, if a thin wire were stretched with images taken at 1 Hz, the incremental strain would represent the change in length of the wire between two frames divided by the wires in the first of the two frames. The cumulative strain would represent the change in length of the wire relative to the original length of the wire, before being stretched. Incremental and cumulative strains[23, 24] were calculated by taking a spatial average of strains throughout each wall at successive time points, using the roipoly function in Matlab (Natick, MA) to specify the polygonal region of interest. Both whole-wall (WALL; Figure 2.6A, outlined in black) and smaller mid-wall regions of interest (MID-WALL; Figure 2.6B, black squares) were used for strain quantification in order to provide large-scale data and variance in radial strain within the region of interest (modified from previous work [24]), respectively. Mid-wall incremental strains were determined using an ROI toward the middle of each wall during the ECG when the peak incremental strain occurred (Figures 2.7C & 2.8C). Normality of the strains within the mid-wall region of interest was confirmed using the Kolmogorov-Smirnov test ($p \leq 0.05$). End-systolic mid-wall cumulative strain was also calculated using a region of interest toward the middle of each wall (Figures 2.7D & 2.8D). Standard errors for regional incremental and cumulative strains were calculated using strain values within each region of interest. Statistical significance was determined using analysis of variance (ANOVA) and Tukey's test. All animal work was approved by the Institutional Animal Care and Use Committee of Columbia University.

2.2.5 – Statistical Analysis

Data were analyzed using the analysis of variance (ANOVA) test. Data showing significance ($p \leq 0.05$) were further analyzed using either a Student's T-test, Tukey or Bonferroni post-hoc tests.

2.3 – Results

2.3.1 – Cardiac Fibers at the Right Ventricular Apex (RVA) Exhibit Disarray

To examine the structure of the ventricular walls and septum, histological techniques were used to enhance visualization of fiber orientation in samples obtained from rats and canines. Rat hearts were used due to their low epicardial fat and to facilitate the analysis of entire ventricular walls. Due to the thinness of rat heart walls, histological specimens are representative of both epicardium and endocardium.

While disarray is used without formal definition in many cardiac structural studies, in this article disarray refers to abrupt changes in myocyte orientation signifying loss of straight end-to-end coupling. In contrast with the LV and septal regions, myocyte disarray in the RV was a notable recurring theme in the samples, with cell-cell apposition typically occurring at or near the RVA region (Figures 2.1A-C and 2.2A-B, left column). There is significant variance in the degree and extent of this disarray, as well as its location, consistent with the highly variable penetrance of ARVC and arrhythmia development in clinical cases.

To quantify this disarray, histological sections were color-mapped with shades of grey corresponding to the local fiber direction. In the RV, cell-cell juxtaposition ranged from 0 to 90 degrees, whereas a more continuous change in fiber orientation was observed in the LV and septal regions as evidenced by the proximal localization of white and black cells in the gray-scale mapped images of the right ventricle (Figures 2.1A-C and 2.2A-B, right column). In the rat

RV, 5.7 percent of cells contained vertically oriented fibers, while left ventricles and septums had 1.1 and 0.7 percent, respectively (Figure 2.1D; $p \leq 0.05$ for LV vs RV, $p \leq 0.01$ for SEP vs RV). In the canine RV, 37.75 percent of cells contained vertically oriented fibers, while left ventricles had 0.375 percent, respectively (Figure 2.2C; $p \leq 0.05$ for LV vs RV). The right ventricular walls exhibit greater black/white distributions that are either focally located or randomly scattered, suggesting a degree of disarray in the right ventricular walls. In contrast, the left ventricular and septal walls exhibit more uniformity in their gray-box distribution.

2.3.2 – Cell-Cell Junctional Protein Localization is Altered Near the RVA

In addition to overt structural disarray in the RVA region, immunohistochemical staining was performed in rat heart sections to assess the localization of both cadherin and plakoglobin at cell junctions. Cadherins are adhesion molecules that hold together adjacent myocytes at their intercalated discs. Plakoglobin is a desmosomal protein that links desmin across adjacent myocytes. Plakoglobin is additionally implicated in ARVC, and its expression is altered even in cases where the disease-causing mutation is not in plakoglobin itself.[25] Thus there is reason to believe that plakoglobin may help stabilize conduction and/or mechanical support pathways.

Far from the RVA, cadherin staining was strong and similar in the left ventricular (Figure 2.3A), right ventricular (Figure 2.3B) and septal (Figure 2.3C) walls, mostly localizing at the end-to-end junctions between adjacent cardiomyocytes. Cadherin signals near the RVA exhibited diminished intensity levels, relative to the rest of the wall, with fiber apposition evident in the RVA region (Figure 2.3D & 2.3F; $p=0.07$). Plakoglobin also exhibits a similar drop-off in intensity near the RVA ($p \leq 0.05$), suggesting diminished desmosomal expression in addition to fiber disarray (Figure 2.3E-F). Intercalated disk orientation near the RVA exhibits lower degrees

of end-to-end localization and regularity. These results are consistent across the hearts examined. Since desmosomes play a supporting role in gap-junctional architecture, altered electromechanical coupling in this region may account for previously observed idiopathic ventricular arrhythmias.[26]

2.3.3 – Elastography Reveals Persistent, Elevated Strain in the Right Ventricle

Elastography measurements of incremental (change from frame to frame) and cumulative (change relative to end-diastole) mechanical strains were acquired along the length of the ventricular walls and septum of a canine heart (Figures 2.4 and 2.5 showing incremental and cumulative strain superimposed on the echocardiography data, respectively). Canine hearts were used due to similarity of their physiology to the human heart, thus being well-suited for elastography measurements.

The RVA exhibits strong sharp changes in the distribution of both incremental strain and cumulative strain (Figures 2.6A-B). In particular, there are sharp transition regions of strain near the RVA, and especially in Heart 1, peak strains occur near the RVA region. These data suggest that the RVA may be prone to unusual mechanical load distributions due to local load heterogeneity, and in some cases, experience elevated loading.

Quantitative analysis of strain data reveals elevated and sustained incremental and cumulative strains within the RV wall, as compared to the LV wall, during systole (Figures 2.7A-B & 2.8A-B). Mid-wall incremental systolic strains are $0.0056 \pm 5.5\text{x}10^{-4}$ and $0.0045 \pm 2.2\text{x}10^{-4}$ in the right ventricle and $0.0024 \pm 5.3\text{x}10^{-5}$ and $0.0017 \pm 4.0\text{x}10^{-5}$ in the left ventricle, respectively, corresponding to 133 and 165 percent increases in incremental strain (Figures 2.7C & 2.8C; $p \leq 0.01$). Mid-wall incremental systolic strains are $0.0043 \pm 1.6\text{x}10^{-5}$ and $0.0017 \pm$

$2.5x10^{-4}$ in the right ventricular apex. Since incremental strains represent the change over a short time-span, higher incremental strains suggest a more abrupt load on the myocytes.

Whole-wall cumulative strains during systole are persistently elevated for the right ventricle compared to the left ventricle during systole, although not for diastole (Figures 2.7B & 2.8B). Further, data demonstrate that changes in cumulative systolic strains (end systolic strain minus beginning systolic strain) in the RV wall are greater than that of the LV wall. Mid-wall cumulative end-systolic strains are 0.15 ± 0.026 and 0.11 ± 0.013 in the right ventricle and 0.094 ± 0.0058 and 0.077 ± 0.0014 in the left ventricle, representing 1.6 and 1.4-fold increases in cumulative strain (Figures 2.7D & 2.8D; $p \leq 0.01$). Mid-wall cumulative end-systolic strains are 0.061 ± 0.010 and 0.059 ± 0.007 in the right ventricular apex. Similar elevations are found for diastolic strains. The cumulative strain values obtained for the LV are consistent with those found in literature, from both experimental observations and computational studies, indicating a peak strain of approximately 10% near the basal region of the heart from diastole to systole.[27, 28]

These data show that the RV wall bears higher strains for longer periods of time, has elevated changes in strain over short times, and near the RVA, experiences heterogeneity in strain distribution in a small volume. Interestingly, both mid-wall and whole-wall septal cumulative strains are comparable to, or greater than, RV cumulative strains. Additionally, the RVA itself does not exhibit particularly elevated strain magnitudes (incremental or cumulative), compared to the rest of the heart. Thus, elevated, persistent and heterogeneous mechanical strains by themselves are likely not sufficient to explain the RVA as a site for conduction abnormalities.

2.4 – Discussion

The work in this chapter was meant to characterize the mechanical strains and structural properties of the right ventricular myocardium. Of particular interest in our investigation was the right ventricular apex, a region notorious for disease development. We show, via tissue-level examination of cardiac structure and mechanical strain that (1) the region near the right ventricular apex exhibits structural disarray, (2) the right ventricular apical region exhibits less organized intercalated disk orientation and diminished desmosomal expression, and (3) there are persistent, elevated strains and changes in strain over short distances in the right ventricle, during systole. Disarray near the RVA region likely contributes to structural weakness since the lateral adhesion strength of the fibers is likely lower than the end-to-end strength. Further, during systole, when the intramuscle strength needs to be high to maintain tissue cohesion, the right ventricle, and sometimes the RVA, experiences elevated strains, compared to the left ventricle. Thus, heterogeneous fiber orientation, coupled with increased incremental strains, effectively create a "weak spot" in the heart. The diminishment or disorganization of plakoglobin near this region may further weaken the heart or lead to conduction alterations.

Our results thus support the "biomechanical" hypothesis, and provide supporting evidence for the need to study how ARVC-causing mutations may affect cell-cell adhesion strength and junctional protein localization in the presence of physiologically relevant mechanical stimuli (Chapter 3). While our study does not address a specific disease process, some motivation for examination of the RVA region came from ARVC. One primary hypothesis for the etiology of ARVC is that defects in cell-cell adhesion lead to destabilization of cell-cell interactions and disruption of junctional associations. Observations that desmosomal mutations causing ARVC do not generally lead to defects in other desmosome-expressing tissues (with skin/hair involvement being a notable exception) support this hypothesis, since the heart tissue is

under persistent, cyclic, elevated mechanical stresses. Our study is consistent with this hypothesis and explains further why the RVA has mixed results as a target for cardiac pacing.

To test our biomechanical hypothesis we did not examine disease model hearts, opting instead to examine cardiac structures and strains to determine how they may contribute to disease development. For example, cardiac structure appears unaltered in the early stages of conditions such as ARVC,[29] manifesting primarily after puberty. Thus, ARVC (and other conduction abnormalities) may not necessarily be the result of a priori alterations in cardiac tissue; they may simply initially manifest at hot spots such as the RVA. The variability we report may also explain why ARVC does not always manifest primarily at the triangle of dysplasia (or indeed, necessarily the right ventricle).

Examination of intact bovine hearts revealed a significant fatty deposit around the superior circumference of the heart, some mild fatty streaks following the left-anterior descending coronary artery, and notably, the right-ventricular apical region, but not the primary cardiac apex (Figure 2.9). As bovine (and canine) species can naturally develop phenotypes similar to the ARVC phenotype observed in humans, the presence of fatty streaks in the native bovine heart may indicate a predisposition for fibrous tissue infiltration near the right ventricular apex that may be exacerbated under disease conditions. Further, superficial examination of the heart structure shows that the bovine heart RVA region exhibits similar fiber disarray observed in rat hearts. Thus, the phenomenon we report is likely broadly applicable across mammalian hearts and may explain the presence of ARVC-like syndromes in cows and dogs, and provide support for use of different mammalian species in our analysis. Further examination, using more sophisticated techniques (such as diffusion-tensor imaging), direct mechanical testing of the RVA tissue and molecular analysis of RVA mechanotransduction, are warranted. Examination of

the other locations of the triangle of dysplasia may be insightful, but were not done in this study because of reduced roles in cardiac conduction issues and difficulty of access for quantitative analysis. Heterogeneity in general fiber disarray and mechanical strains in the present study offer a potential explanation for the varying penetrance in ARVC development as well as variability in cardiac pacing using the RVA.[3, 4]

We show that healthy right ventricles exhibit fiber disarray and diminished plakoglobin expression, specifically at the right ventricular apex, and experience elevated strains during systole relative to the left ventricle. Together, these results provide supporting evidence for why the RVA is a hot spot for development of arrhythmias. In particular, these results support the "biomechanical" hypothesis that regions exhibiting both weakened structure and elevated strains are likely to be a focal point for cardiac conduction abnormalities, and motivate our need to study the effects of ARVC-causing proteins on cell-cell adhesion and junctional protein localization in the presence of mechanical stimuli.

2.5 – Figures

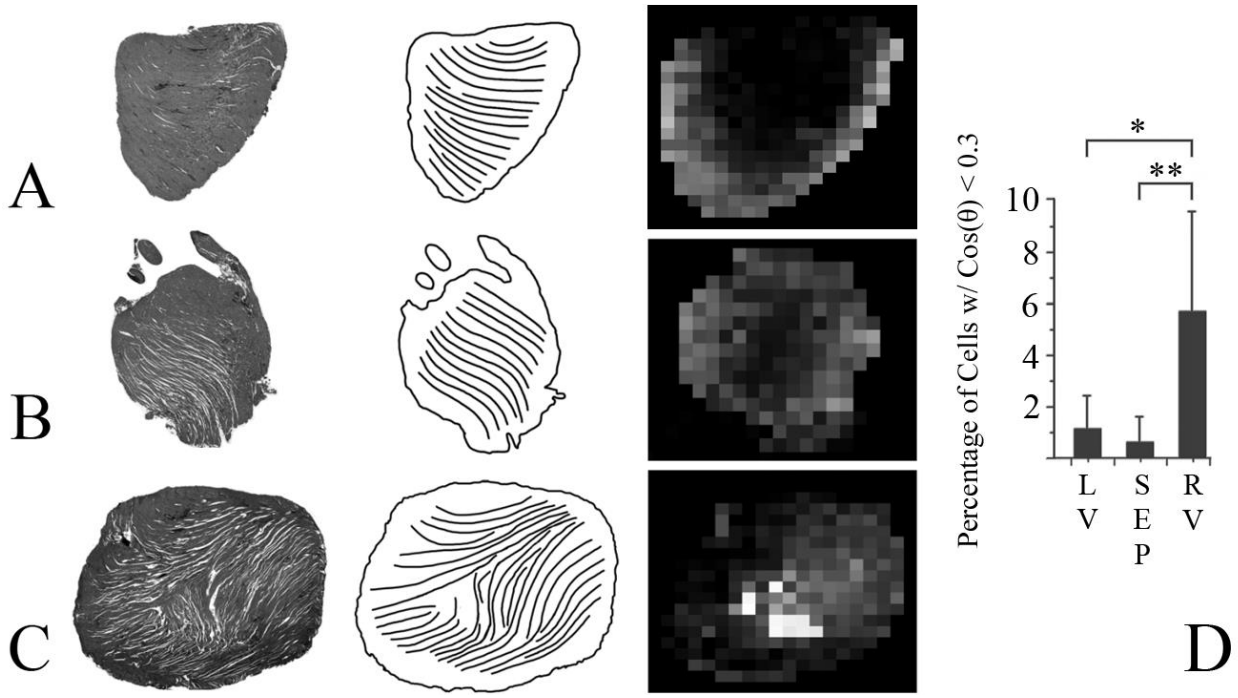

Figure 2.1: Fiber disarray occurs at the right ventricular apex in the mouse heart - Representative epicardial sections of (A) left-ventricular, (B) septal, and (C) right-ventricular regions of the rat heart with streamlines (line plots, middle column) to enhance visualization of myocyte fiber direction. Color mapping of fiber orientation in left-ventricular, septal, and right-ventricular sections (right column) shows a localization of vertical fibers (white) near the RVA region apposing fibers with a horizontal orientation (black), in contrast with the left-ventricular and septal sections. (A-C) Scale bar = 2mm; (D) Quantification of angle mapping in left-ventricular (LV), septal (SEP), and right-ventricular rat heart sections showing the percentage of cells where $\cos(\theta) < 0.3$. * $p \leq 0.05$; ** $p \leq 0.01$

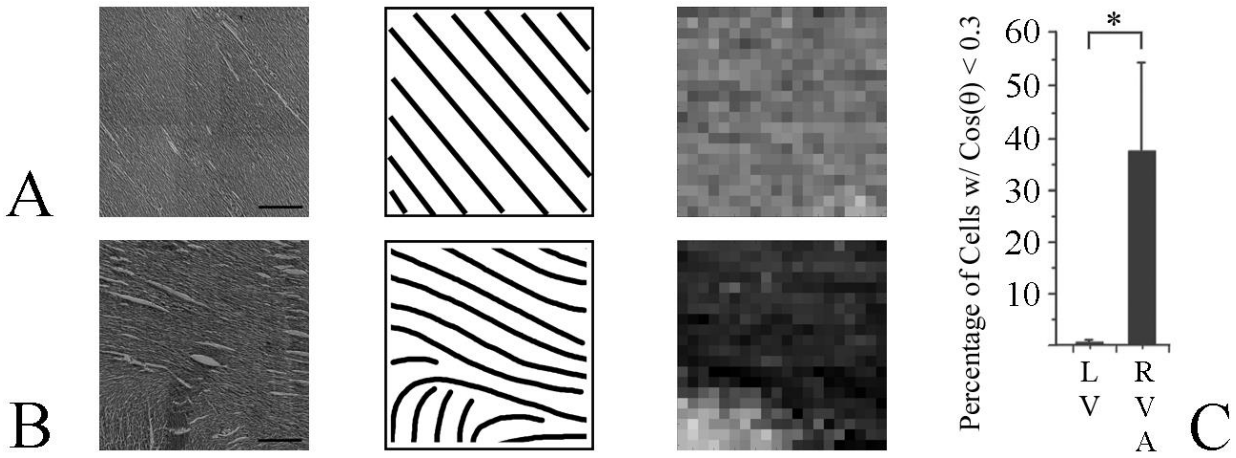

Figure 2.2: Fiber disarray occurs at the right ventricular apex in the canine heart - Representative epicardial sections of (A) left-ventricular, and (B) right-ventricular regions of the canine heart with streamlines (line plots, middle column) to enhance visualization of myocyte fiber direction. Color mapping of fiber orientation in left-ventricular, septal, and right-ventricular sections (right column) shows a localization of vertical fibers (white) near the RVA region apposing fibers with a horizontal orientation (black), in contrast with the left-ventricular section. (A-B) Scale bar = 500 μm; (C) Quantification of angle mapping in left-ventricular (LV) and right-ventricular canine heart sections showing the percentage of cells where $\cos(\theta) < 0.3$. * $p \leq 0.05$; ** $p \leq 0.01$

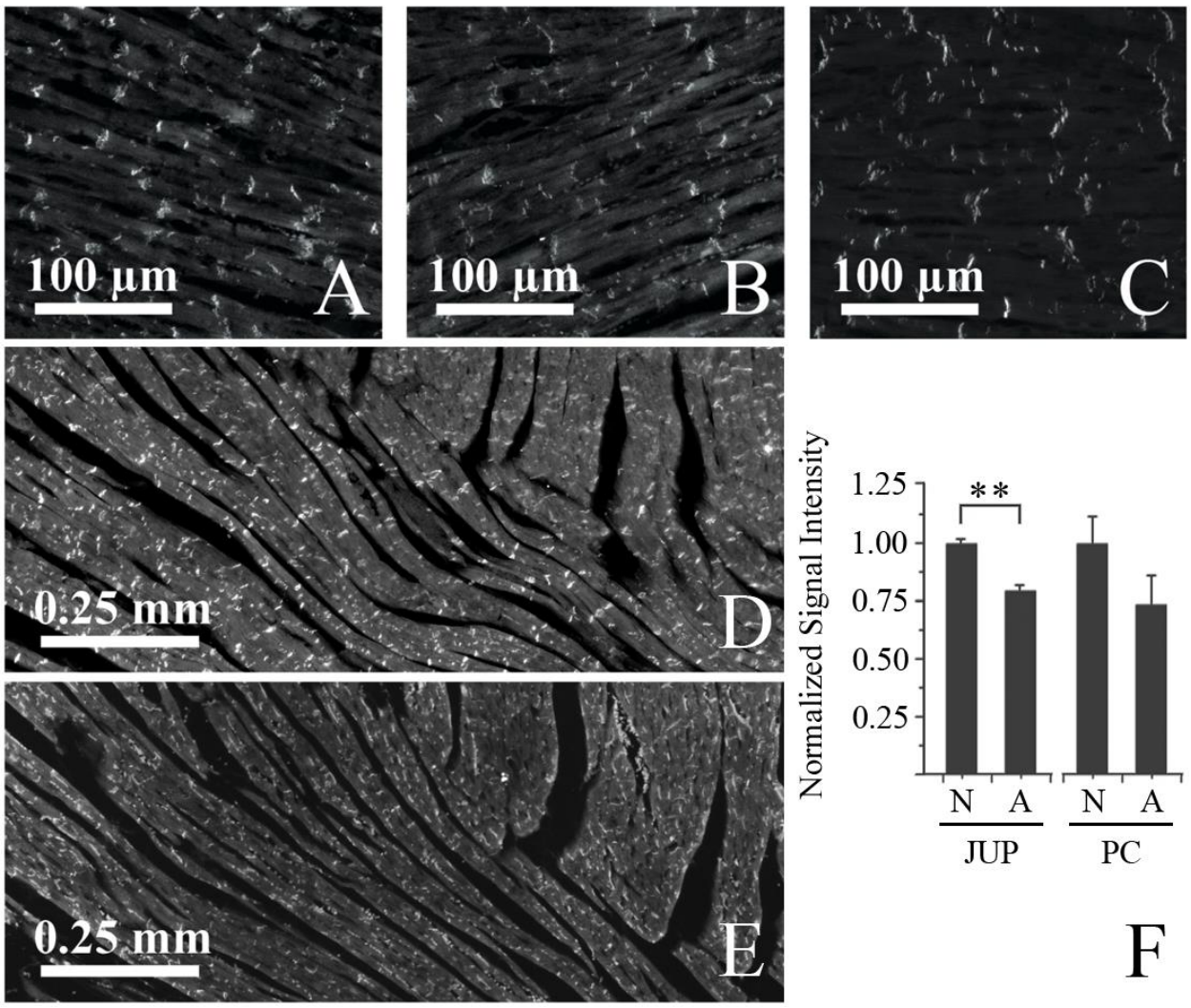

Figure 2.3: Diminished plakoglobin expression occurs at the right ventricular apex in the mouse heart - (A) Left-ventricular, (B) right-ventricular, and (C) septal myocardial samples immunostained against pan-cadherin. The localization of expression is predominantly at the end-to-end junctions of the myocytes. Scale bar = 100 µm. (D) Cadherin stained region of cardiac tissue including the RVA and some tissue peripheral to the RVA. (E) Plakoglobin stained region of cardiac tissue including the RVA and some tissue peripheral to the RVA. The upper-middle region, representing the RVA, exhibits weaker staining and less organization of intercalated disks. Scale bar = 250 µm. (F) Quantification of plakoglobin (JUP) and pan-cadherin (PC) signal intensity in non-apical (N) and apical (A) regions of the right ventricle. ** $p \leq 0.01$

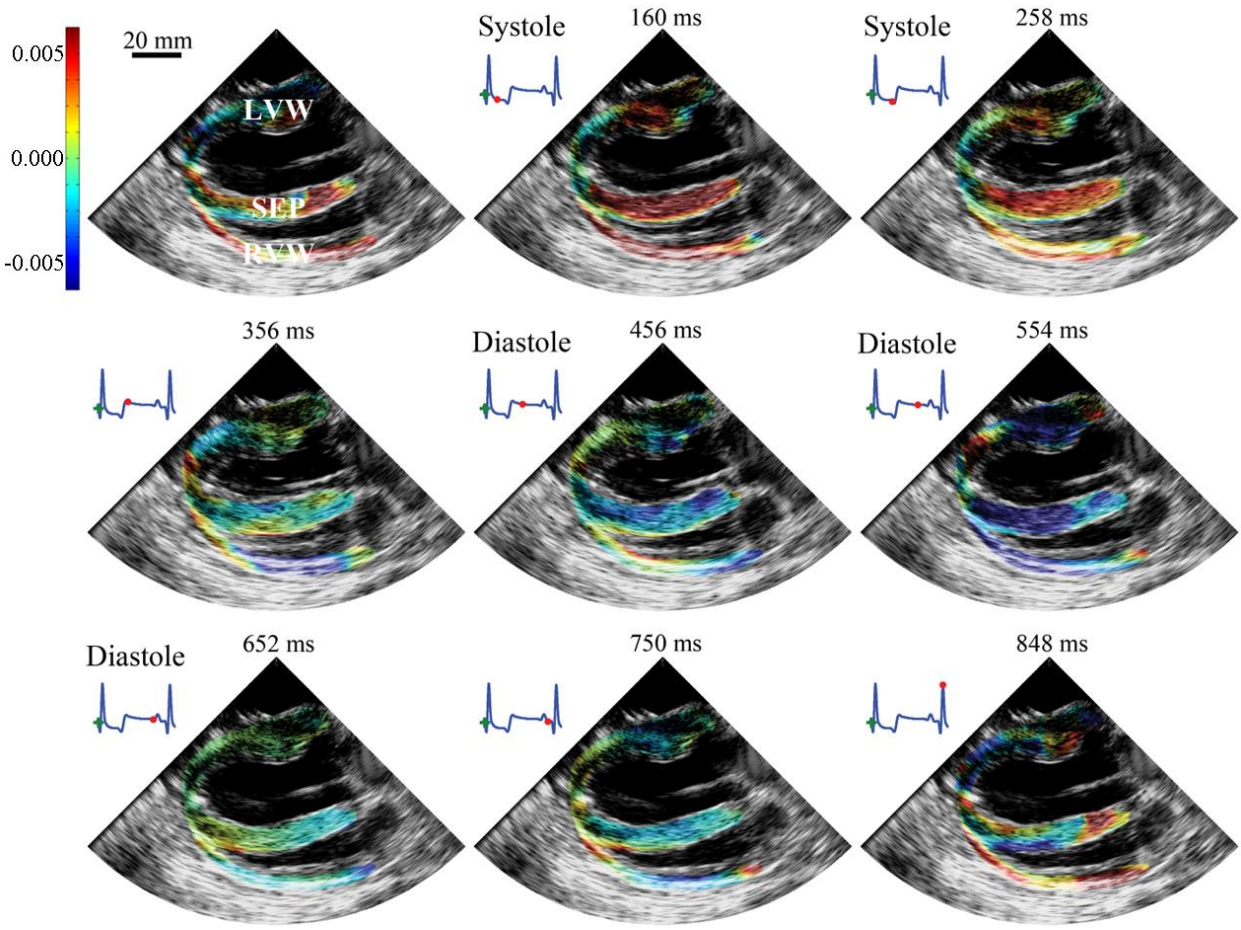

Figure 2.4: Elevated incremental strains occur at the right ventricle during systole - Spatial distribution of incremental radial strains, superimposed on echocardiogram, across canine ventricular walls at different time points in one complete ECG cycle (denoted by red dots). The left ventricular wall (LVW) is shown at the top of the image, followed by the septum (SEP) in the middle and the right ventricular wall (RVW) at the bottom. Incremental strains are superimposed against the acquired echocardiography data.

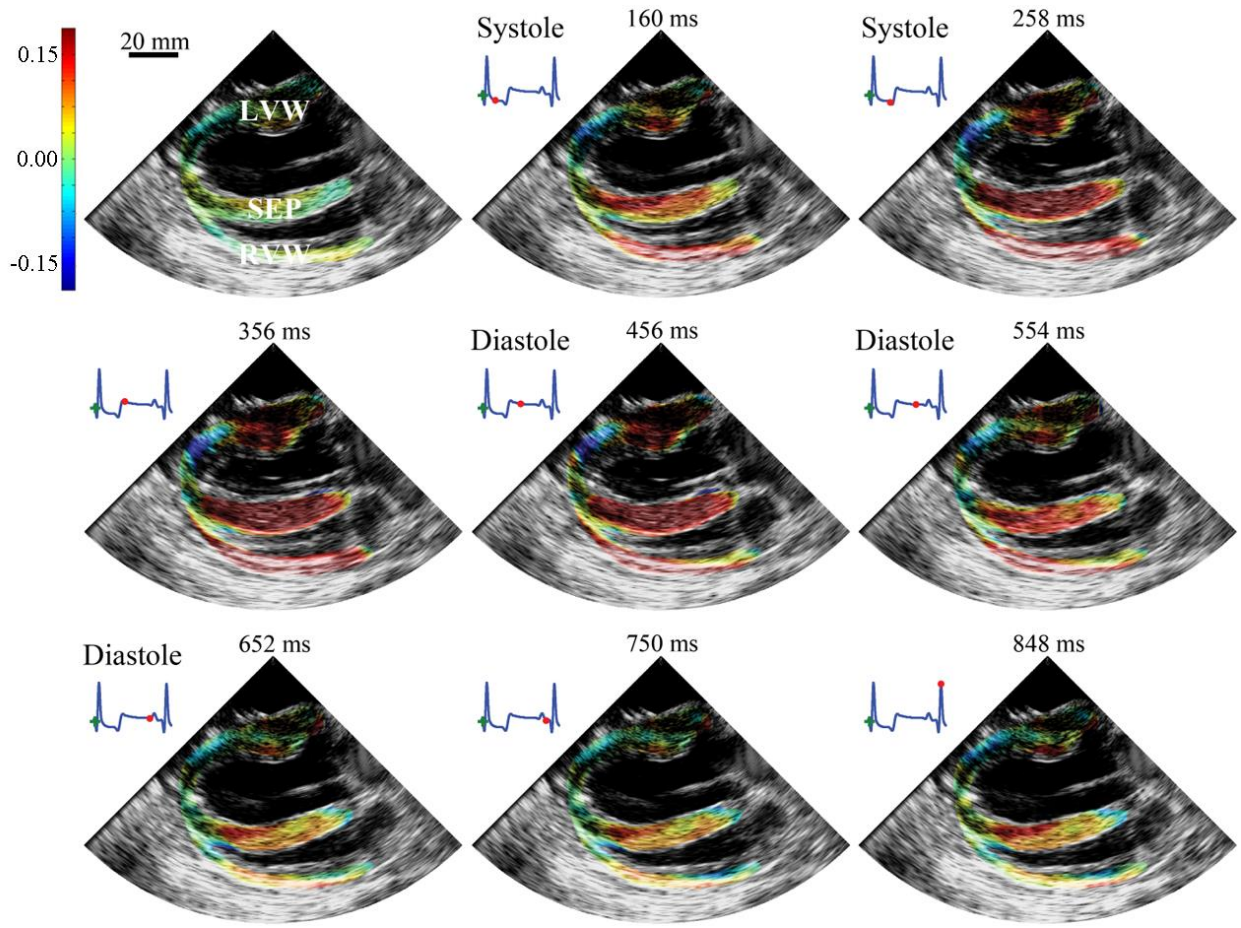

Figure 2.5: Elevated cumulative strains occur at the right ventricle during systole - Spatial distribution of cumulative radial strains, superimposed on echocardiogram, across canine ventricular walls at different time points in one complete ECG cycle (denoted by red dots). The left ventricular wall (LVW) is shown at the top of the image, followed by the septum (SEP) in the middle and the right ventricular wall (RVW) at the bottom. Cumulative strains are superimposed against the acquired echocardiography data.

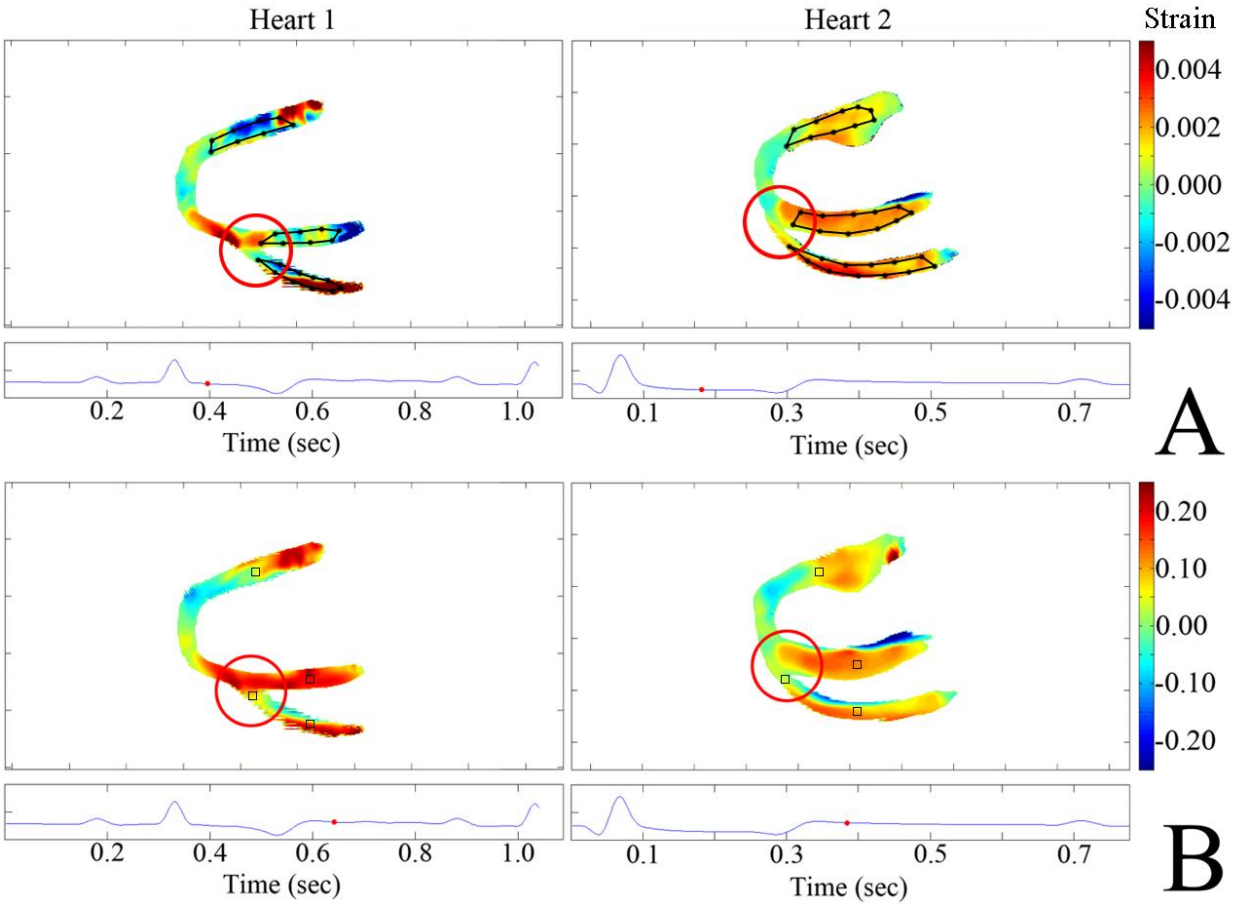

Figure 2.6: Heterogeneous strain distributions occur at the right ventricular apex - Spatial distribution of (A) incremental strains during systole and (B) cumulative radial strains near the beginning of diastole, showing a transition in strain magnitude near the RVA (circled in red), over a short distance compared to a similar transition over the cardiac apex. Black outlines (A) are used to identify regions used for whole-wall strain analysis. Black squares (B) are used to identify regions used for mid-wall strain analysis.

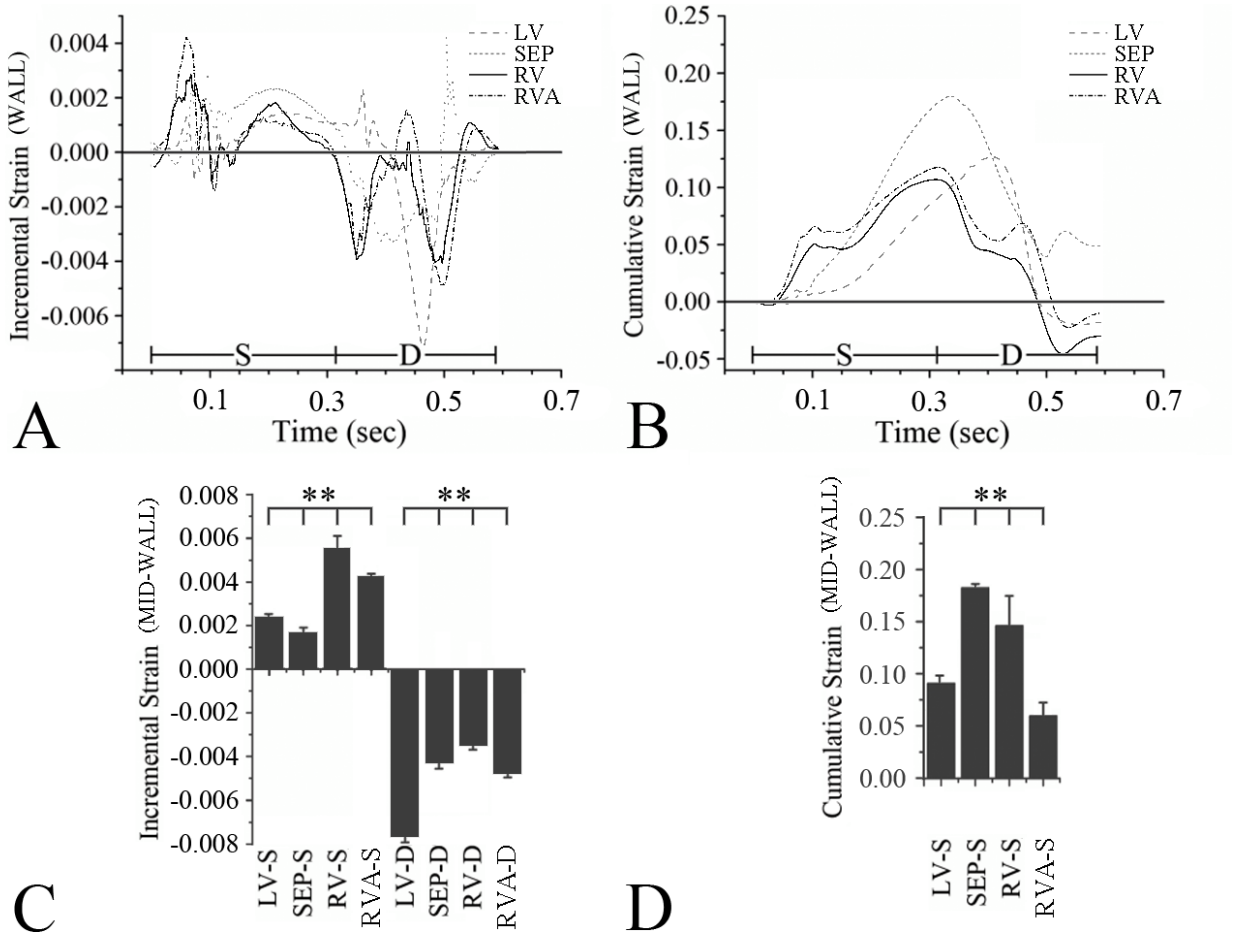

Figure 2.7: Quantification of incremental and cumulative strains in the canine Heart 1 - Incremental (A) and cumulative (B) strains within canine Heart 1 during systole (S, 0-310 ms) and diastole (D, 310-595 ms). Sustained, elevated strains are observed within the right ventricle (RV) as compared to the left ventricle (LV) during systole. Mid-wall incremental strains (C) and end-systolic mid-wall cumulative strains (D) show elevated RV strains compared to LV strains. ** $p \leq 0.01$

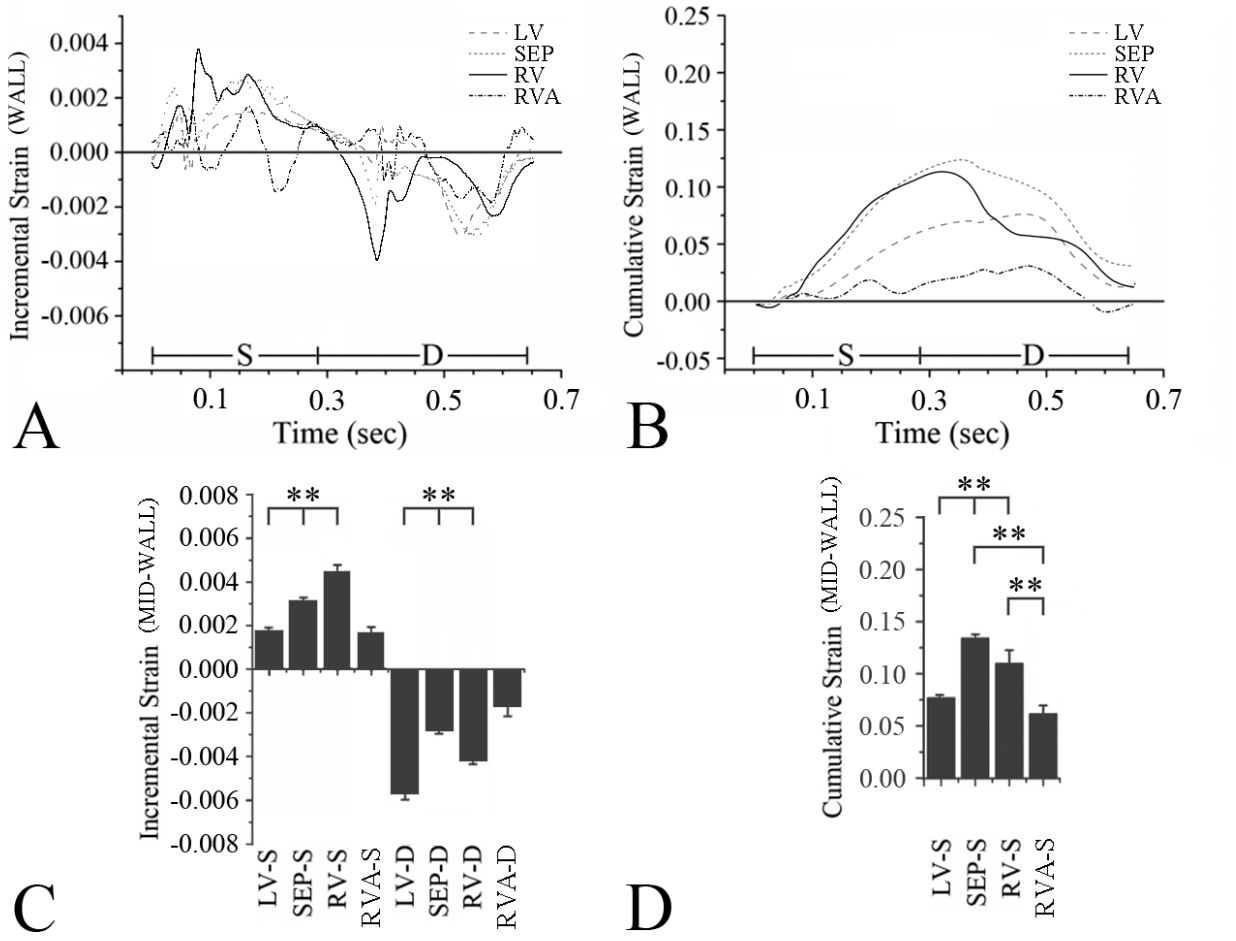

Figure 2.8: Quantification of incremental and cumulative strains in the canine Heart 2 - Incremental (A) and cumulative (B) strains within canine Heart 2 during systole (S, 0-290 ms) and diastole (D, 290-645 ms). Sustained, elevated strains are observed within the right ventricle (RV) as compared to the left ventricle (LV) during systole. Mid-wall incremental strains (C) and end-systolic mid-wall cumulative strains (D) show elevated RV strains compared to LV strains. ** $p \leq 0.01$

Figure 2.7: Healthy bovine hearts exhibit fatty deposits along the triangle of dysplasia - Intact bovine heart. Note the significant fatty deposit around the superior circumference of the heart, some mild fatty streaks following the left-anterior descending coronary artery, and notably, the right-ventricular apical region (red circle), but not the primary cardiac apex.

2.6 – Appendix

```
%Select grid points left to right, up to down
%image should be 16bit format through ImageJ
%Image should be preferably around 2.5 MB

image = uigetfile;
imagedata = imread(image);
imagedata = uint16(imagedata);


H = input('How Many Cells in the Y Direction?');
W = input('How Many Cells in the X Direction?');

[ny,nx] = size(imagedata);

i=1;

for j = 1:floor(ny./H)-1:((H-1)*(floor(ny./H)));

    for k = 1:floor(nx./W)-1:((W-1)*(floor(nx./W)));

        image1=imagedata([j:(j+(ny./H))],[k:(k+(nx./W))]);
        imshow(image1,'InitialMagnification','fit');
        O(i,:) = ginput(1);
        P(i,:) = ginput(1);
        i=i+1;

    end
end
```

2.7 – References

1. Gillis AM. Redefining physiologic pacing: Lessons learned from recent clinical trials. *Heart Rhythm*. 2006;3:1367-1372
2. Furman S, Schwedel JB. An intracardiac pacemaker for stokes-adams seizures. *N Engl J Med*. 1959;261:943-948
3. Grover M, Glantz SA. Endocardial pacing site affects left ventricular end-diastolic volume and performance in the intact anesthetized dog. *Circ Res*. 1983;53:72-85
4. Leclercq C, Gras D, Le Helloco A, Nicol L, Mabo P, Daubert C. Hemodynamic importance of preserving the normal sequence of ventricular activation in permanent cardiac pacing. *Am Heart J*. 1995;129:1133-1141
5. Eckardt L, Kirchhof P, Schulze-Bahr E, Rolf S, Ribbing M, Loh P, Bruns HJ, Witte A, Milberg P, Borggrefe M, Breithardt G, Wichter T, Haverkamp W. Electrophysiologic investigation in brugada syndrome - yield of programmed ventricular stimulation at two ventricular sites with up to three premature beats. *Eur Heart J*. 2002;23:1394-1401
6. Prinzen FW, Peschar M. Relation between the pacing induced sequence of activation and left ventricular pump function in animals. *Pace*. 2002;25:484-498
7. Ho SY, Nihoyannopoulos P. Anatomy, echocardiography, and normal right ventricular dimensions. *Heart*. 2006;92:I2-I13
8. Sheehan F, Redington A. The right ventricle: Anatomy, physiology and clinical imaging. *Heart*. 2008;94:1510-1515
9. Marcus FI, Fontaine GH, Guiraudon G, Frank R, Laurenceau JL, Malergue C, Grosgogeat Y. Right ventricular dysplasia - a report of 24 adult cases. *Circulation*. 1982;65:384-398

10. Lobo FV, Heggtveit HA, Butany J, Silver MD, Edwards JE. Right ventricular dysplasia: Morphological findings in 13 cases. *Can J Cardiol*. 1992;8:261-268

11. Thiene G, Nava A, Corrado D, Rossi L, Pennelli N. Right ventricular cardiomyopathy and sudden death in young people. *N Engl J Med*. 1988;318:129-133

12. Sen-Chowdhry S, Lowe MD, Sporton SC, McKenna WJ. Arrhythmogenic right ventricular cardiomyopathy: Clinical presentation, diagnosis, and management. *Am J Med*. 2004;117:685-695

13. Ophir J, Cespedes I, Ponnekanti H, Yazdi Y, Li X. Elastography - a quantitative method for imaging the elasticity of biological tissues. *Ultrasonic Imaging*. 1991;13:111-134

14. Ophir J, Alam SK, Garra B, Kallel F, Konofagou E, Krouskop T, Varghese T. Elastography: Ultrasonic estimation and imaging of the elastic properties of tissues. *P I Mech Eng H*. 1999;213:203-233

15. Bonnefous O, Pesque P. Time domain formulation of pulse-doppler ultrasound and blood velocity estimation by cross-correlation. *Ultrasonic Imaging*. 1986;8:73-85

16. Hein IA, Obrien WD. Current time-domain methods for assessing tissue motion by analysis from reflected ultrasound echoes - a review. *Ieee T Ultrason Ferr*. 1993;40:84-102

17. Dejong PGM, Arts T, Hoeks APG, Reneman RS. Determination of tissue motion velocity by correlation interpolation of pulsed ultrasonic echo signals. *Ultrasonic Imaging*. 1990;12:84-98

18. Konofagou EE, D'Hooge J, Ophir J. Myocardial elastography - a feasibility study in vivo. *Ultrasound Med Biol*. 2002;28:475-482

19. Kwong KF, Schuessler RB, Green KG, Laing JG, Beyer EC, Boineau JP, Saffitz JE. Differential expression of gap junction proteins in the canine sinus node. *Circ Res*. 1998;82:604-612

20. Provost J, Lee WN, Fujikura K, Konofagou EE. Electromechanical wave imaging of normal and ischemic hearts in vivo. *Ieee Transactions on Medical Imaging*. 2010;29:625-635

21. Wang SG, Lee WN, Provost J, Luo JW, Konofagou EE. A composite high-frame-rate system for clinical cardiovascular imaging. *Ieee T Ultrason Ferr*. 2008;55:2221-2233

22. Kallel F, Ophir J. A least-squares strain estimator for elastography. *Ultrasonic Imaging*. 1997;19:195-208

23. Konofagou EE, Fung-Kee-Fung S, Luo J, Pernot M. Imaging the mechanics and electromechanics of the heart. *Conf Proc IEEE Eng Med Biol Soc*. 2006;Suppl:6648-6651

24. Lee WN, Provost J, Fujikura K, Wang J, Konofagou EE. In vivo study of myocardial elastography under graded ischemia conditions. *Phys Med Biol*. 2011;56:1155-1172

25. Asimaki A, Tandri H, Huang HD, Halushka MK, Gautam S, Basso C, Thiene G, Tsatsopoulou A, Protonotarios N, McKenna WJ, Calkins H, Saffitz JE. A new diagnostic test for arrhythmogenic right ventricular cardiomyopathy. *New England Journal of Medicine*. 2009;360:1075-1084

26. Navarrete A. Idiopathic ventricular tachycardia arising from the right ventricular apex. *Europace*. 2008;10:1343-1345

27. Takayama Y, Costa KD, Covell JW. Contribution of laminar myofiber architecture to load-dependent changes in mechanics of lv myocardium. *Am J Physiol-Heart C*. 2002;282:H1510-H1520

28. Usyk TP, Mazhari R, McCulloch AD. Effect of laminar orthotropic myofiber architecture on regional stress and strain in the canine left ventricle. *J Elasticity*. 2000;61:143-164

29. Kaplan SR, Gard JJ, Protonotarios N, Tsatsopoulou A, Spiliopoulou C, Anastasakis A, Squarcioni CP, McKenna WJ, Thiene G, Basso C, Brousse N, Fontaine G, Saffitz JE. Remodeling of myocyte gap junctions in arrhythmogenic right ventricular cardiomyopathy due to a deletion in plakoglobin (naxos disease). *Heart Rhythm*. 2004;1:3-11

3 Characterizing the Mechanical and Signaling Properties of Cardiac Myocytes Expressing ARVC-Causing Plakoglobin

3.1 – Introduction

More than half of ARVC patients exhibit one or more mutations in genes encoding desmosomal proteins.[1] This has led many investigators to suggest that ARVC is a "disease of the desmosome" in which defective cell-cell adhesion plays a critical pathogenic role. In support of this widely held hypothesis are electron microscopy studies of patient endomyocardial biopsies and mouse models of human disease showing decreased numbers of desmosomes in ventricular myocardium and apparent clefts or widening of various components within the intercalated disk.[2-4] Delmar and associates have shown that knockdown of plakophilin-2 in neonatal rat cardiac myocytes in vitro greatly reduces cell-cell adhesion strength,[5] and we have previously shown that, when expressed in HEK cells, mutant forms of plakoglobin linked to ARVC can alter cell stiffness or cause a similar marked loss of cell-cell adhesion strength.[6] There is also clinical evidence implicating abnormal biomechanical factors in ARVC. For example, recent findings have revealed that ARVC progression may be exacerbated by strenuous exercise.[7] Additional motivation comes from our findings presented in Chapter 2, where we show that the right ventricular (RV) apex, an area preferentially affected in ARVC, exhibits diminished junctional plakoglobin localization and elevated incremental strains.[8] Noting that the function of desmosomes is to provide tissues with their mechanical strength, regions of diminished plakoglobin expression may have weakened tissue cohesion, potentially creating a mechanically weak spot in the heart. Furthermore, ARVC may be part of a cardiocutaneous syndrome in which the skin phenotype appears to be directly related to mechanical stress. One such condition is Naxos disease which, in addition to ARVC, is characterized by keratoderma of

the palms and soles arising after birth once these regions are subjected to mechanical stresses during normal daily activities. However, while these observations all suggest that mechanical stress plays a critical role in promoting the ARVC phenotype, the underlying mechanisms remain poorly defined and there is no direct evidence of weakened cell-cell adhesion in the hearts of patients with ARVC.

Previous studies of mechanotransduction in cardiac myocytes have characterized responses of monolayers of cultured myocytes to stretch, but responses to shear stress may also be particularly pertinent.[9-11] In vivo, cardiac myocytes are organized into a laminar sheet-like architecture with loose collagenous coupling between sheets. Relative movement of these laminar sheets during the cardiac cycle may cause direct shearing between adjacent sheets or shear from interstitial fluid motion.[12, 13] Canine studies, for example, have identified myocardial shear as a significant factor in wall thickening.[14, 15] Additionally, short-term fluid shear stresses of 90 to 600 mdyn/ cm^2 regulate expression of a wide variety of cardiac markers in rat cardiac myocytes, including the contractile proteins α-sarcomeric actin and troponin-T, the gap junction protein connexin43 (Cx43), and the cell-cell adhesion protein N-cadherin without affecting phosphorylation of p38, an established marker of cell apoptosis.[16, 17] In particular, regulation of cell-cell adhesion proteins may play an important role in ARVC pathogenesis, contributing to the adhesion defects often associated with this condition. To gain greater insights into potential mechanisms by which desmosomal mutations cause ARVC, we characterized biomechanical properties and responses to shear stress in neonatal rat ventricular myocytes expressing two distinct mutant forms of the desmosomal protein plakoglobin which have been linked to ARVC in patients. We used atomic force microscopy to measure cell stiffness. Although several techniques exist to measure the elasticity of cells (i.e. – magnetic twisting cytometry,[18]

micropipette aspiration,[19] microindentation,[20-22] etc.), atomic force microscopy (AFM) is the most widely applied, reliable technique with the least potential for damaging the cells being studied. Using AFM, we show that the cardiac myocytes expressing ARVC-causing mutant plakoglobin exhibit no significant changes in cell-cell stiffness. Furthermore, our initial investigation into cell-cell adhesion (using aggregate assays) showed no significant differences in cells expressing mutant plakoglobin, relative to control cells. Because defective intercellular adhesion is widely believed to play a role in ARVC pathogenesis, we decided to confirm our findings with dispase assays (which also showed no differences in cell-cell adhesion strength).

Changes in mechanotransduction may also contribute to ARVC pathogenesis. Specifically, changes at the molecular level may compound any changes in adhesion that occur form the expression of mutant plakoglobin. Therefore, in addition to examining cell-cell adhesion, we investigate changes in junctional protein distribution, apoptosis, and ERK phosphorylation. We determined that cells expressing mutant plakoglobin were unable to remodel plakoglobin, as well as N-cadherin, at cell-cell junctions, suggesting mutant plakoglobin expression can destabilize both desmosomal and non-desmosomal junctions. With cell death being a hallmark characteristic of ARVC, we performed TUNEL assays to show that mutant plakoglobin expression led to an increase in apoptosis. We also investigate ERK phosphorylation, which is involved in hypertrophic response in cardiac myocytes, and is responsive to shear stress.[16] Cardiac myocytes can respond to increased mechanical loading by undergoing hypertrophy, and desmosomal integrity has been shown to affect the hypertrophic response in cardiac myocytes.[23, 24] Despite the belief that ARVC-causing mutations result in desmosomal destabilization, we show that ERK phosphorylation is not disrupted by the expression of ARVC-causing plakoglobin. Finally, we perform pharmacological interrogation to

restore the wild-type phenotype in our disease model. Overall, we observed no differences in biomechanical properties. Instead, myocytes expressing mutant plakoglobin exhibited abnormal responses to mechanical stress that were corrected by SB216763, which is a well-documented inhibitor of GSK3β.[25-28]

3.2 – Methods

3.2.1 – Cell Culture and Transfection

Primary cultures of neonatal rat myocyte cultures (NRVM) were prepared from ventricles of 1-day old Wistar rat pups (Charles River, Indianapolis) as previously described.[29] Hearts from 10 neonatal rats were removed and finely minced. The pieces were serially digested in a dissociation solution (Ca^{2+}/Mg^{2+}-free Hanks balanced salt solution, GIBCO) containing 0.1% trypsin, 60 μg/ml pancreatin (Sigma, MO), 20 units/ml penicillin and 20 μg/ml streptomycin. Cells were seeded at a density of 310K cells/cm^2. NRVM were cultured on collagen-coated glass slides in M199 media (Life Technologies, NY) supplemented with 5% fetal calf serum (Sigma, MO) and 100 μM BRDU (Sigma, MO). After 2 days in culture (or immediately following isolation for cell aggregate cultures), cells were exposed for 1 hour at 37 ^oC to adenoviruses containing wild-type human plakoglobin, or plakoglobin constructs with either the S39_K40insS mutation (linked to autosomal dominant ARVC) or the 2057del2 mutation (linked to Naxos disease). Cells transfected with virus containing wild-type plakoglobin were used to control for viral transfection and possible effects related to over-expression. Adenovirus containing green fluorescent protein (GFP) was used to monitor transfection efficiency. Viruses were obtained through a collaboration with the Saffitz Lab at Beth Israel Deaconess Medical Center (Boston, MA). The wild-type plakoglobin construct and both mutant forms of plakoglobin included a V5

epitope tag to facilitate exogenous protein identification by immunostaining and immunoblotting. Recombinant adenoviral constructs were created using the ViraPower Adenoviral Expression system (Invitrogen) using a pAd/CMV/V5-DEST vector through LR clonase-mediated recombination. Experiments were performed 24 hours after adenoviral transfection. All animal work was performed in accordance with the Institutional Animal Care and Use Committee of Columbia University.

3.2.2 – Cell-Cell Adhesion Assays

Cell-cell adhesion strength was measured using dispase assays and cell aggregate assays. Dispase assays were performed using monolayers of transfected NRVM on collagen-coated glass chamber slides. Monolayers were pre-treated with 10 μM blebbistatin for 20 minutes to minimize contractions, followed by a solution containing 2.4 U/mL dispase and 10 μM blebbistatin for 30 minutes at 37 ºC and 1% CO2. Intact cell sheets that had lifted off the culture dish were agitated for 3 min in a rotary shaker at 70 rpm, and the number of fragments was quantified using ImageJ.[5, 6] To further validate the dispase assays, additional studies were performed in monolayers of NRVM treated with 1 μM cytochalasin-D for 1 hour (post-lift), or in non-transfected monolayers exposed to a specific siRNA against plakoglobin or N-cadherin, as previously described,[30] to compare effects on adhesion strength caused by desmosomal protein knockdown versus expression of mutant desmosomal proteins. Non-targeting siRNA was used to control for the effects of the transfection process. As both adenoviral and siRNA treatments are forms of transfection, in this study we restrict our use of the term ‘transfection’ to refer to adenoviral transfection, and ‘knockdown’ to refer to siRNA transfection. Cell aggregate assays, a commonly used assay for studying cell-cell adhesion, were performed by seeding 20 μL hanging

drops of culture media with 10,000 cardiac myocytes. Three days later, cell aggregates were agitated by pipetting, and the number of resulting fragments was quantified using integrated morphometry analysis in Metamorph.

3.2.3 – Immunoblotting

Immunoblotting was performed as previously described.[30] Cultured NRVM were lysed in standard RIPA lysis buffer containing 500 nM phenylmethanesulfonyl fluoride, 50 mM sodium fluoride, 1 mM sodium orthovanadate, 10 mM sodium pyrophosphate, and protease inhibitor cocktail. Samples were solubilized in LDS sample buffer supplemented with 5% v/v 2-mercaptoethanol. Total protein concentration was determined by Bradford assay (Sigma). Soluble fractions containing equal amounts of total protein were separated using SDS polyacrylamide gel electrophoresis and transferred onto PVDF membranes (Millipore, MA). Immunoblotting was performed using the following mouse anti-human antibodies: anti-plakoglobin (Sigma 1:2000), anti-phosphorylated ERK1/2 (Cell Signaling 1:1000), anti-total ERK1/2 (Cell Signaling 1:1000), anti-Rnd1 (Santa-Cruz Biotechnology 1:200), anti-Isg15 (Santa-Cruz Biotechnology 1:200) and horseradish peroxidase-conjugated goat anti-mouse secondary antibody (Biorad 1:1000). Blots were developed with ECL reagents (Perkin Elmer, MA) and imaged using a FUJI imaging unit (Fujifilm, CT). Relative band intensities were quantified using ImageJ, with values normalized to loading controls (total-ERK 1/2 for phosphorylated-ERK 1/2).

3.2.4 – Atomic Force Microscopy

Atomic force microscopy (AFM) was performed using a BioScope Catalyst AFM mounted on an Olympus IX-81 inverted light microscope (Olympus, PA). A silicon-nitride DNP probe (Bruker, CA) was used to characterize the stiffness of control myocytes and cells expressing mutant forms of plakoglobin. Indentations of 400 nm were made on the surface of the cells. The elastic modulus was determined using the force (calculated as a product of the cantilever's spring constant and tip deflection), and the deflection vs. displacement data fit to an eighth-order polynomial, as previously described.[31, 32] Readings were acquired between consecutive contractions (which were easily visible on the AFM real-time readout) without further treatment. Five measurements from each cell were acquired and averaged to yield 'whole-cell' stiffness.

3.2.5 – Shear Flow

NRVM were sheared under oscillatory flow conditions in a parallel-plate shear chamber at 0.06 Pascal (Pa) for 4 hours at 37ºC. Thereafter, the cells were either immunostained for plakoglobin/N-cadherin or lysed for immunoblotting measurements of plakoglobin, V5, and phosphorylated or total ERK. The shear level was estimated by (1) using a parallel plate model to simulate the shear induced by adjacent myocardial sheets,[17] and (2) using a range of shear stresses that have been previously shown to induce ERK phosphorylation without activation of the p38 pathway.[16] The formula used to calculate the shear level was derived by applying a force balance to incremental unit of fluid, and solving for the shear stress at the walls of two parallel plates (Figure 3.1). The relationship was derived as follows:

$$P(dx\,dz) - \left(P + \frac{\partial P}{\partial x}dx\right)(2y\,dz) - 2\tau\,dx\,dz = 0$$

$$\tau = -y\frac{\partial P}{\partial x} = \mu\frac{dV}{dy}$$

By solving for $\frac{dV}{dy}$, and applying the boundary condition $V\left(y = \frac{H}{2}\right) = 0$, we can determine the velocity profile within the parallel plate:

$$V = \frac{1}{2\mu}\frac{\partial P}{\partial x}\left(\frac{H^2}{4} - y^2\right)$$

Integrating between $-\frac{H}{2}$ and $\frac{H}{2}$, we can determine our relationship for applied shear stress:

$$Q = \int V\, dA_c \rightarrow \tau = -y\left(\frac{12\mu Q}{DH^3}\right)$$

$$\tau_{wall}\left(y = \frac{H}{2}\right) = \frac{-6\mu Q}{H^2 D}$$

where τ_{wall} represents the shear stress applied to our cells (0.06 Pa), Q represents the fluid flow rate into the chamber, μ represents the fluid viscosity (6.5 x 10^{-4} Ns/m^2), and H and D the dimensions of the parallel plate chamber. By designing the chamber to have a channel height of H = 7.87 x 10^{-4} m, a depth of D = 12.7 x 10^{-3} m, we can determine the fluid flow rate necessary to apply a peak shear stress of 0.06 Pa (Figure 3.2). Oscillatory shear stress (sinusoidal waveform; 1Hz peak to peak) was applied to the cells by using syringes (Hamilton, NV; #81020 1710TLL 100uL SYR) connected to the shear chamber with silicone tubing (Instech, PA; #P625/10K.093) to create fluid flow through the chamber.

Minimal shear control experiments were performed by shearing untransfected myocytes at the lowest possible shear setting to ensure that media was refreshed above the cell monolayer, but at flow rates well below reported response shear stress levels (≤ 0.01 Pa). In some experiments, cells were incubated with SB216763 (5 μM) for 24 hours before shearing and throughout the duration of shear to determine if this compound, identified in a previous chemical

screen in a zebrafish model of ARVC,[11] could reverse changes in cell mechanical and mechanotransduction properties caused by expression of mutant plakoglobin.

3.2.6 – Immunofluorescence

NRVM were immunostained based on established protocols.[33] Cells were simultaneously blocked and permeabilized for 45 minutes in 3% normal goat serum, 1% w/v BSA, and 0.15% Triton X-100 in PBS, followed by an overnight incubation at 4°C with either mouse-monoclonal anti-plakoglobin (Sigma; 1:1500 in blocking buffer) or anti-N-cadherin (Sigma; 1:1500) antibodies. Samples were then incubated with secondary antibody (Invitrogen; 1:1500) for 2 hours at room temperature. The immunostained preparations were imaged at 40x (1.3 NA) using an Olympus IX-81 inverted confocal microscope. Each image was subsequently masked to isolate cell junctions, allowing for discrete quantification of junctional immunoreactive signal. Images were analyzed using quantitative confocal microscopy as previously described.[6, 34] Each image was masked to isolate cell junctions, allowing for discrete quantification of junctional immunoreactive signal. Using ImageJ, the same threshold was applied to each image. The fraction of junctional pixels above threshold was calculated by dividing the number of pixels above threshold by the total number of pixels in the image.

3.2.7 – Apoptosis Assay

Terminal deoxynucleotidyl transferase dUTP nick end labeling (TUNEL) assays were performed using an *in situ* cell death detection kit (Roche Diagnostics, Basel, Switzerland) as previously described.[30] Adherent cells were fixed in 4% paraformaldehyde for 1 hour at room temperature, permeabilized with 0.1% Triton X-100 for 2 minutes on ice, and then incubated in

50μL of TUNEL reaction mixture at 37 ºC for one hour in the dark. Samples were analyzed directly using fluorescence microscopy.

3.2.8 – RNA Isolation and Microarray Analysis

Total RNA was isolated from neonatal rat ventricular myocytes using the Qiagen RNeasy Kit according to the manufacturer's recommended protocol. Cells were cultured and transfected to express NX plakoglobin as described in Methods Section 3.2.1. Shear assays were performed 24 hours after adenoviral transfection, using time-matched controls. For SB216763-treated cases, cells were exposed to the drug immediately after transfection. All samples were lysed in parallel using 350 μL of RLT buffer. Lysates were passed through the RNeasy spin columns to capture the RNA. Following two washes with 500 μL of RPE buffer, RNA was eluted in 50 μL of RNase-free water. RNA concentration was measured using a Nanodrop spectrophotometer (Thermo Scientific), and samples were sent to the Yale Center for Genome Analysis for processing using the Affymetrix Rat ST 2.0 gene array.

3.2.9 – Statistical Analysis

Data sets with more than 3 independent groups were analyzed using the non-parametric Kruskal-Wallis analysis of variance (ANOVA) test in Prism. Data showing significance ($p \leq 0.05$) were further analyzed using Dunn's *post hoc* test for multiple comparisons. For data sets involving fewer than 3 independent groups, data were analyzed using the Mann-Whitney test. Differences were considered to be statistically significant and indicated with * when $p \leq 0.05$ or ** when $p \leq 0.01$. Error bars are plotted as the standard deviation of the data.

3.3 – Results

3.3.1 – Expression of ARVC-Causing Mutant Plakoglobin in Cardiac Myocytes

Immunostaining with an antibody against the V5 epitope tag in myocytes transfected to express epitope-tagged wild-type (WT PG), Naxos (2057del2 PG) or S39_K40insS (InsS PG) confirmed the localization of exogenous plakoglobin at cell junctions, and in the case of 2057del2 PG transfected cells, also within the nucleus (Figure 3.3A). Only background levels of signal were seen in non-transfected control cells (Figure 3.3A). Immunostaining with an antibody against an N-terminal epitope in plakoglobin showed a similar pattern of signal distribution (Figure 3.3B). Quantification of immunoblots of transfected cardiac myocyte lysates with an anti-plakoglobin antibody confirmed expression of exogenous plakoglobin at levels comparable to that of the endogenous protein (Figure 3.3C). All lysates contained endogenous plakoglobin, while lysates from WT PG and InsS PG transfected myocytes also showed a second, more slowly migrating band corresponding to the exogenous form of plakoglobin containing the V5 tag. As expected, the 2057del2 PG protein was smaller than the endogenous protein because the Naxos mutation results in a premature stop codon and truncation of the C-terminus. Transfection with a GFP virus confirmed >90 percent viral efficiency, and was used to determine the multiplicity of infection for the WT, InsS and NX viral constructs (Figure 3.3D).

3.3.2 – Cell-Cell Adhesion Strength and Stiffness Unaffected by Mutant Plakoglobin Expression

Dispase assays were used to determine whether expression of mutant desmosomal proteins affected the strength of cell-cell adhesion. Aggregate assays were used to confirm the findings of the dispase assay. As shown in Figure 2A and B, the number of fragments resulting from mechanical agitation of monolayers in the dispase assay (Figure 3.4A) or cell clusters in the

cell aggregate assay (Figure 3.4B) or was not significantly different among the control myocytes and myocytes expressing either mutant form of plakoglobin. As a control experiment to determine if the dispase assay was sensitive enough to detect changes in cell-cell adhesion, control monolayers were exposed to 1 μM cytochalasin-D and then lifted from the culture dish and subjected to rotary agitation. As shown in Figure 3.4C, treatment with cytochalasin-D caused 3.0- and 3.5-fold increases in monolayer fragmentation after 1 and 3 minutes of agitation, respectively, thus providing independent confirmation that the dispase assay sensitively detects changes in cell-cell adhesion strength.

The apparent lack of effect of mutant plakoglobin on adhesion is different than previous studies[5] reporting reduced adhesion in cardiac myocytes following siRNA knockdown of expression of the desmosomal protein plakophilin-2 in which dominant mutations are often found in ARVC patients. To determine whether the effects on cell adhesion are different following knockdown of a desmosomal protein versus expression of a disease-causing mutation, we treated non-transfected myocytes with two different specific siRNAs against plakoglobin. As shown in Figure 3.4D, treated cells exhibited a marked reduction in plakoglobin expression. Both siRNAs led to between 2.0- and 2.7-fold increases in monolayer fragmentation relative to time-matched controls after 1 or 3 minutes of agitation, whereas treatment with a negative siRNA had no effect on cell-cell adhesion. Knockdown efficiency was quantified by western blot. TUNEL assays were used to exclude reduced cell viability as a possible cause of increased sheet fragmentation (3.4E). Suppression of N-cadherin showed a similar reduction in cell-cell adhesion strength, suggesting this effect is not limited to the suppression of desmosomal proteins, but other adhesion proteins as well (Figure 3.4F). Taken together, these results indicate that expression of exogenous plakoglobin at levels comparable to that of the endogenous protein

does not significantly affect cell-cell adhesion strength, whereas knockdown of the endogenous protein has a marked effect in reducing adhesion.

3.3.3 – Shear Stress Induces Junctional Plakoglobin and N-Cadherin Remodeling

A custom oscillatory shear device and parallel plate flow chamber were used to shear control and transfected myocytes. In response to oscillatory fluid shear at 0.06 Pa, control and WT PG transfected myocytes exhibited between 2.3 and 3.3-fold increases in immunoreactive signal for junctional plakoglobin (Figure 3.5A and B) compared to unsheared cells. In contrast, myocytes expressing the 2057del2 PG or InsS PG mutants failed to increase junctional plakoglobin signal following shear. A considerable amount of the plakoglobin in myocytes expressing the 2057del2 PG mutation was distributed within cells in a distinct perinuclear pattern, but there was little if any change in either the amount or distribution of plakoglobin signal in response to shear. To determine whether SB216763 could restore the control-level response to shear in cells expressing mutant plakoglobin, we repeated experiments in cultures exposed to 5 μM SB216763 for 24 hours. As shown in Figures 3.5C, cells expressing either InsS PG, 2057del2 PG, or 1851del123 PKP exhibited robust increases in junctional signal for plakoglobin in response to oscillatory shear equivalent to the response in control cells and cells expressing wild-type proteins (2.0-, 2.2-, and 2.6-fold increases in 2057del2 PG, InsS PG and 1851del123 PKP cells, respectively). Neither shear stimulation nor treatment with SB216763 altered the overall expression of plakoglobin in WT and Naxos cells (Figure 3.5D). Thus, failure to increase junctional signal for plakoglobin in response to shear can be normalized by SB216763 in cells expressing mutant plakoglobin without alter plakoglobin expression levels.

Control and WT PG cells also showed 2- and 1.6-fold increases in junctional signal for N-cadherin, respectively, following oscillatory shear (Figure 3.6A-B). In contrast, cells expressing either mutant form of plakoglobin failed to increase junctional N-cadherin signal in response to shear (Figure 3.6A-B). As was seen for plakoglobin, SB216763 restored the ability of cells expressing mutant plakoglobin to increase junctional N-cadherin signal in response to shear (Figure 3.6C; 1.9- and 1.7-fold increases in 2057del2 PG and InsS PG cells, respectively, compared with 1.6- and 2.1-fold increases in control and WT PG cells).

In view of the increased signals for junctional plakoglobin and N-cadherin in control and WT PG cells following shear, we repeated studies of cell mechanical properties to determine if there was a correlation between the amount of junctional protein signals and measures of cell-cell adhesion strength. As shown in Figure 3.6D, there was no significant change in cell-cell adhesion strength following shear in control myocytes or myocytes expressing mutant plakoglobin. Thus, within the limits of these assays, there appears to be no apparent relationship between the amount of junctional immunoreactive signals for plakoglobin or N-cadherin and cell-cell adhesion.

We next used AFM to measure cell stiffness.[35] Whereas our previous studies have shown a change in cell stiffness in HEK epithelial cells expressing the InsS PG (but not the 2057del2 PG) mutation in plakoglobin,[6] we found no such change in stiffness in cardiac myocytes expressing either mutant form of plakoglobin (Figure 3.6E).

3.3.4 – Shear Stress Causes Disparate Changes in Apoptosis Without Altering ERK Phosphorylation

Apoptosis is increased in the myocardium of patients with ARVC,[36] and myocytes expressing the 2057del2 PG mutant form of plakoglobin exhibit increased apoptosis rates under basal condition with even greater apoptosis in response to cyclical stretch.[11] To determine if a similar response occurs in oscillatory shear, we measured apoptosis by TUNEL assays. As shown in Figure 3.7A, myocytes expressing 2057del2 PG showed elevated levels of apoptosis in response to shear stress, relative to unsheared cells. In contrast, myocytes expressing the InsS PG variant of plakoglobin exhibited no changes in apoptosis with exposure to oscillatory shear, although the mean level of apoptosis was elevated relative to control cells. Treatment with SB216763 returned apoptosis levels to control levels in myocytes expressing 2057del2 PG (Figure 3.7B).

We next assessed whether ERK phosphorylation may be disrupted by ARVC mutant plakoglobin. Immunoblotting performed on myocytes exposed to oscillatory shear flow confirmed an increase in the amount of phosphorylated ERK (p-ERK) in response to shear for control and WT PG myocytes, as well as cells expressing mutant forms of plakoglobin (Figure 3.7C). After 10 minutes, control, WT PG, 2057del2 PG and insS PG transfected myocytes exposed to oscillatory shear exhibited 3.3-, 3.2-, 4.2-, and 3.5-fold increases in p-ERK relative to unsheared controls, respectively.

3.3.5 – SB216763, But Not GSK3 Knockdown, Rescues Wild-Type Phenotype

Treatment with SB216763 was able to recover the wild-type phenotype in cells expressing ARVC-causing mutant plakoglobin. SB216763 selectively inhibits glycogen synthase kinase-3 (GSK3) by competitively binding to the GSK3 ATP-binding site, and it has been shown to have protective effects in a variety of cell types.[11, 37-40] To determine if GSK3 inhibition was the mechanism by which cells expressing mutant plakoglobin recovered the wild-type

phenotype, we treated WT, InsS and NX transfected myocytes with a specific siRNA against GSK3, and exposed the cells to shear stress. SiRNA-mediated suppression of GSK3 did not recapitulate the effects of SB216763 treatment. Junctional remodeling was unaffected in WT cells, exhibiting 2.7- and 2.0-fold increases in junctional plakoglobin signal is response to shear stress relative to unsheared controls following treatment with non-targeting or GSK3 siRNA, respectively (Figure 3.8A-B). InsS and NX cells did not recover the ability to remodel cell junctions following GSK3 siRNA treatment (Figure 3.8B).

While the reported function of SB216763 is to selectively inhibit GSK3, suppression of GSK3 does not mimic the effects of SB216763, suggesting the compound has a secondary function. To gain further insight into the mechanism by which SB216763 is able to restore the wild-type phenotype in cells expressing mutant plakoglobin, we performed microarray analysis on NX cells treated with SB216763 and exposed to shear stress (Figure 3.8C). Microarray analysis revealed >100 genes that were differentially expressed. Immunoblotting for certain gene targets identified in the microarray analysis was performed on WT and NX cells. Targets were selected based on the level of differential expression (greater than 2-fold increase and $p < 0.05$), and their role in regulating cytoskeletal or junctional protein distribution. As shown in Figure 3.8D, neither gene product showed significant differences in expression levels between WT and NX cells with SB216763 treatment, although immunoblotting results from NX cells did confirm the microarray results.

3.4 – Discussion

In the broader scope of this thesis, the work in this chapter was meant to assess changes in the mechanical and signaling properties of cardiac myocytes expressing ARVC-causing

mutant plakoglobin. The key observation from the data presented is that expression of ARVC-linked mutant plakoglobin in ventricular myocytes in amounts roughly equivalent to that of the native protein, has no apparent effect on cell mechanical properties *per se* (no change in cell stiffness or cell-cell adhesion strength) but instead has a marked effect on how cells respond to mechanical stimulation. This is an important distinction that has significant implications about how mutations in desmosomal proteins cause the complex disease phenotypes seen in patients with ARVC. It is widely believed that defective intercellular adhesion plays an important pathogenic role in ARVC patients with desmosomal mutations, but direct evidence for this hypothesis has been lacking. It has been previously reported that knockdown of desmosomal proteins can result in a dramatic decrease in cell-cell adhesion strength.[5] To reconcile the apparent discrepancy between this observation and the present study, we used two separate siRNAs targeting different regions to knock down expression of plakoglobin, and in both cases observed a similar marked decrease in cell-cell adhesion strength. This highlights important differences in the pathophysiological consequences of suppression of a desmosomal protein versus expression of a mutant form of a desmosomal protein. In this regard, it appears that mutant desmosomal proteins are expressed in the myocardium of patients with ARVC. This is certainly true in Naxos disease which, although inherited as a recessive trait, is not related to loss of gene expression but rather to expression of mutant plakoglobin with a gene-dosage effect. Indeed, germline deletions of plakoglobin, desmoplakin and plakophilin all cause embryonic lethal phenotypes in mice,[41-44] providing further evidence that ARVC is related to expression of mutant proteins rather than haploinsufficiency. While it should not be surprising that knockdown of a desmosomal gene leads to loss of cell-cell adhesion, our results show that

expression of a mutant desmosomal gene has a different effect which is more likely to reflect the pathophysiology of the disease in patients.

Another interesting related observation from our study is the apparent lack of correlation between the amount of immunoreactive signal for plakoglobin at cell-cell junctions and the strength of cell-cell adhesion. While there is likely a positive correlation between desmosome number and immunoreactive signal intensity, many factors (i.e. - variations in antibody binding specificity, macromolecular crowding, and epitope accessibility) can make the exact relationship difficult to determine. Our data are consistent with the idea that redistribution of plakoglobin from junctional to intracellular/intranuclear sites, a feature seen in both patients and experimental models of ARVC, has no major effect on cell-cell adhesion strength but rather leads to abnormal responses to mechanical stimuli that appear to be a fundamental part of the disease pathway in ARVC. Finally, we have previously reported that when HEK cells overexpress the 2057del2 PG mutation, there is a marked reduction in cell-cell adhesion strength without a change in cell stiffness, whereas overexpression of the InsS PG mutation in HEK cells has the opposite effects. The discrepancy between previous results and those presented in this study may result from differences in cell type, and the disparate roles of desmosomes in cardiac myocytes and HEK cells. It is possible that the robust actin-myosin network present in cardiac myocytes, but not in HEK cells, may mask any minor alterations in cell stiffness that result from the expression of mutant desmosomal proteins. The results of the present study reinforce the important idea that epithelial cells are not necessarily good surrogates for cardiac myocytes, and changes in HEK cells expressing cardiomyopathy-related disease mutations must be interpreted with caution.

The lack of differences in cell-cell adhesion between control and myocytes expressing mutant plakoglobin motivated our search for a molecular mechanism underlying the

pathogenesis of ARVC. Thus, we chose to investigate (1) ERK phosphorylation, a documented promoter of myocyte hypertrophy *in vitro* and *in vivo*,[16, 45, 46] and (2) apoptosis. While ERK phosphorylation (before and after shear) remained unaffected by the expression of ARVC-causing mutant plakoglobin, apoptosis was elevated in myocytes expressing 2057del2 PG. Cardiac myocytes have been shown to undergo hypertrophy as a response increased mechanical loading in order to restore wall stresses to normal levels.[47-49] Cell-cell adhesion defects are often associated with ARVC-pathogenesis, so it was surprising that ERK phosphorylation, the short-term response to stimuli, was unaltered in cells expressing ARVC-causing mutant proteins. We expect that defects in cell-cell adhesion would alter the stress/strain balance on the myocardium, with cardiac myocytes responding by undergoing sustained hypertrophy (to compensate for decreased force generation). Our findings support the hypothesis that apoptosis, and not cell-cell adhesion, likely play a more significant role in ARVC pathogenesis. Noting the nuclear localization of plakoglobin in these cells, elevated levels of apoptosis is consistent with work by Garcia-Gras *et al* that suggests nuclear localization of plakoglobin can recapitulate the ARVC phenotype (i.e. – adipogenesis, fibrogenesis, and myocyte apoptosis).[50]

Treatment of myocytes expressing mutant plakoglobin with SB216763 attenuated apoptosis back to control levels in myocytes expressing the 2057del2 PG and InsS PG mutations. Furthermore, SB216763 treatment recovered junctional remodeling of plakoglobin and N-cadherin in cells expressing 2057del2 PG, InsS PG mutant proteins. The fact that SB216763 was able to alter the subcellular distribution of plakoglobin without changing the level at which the protein is expressed further supports the hypothesis SB216763 corrects underlying defects in protein trafficking.[11] Attenuation of apoptosis may be explained by a decrease in the suppression

of canonical wnt/beta-catenin signaling by nuclear plakoglobin, as evidenced by the loss of the nuclear localization of plakoglobin.

SiRNA-mediated suppression of GSK3 in myocytes expressing ARVC-causing mutant proteins did not recover the wild-type ability to increase junctional plakoglobin signal in response to shear stress. Although SB216763 is a well-documented inhibitor of GSK3,[25-28] these data suggest that additional mechanisms may be involved in the recovery of the wild-type phenotype in InsS and NX cells. The inability for GSK3 suppression to recapitulate the wild-type phenotype motivated our search for a molecular mechanism. Interestingly, treatment with SB2, exposure to shear stress, and a combination of both treatments all caused a number of genes to be differentially expressed in NX cells. We identified two key differentially expressed genes associated with cytoskeletal remodeling (Rnd1) and protein transport (Isg15), and performed immunoblotting to determine if the expression of these genes was altered in NX cells, relative to WT cells. Although no significant differences in Rnd1 or Isg15 expression were observed between NX and WT cells following treatment with SB216763, the microarray analysis did identify several other interesting targets (associated with Rho GTPase signaling, protein shuttling, and cytoskeletal remodeling). Further investigation is necessary to elucidate the exact mechanism by which SB216763 restores the wild-type phenotype.

We conclude that ARVC-causing mutations in plakoglobin lead to altered cellular distribution of plakoglobin and N-cadherin, as well as increased apoptosis in NX cells, without alterations in cell mechanical properties or certain early signaling pathways.

3.5 – Figures

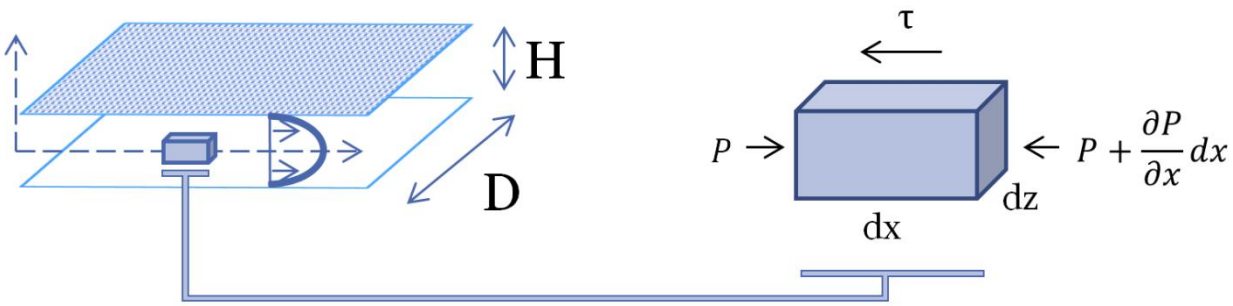

Figure 3.1 – Diagram of shear flow device and force balance: (Left) Diagram showing the dimensions of the shear flow chamber, where 'H' represents the vertical distance between the two parallel plates and 'D' represents the depth of the chamber normal to the direction of flow. (Right) Force balance on an incremental block of fluid used to derive the relationship between shear stress, parallel plate chamber dimensions, and fluid flow rate.

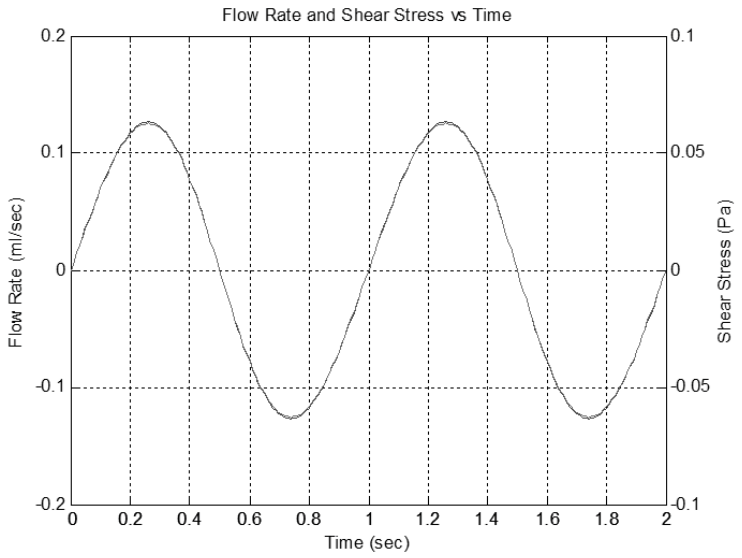

Figure 3.2 – Media flow rate is directly proportional to applied shear stress: As derived in section 3.2.5, the derived expression to calculate applied shear stress is directly proportional to the flow rate of media through the shear chamber. As determined above using Matlab, to achieve a physiologically relevant shear stress level of 0.06 pascals, we flow media in the chamber at a rate of 0.12 mL/sec.

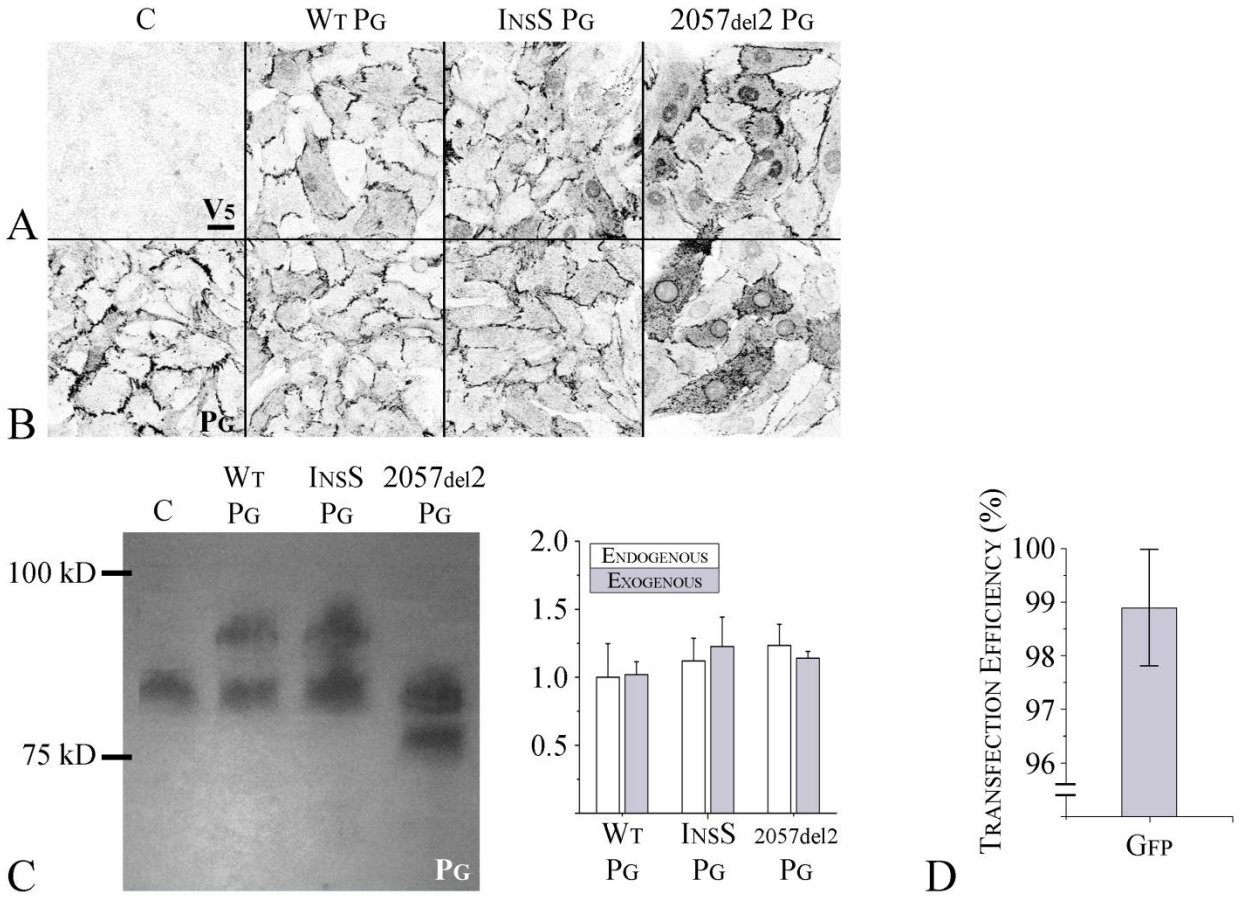

Figure 3.3 – ARVC models express transgenic plakoglobin at endogenous levels: **(A)** V5 immunostaining of control (non-transfected) myocytes (C) and myocytes transfected to express wild-type plakoglobin (WT PG), S39_K40insS (InsS PG), or 2057del2 PG. No signal is seen in non-transfected control cells (thus demonstrating absence of non-specific binding). Normal junctional localization of V5 labeled protein is seen in cells transfected to express WT PG, InsS PG and 2057del2 PG mutants. Cells transfected with 2057del2 PG also show nuclear localization of truncated 2057del2 plakoglobin. **(B)** Immunostaining with an anti-plakoglobin antibody against an N-terminal epitope (which recognizes both endogenous and transfected forms of WT PG, InsS PG and 2057del2 PG) shows a similar pattern. **(C)** Immunoblot (left) using an N-terminal anti-plakoglobin antibody, with quantification (right) showing roughly

equivalent amounts of endogenous plakoglobin and transgene plakoglobin in WT PG, InsS PG and 2057del2 PG cells (n=4). While the control lane shows a single band corresponding to endogenous plakoglobin, the WT PG, InsS PG, and 2057del2 PG lanes exhibit a second band, corresponding to the transgenic plakoglobin. The larger molecular weight of transgenic plakoglobin observed in the WT PG and InsS PG lanes is explained by the addition of a C-terminal V5 tag, connected using a linker peptide. The lower molecular weight transgenic plakoglobin band observed in the 2057del2 PG lane is explained by the truncation of the C-terminal end of plakoglobin – a result of the premature stop codon generated by the frame-shift 2057del2 mutation. **(D)** Quantification of cells transfected with a GFP virus to confirm 98.9 ± 1.1% transfection efficiency (n=5). Scale bars = 20 μm.

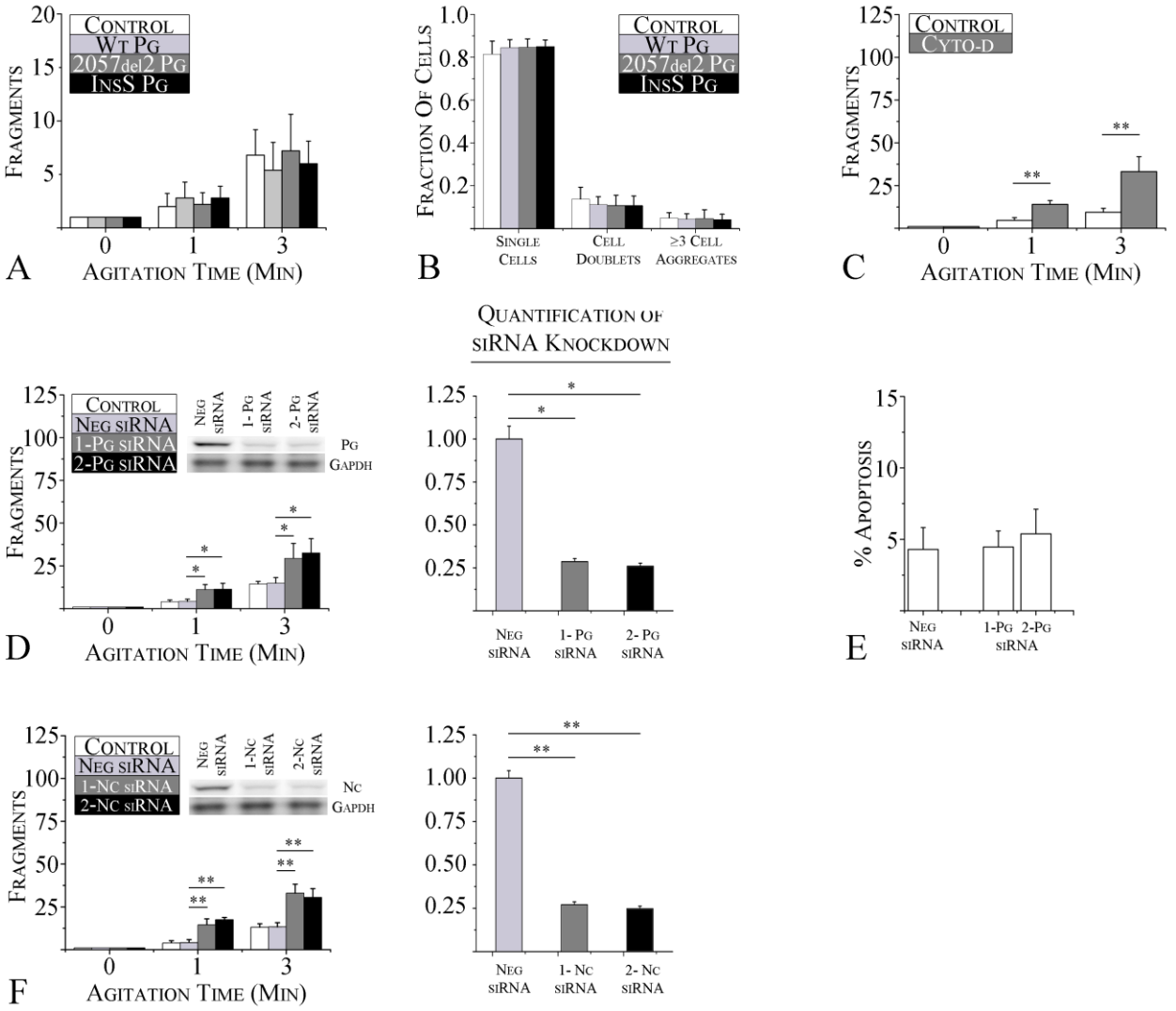

Figure 3.4 - Cell-cell adhesion strength and cell stiffness are unaffected by mutant plakoglobin: **(A)** Quantification of control and mutant plakoglobin-transfected cardiac myocyte monolayer fragmentation in dispase assays before and after 1 or 3 minutes of agitation. Cardiac myocytes expressing mutant plakoglobin show no differences in cell-cell adhesion relative to WT PG (n=5). **(B)** Quantification of cluster sizes in control and transfected cardiac myocytes in cell aggregate assays (n=3). Cardiac myocyte aggregates expressing mutant plakoglobin show no differences in aggregate fragmentation relative to WT PG. **(C)** Dispase assays in normal (non-transfected) cardiac myocytes showing significant reduction in cell-cell adhesion in cells

exposed to 1uM cytochalasin-D (n=5). **(D)** Dispase assays in normal (non-transfected) cardiac myocytes showing significant reduction in cell-cell adhesion in cells following siRNA knock-down of endogenous plakoglobin (n=5). Plakoglobin knock-down was confirmed by immunoblotting (inset), and quantified (right). **(E)** Quantification of apoptosis (percent TUNEL-positive nuclei) in control (C) cells transfected with non-targeting siRNA, or siRNA targeting plakoglobin (n=6). Mechanical shear caused cells to shear off the glass slide, preventing quantification. **(F)** Dispase assays in normal (non-transfected) cardiac myocytes showing significant reduction in cell-cell adhesion in cells following siRNA knock-down of endogenous N-cadherin (Nc) (n=6). N-cadherin knock-down was confirmed by immunoblotting (inset), and quantified (right). *$p < 0.05$; **$p < 0.01$

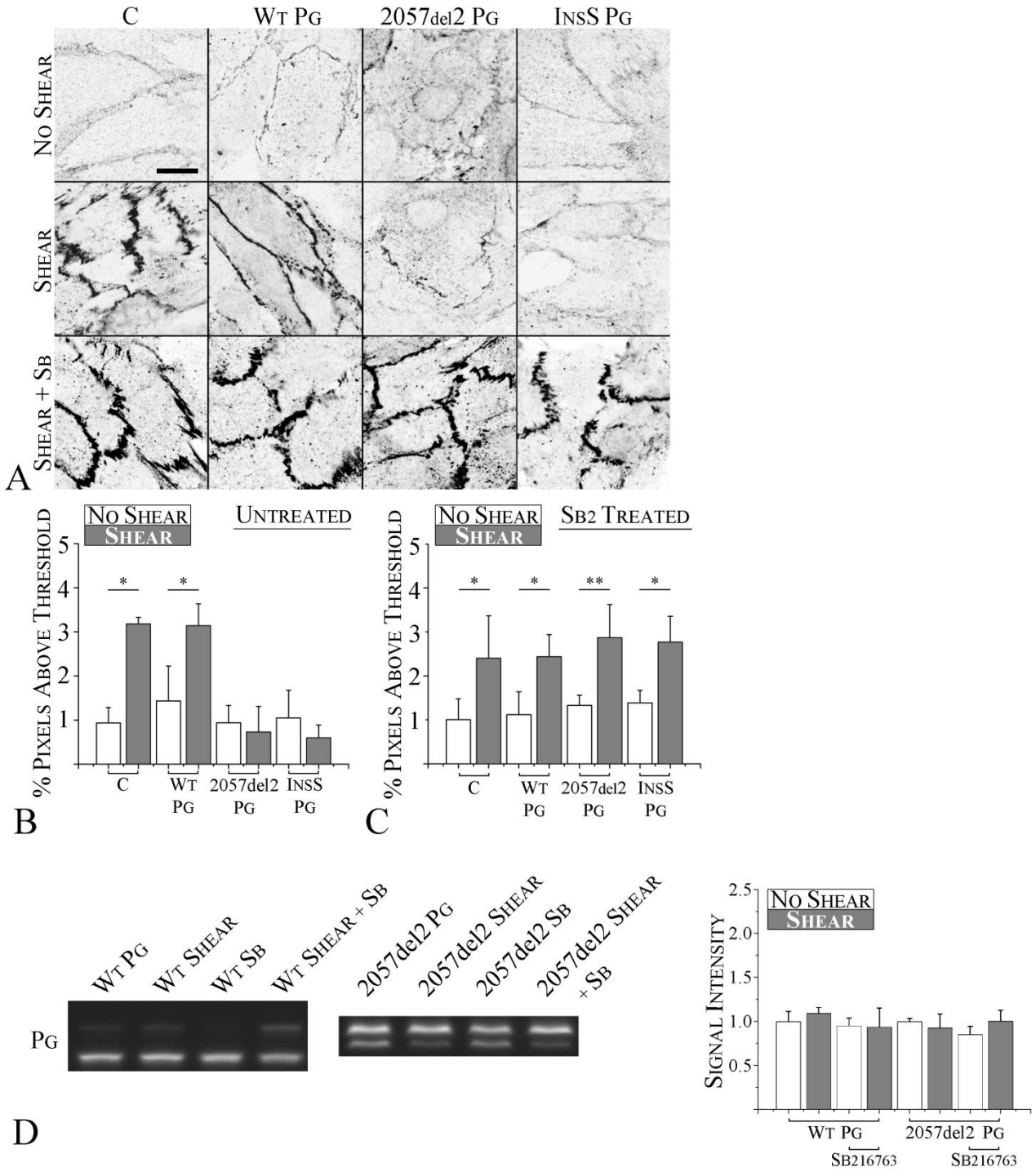

Figure 3.5 – Shear-induced plakoglobin remodeling is reversibly altered in ARVC: **(A)** Immuno-fluorescence images showing the distribution of plakoglobin (N-terminal antibody) in control (C) and transfected cardiac myocytes before (top) and after (middle) exposure to shear, and after

treatment with SB216763 (SB2; bottom). Control and WT PG cells show increased immunoreactive signal with junctional localization after shear, whereas cells expressing InsS PG or 2057del2 PG show no apparent increase in junctional signal after shear. Treatment with the drug restored the normal shear-induced increase in junctional signal in cells expressing mutant plakoglobin or plakophilin. **(B)** Quantification of junctional plakoglobin signal before and after shear in cells transfected to express mutant plakoglobin (n=5). **(C)** Quantification of junctional plakoglobin signal before and after shear in cells transfected to express mutant plakoglobin and treated with SB216763 (n=6). **(D)** Immunoblot (left and middle) and quantification of immunoblots (right) using a N-terminal anti-plakoglobin antibody showing no overt changes in plakoglobin levels in cells expressing WT or 2057del2 PG (n=5) in response to shear or treatment with SB216763. Scale bars = 20 μm. *$p < 0.05$; ** $p < 0.01$

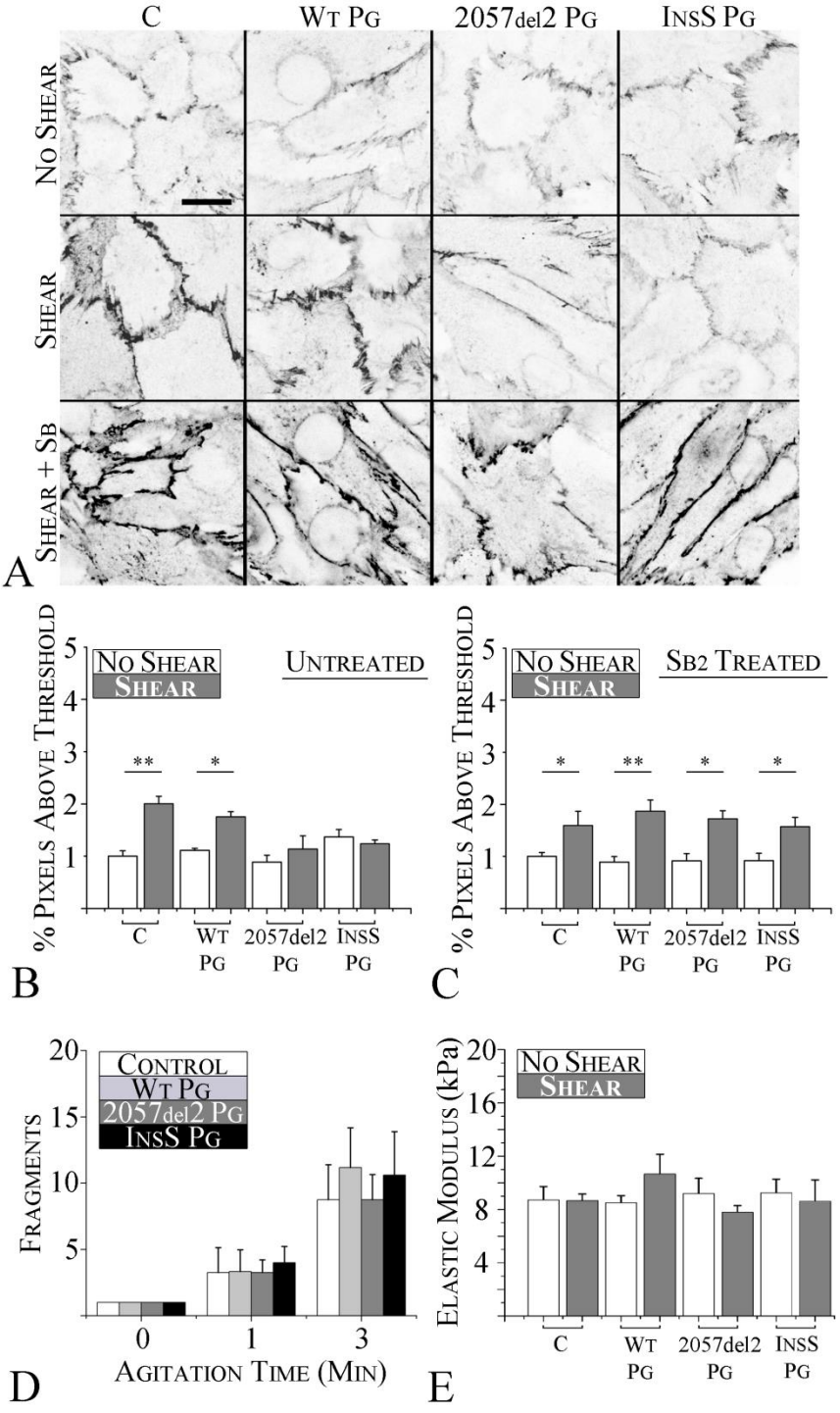

Figure 3.6 - Shear-induced N-cadherin remodeling is reversibly altered in ARVC: **(A)** N-cadherin immunofluorescence images showing the distribution of N-cadherin in control (C) and transfected cardiac myocytes before (top) and after (middle) exposure to shear, and after

treatment with SB216763 (bottom). As seen in Figure 3, control (non-transfected) cells and cells transfected to express wild-type plakoglobin (WT PG) show increased junctional signal for N-cadherin after shear, whereas no shear-induced increase was seen in cells expressing mutant forms of plakoglobin. Treatment with the drug restored the normal shear-induced increase in junctional signal in cells expressing mutant plakoglobin. **(B)** Quantification of junctional N-cadherin signal before and after shear (n=5). **(C)** Quantification of junctional N-cadherin signal before and after shear in cardiac myocytes treated with SB216763 (n=5). SB216763 restored the normal shear-induced increase in junctional N-cadherin signal. **(D)** Dispase assay measurements in control cells (C) and cells expressing transgenic plakoglobin after exposure to mechanical shear stress (n=5). Cardiac myocytes expressing mutant plakoglobin show no differences in cell-cell adhesion as compared to control cells. **(E)** Cell stiffness measurements in control cells (C) and cells expressing wild type or mutant plakoglobin before and after exposure to mechanical shear stress (n=4). Cardiac myocytes expressing mutant plakoglobin show no differences in cell stiffness compared to control cells. *$p<0.05$; **$p<0.01$

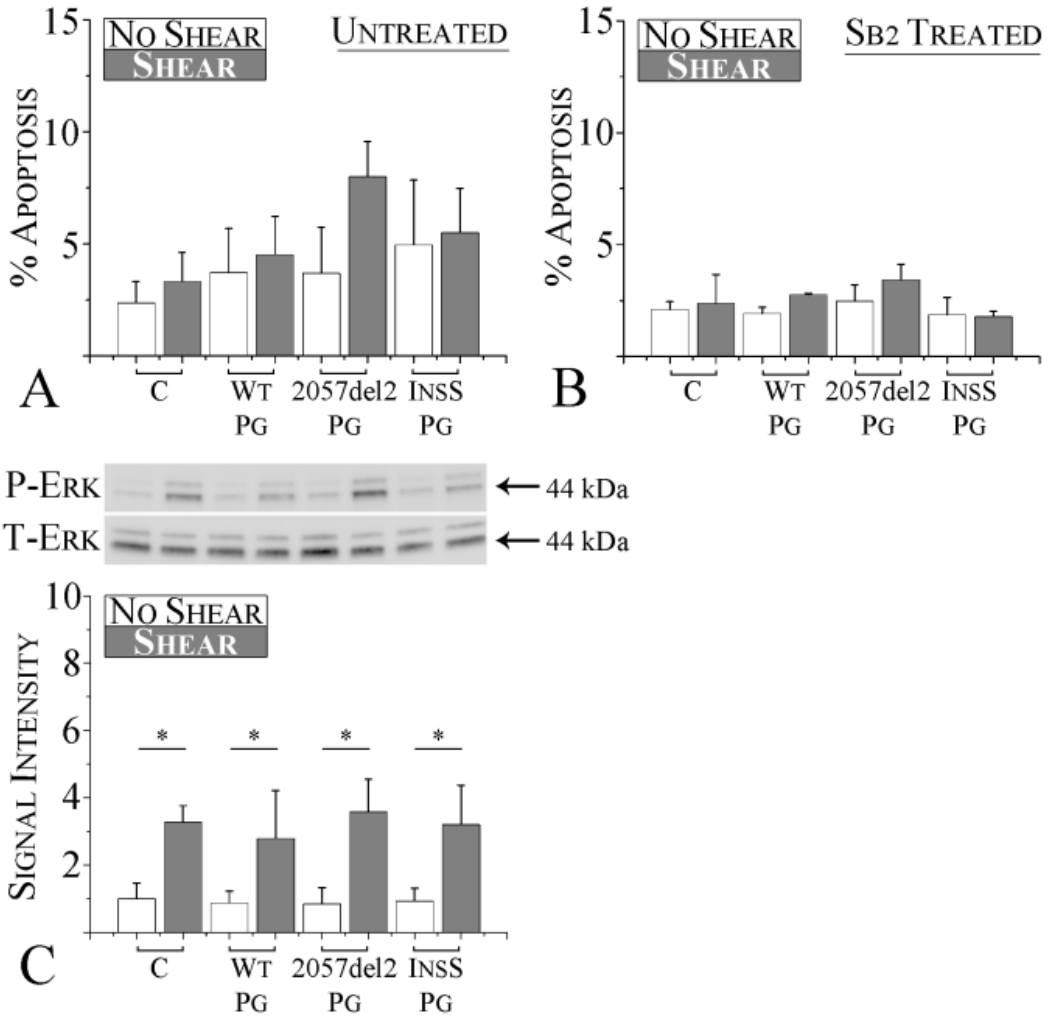

Figure 3.7 - Cell viability, but not ERK phosphorylation, is altered by mutant plakoglobin expression: **(A)** Quantification of apoptosis (percent TUNEL-positive nuclei) in control (C) cells and cells transfected to express wild-type or mutant forms of plakoglobin before and after exposure to shear (n=4). Mechanical shear stress caused an increase in apoptosis in cells expressing 2057del2 PG. **(B)** Quantification of apoptosis (percent TUNEL-positive nuclei) in cells treated with SB216763 (SB2) before and after shear (n=3). SB216763 prevented the shear-induced increase in apoptosis in cells expressing 2057del2 PG. **(C)** Representative immunoblot and quantitative data showing equivalent levels of phospho-ERK activation (P-ERK), with total

ERK (T-ERK) as a loading control, in control cells (C) or cells transfected to express wild-type or mutant forms of plakoglobin (n=3). *$p<0.05$

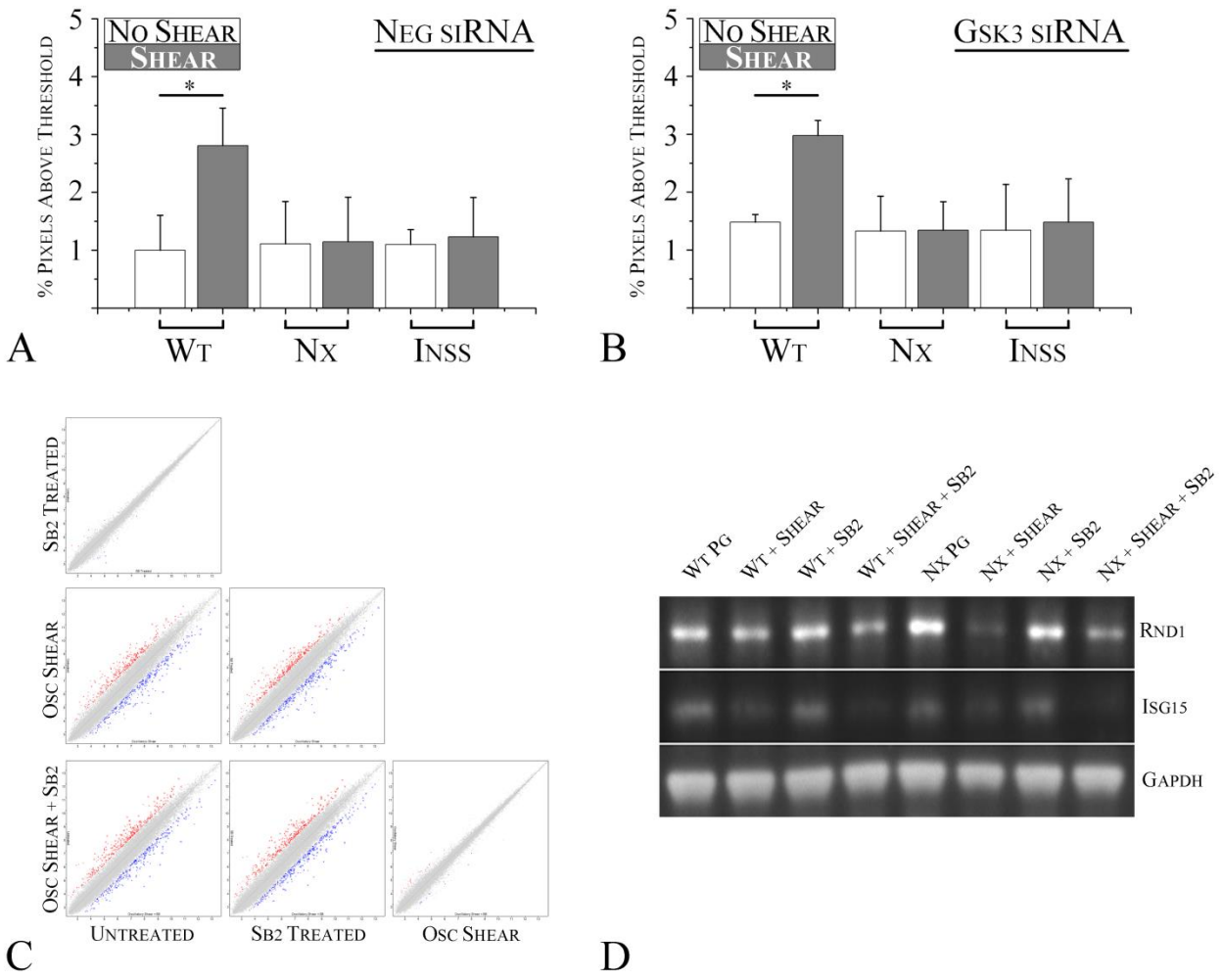

Figure 3.8 - GSK3 Suppression Does Not Mimic the Effects of SB216763: **(A-B)** Quantification of junctional plakoglobin signal before and after shear in cells treated with **(A)** non-targeting (n=3) or **(B)** GSK3 siRNA (n=3). Knockdown of GSK3 did not restore the normal shear-induced increase in junctional signal in cells expressing InsS or NX plakoglobin. **(C)** Scatter plots from microarray data analysis showing differential gene expression when comparing NX cells exposed to shear stress, treated with SB216763, or both (n=3). **(D)** Immunoblots using anti-Rnd1 (top), anti-Isg15 (middle) or anti-GAPDH (bottom) antibodies in WT and NX cells exposed to shear stress, treated with SB216763, or both. Isg15 and Rnd1 were targets identified using microarray analysis. *p< 0.05

3.6 - Appendix

Shear Flow Device and Shear Chamber:

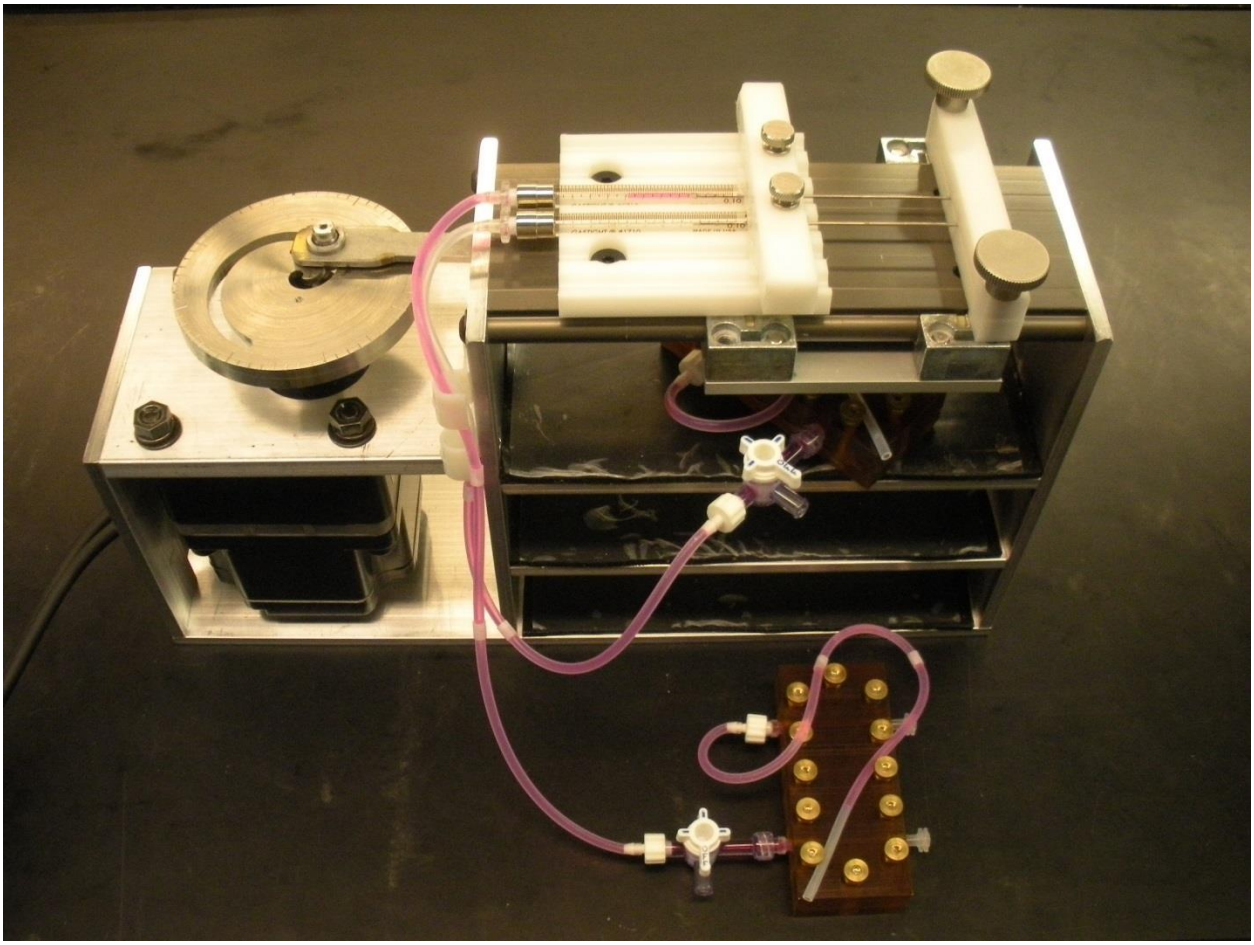

Machine Drawing for Shear Chamber:

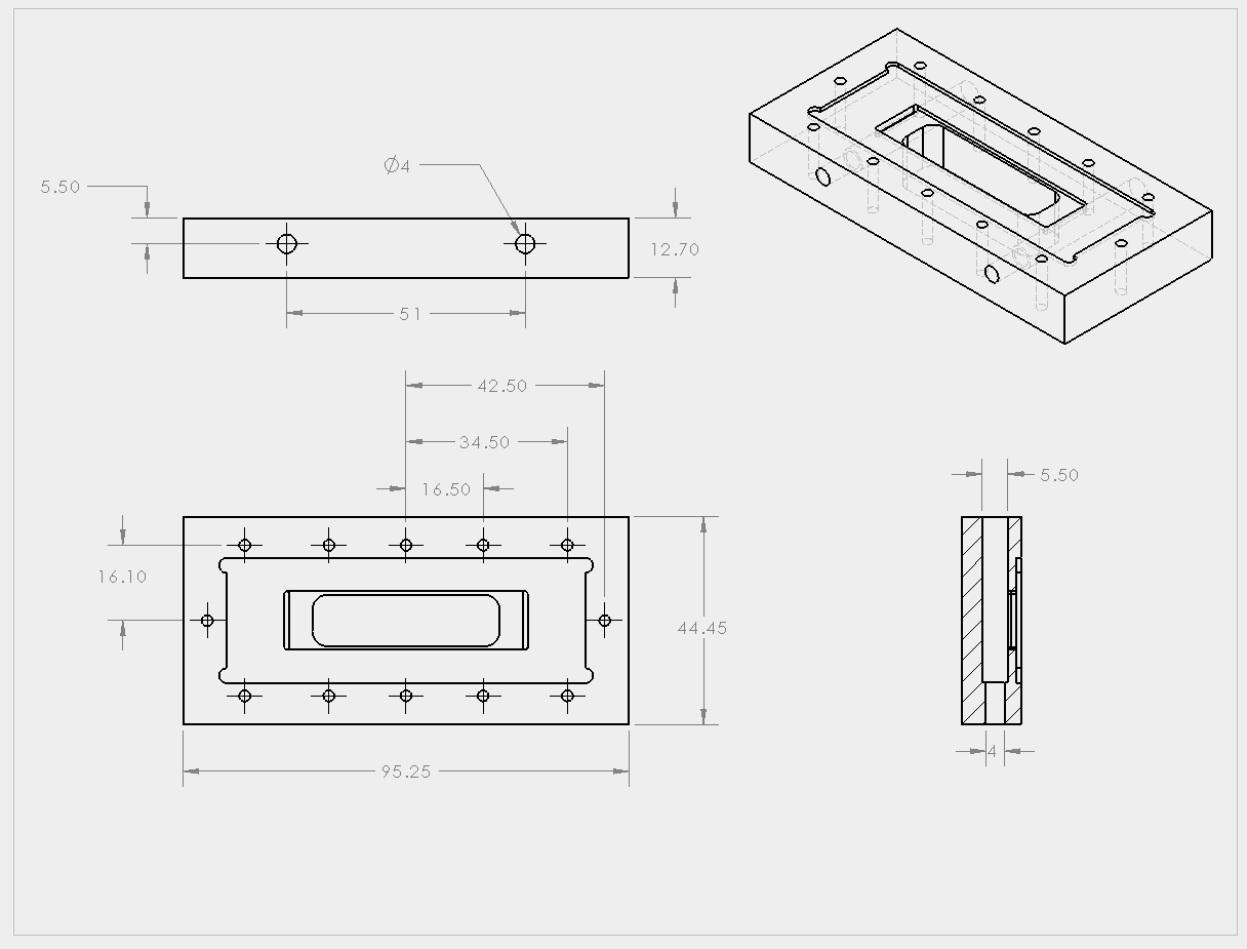

3.7 – References

1. Sen-Chowdhry S, Syrris P, McKenna WJ. Role of genetic analysis in the management of patients with arrhythmogenic right ventricular ysplasia/ardiomyopathy. *J Am Coll Cardiol*. 2007;50:1813-1821
2. Basso C, Czarnowska E, Della Barbera M, Bauce B, Beffagna G, Wlodarska EK, Pilichou K, Ramondo A, Lorenzon A, Wozniek O, Corrado D, Datiento L, Danieli GA, Valente M, Nava A, Thiene G, Rampazzo A. Ultrastructural evidence of intercalated disc remodelling in arrhythmogenic right ventricular cardiomyopathy: An electron microscopy investigation on endomyocardial biopsies. *Eur Heart J*. 2006;27:1847-1854
3. Fujita S, Terasaki F, Otsuka K, Katashima T, Kanzaki Y, Kawamura K, Tanaka T, Kitaura Y. Markedly increased intracellular lipid droplets and disruption of intercellular junctions in biopsied myocardium from a patient with arrhythmogenic right ventricular cardiomyopathy. *Heart Vessels*. 2008;23:440-444
4. Rizzo S, Lodder EM, Verkerk AO, Wolswinkel R, Beekman L, Pilichou K, Basso C, Remme CA, Thiene G, Bezzina CR. Intercalated disc abnormalities, reduced na+ current density, and conduction slowing in desmoglein-2 mutant mice prior to cardiomyopathic changes. *Cardiovasc Res*. 2012;95:409-418
5. Sato PY, Coombs W, Lin XM, Nekrasova O, Green KJ, Isom LL, Taffet SM, Delmar M. Interactions between ankyrin-g, plakophilin-2, and connexin43 at the cardiac intercalated disc. *Circ Res*. 2011;109:193-U160
6. Huang H, Asimaki A, Lo D, McKenna W, Saffitz J. Disparate effects of different mutations in plakoglobin on cell mechanical behavior. *Cell Motil Cytoskel*. 2008;65:964-978

7. Corrado D, Basso C, Pavei A, Michieli P, Schiavon M, Thiene G. Trends in sudden cardiovascular death in young competitive athletes after implementation of a preparticipation screening program. *Jama-J Am Med Assoc*. 2006;296:1593-1601

8. Hariharan V, Provost J, Shah S, Konofagou E, Huang H. Elevated strain and structural disarray occur at the right ventricular apex. *Cardiovascular Engineering and Technology*. 2012;3:52-61

9. Komuro I, Kudo S, Yamazaki T, Zou YZ, Shiojima I, Yazaki Y. Mechanical stretch activates the stress-activated protein kinases in cardiac myocytes. *Faseb J*. 1996;10:631-636

10. Kijima K, Matsubara H, Murasawa S, Maruyama K, Mori Y, Ohkubo N, Komuro I, Yazaki Y, Iwasaka T, Inada M. Mechanical stretch induces enhanced expression of angiotensin ii receptor subtypes in neonatal rat cardiac myocytes. *Circ Res*. 1996;79:887-897

11. Asimaki A, Kapoor S, Plovie E, Arndt AK, Adams E, Liu Z, James CA, Judge DP, Calkins H, Churko J, Wu JC, MacRae CA, Kleber AG, Saffitz JE. Identification of a new modulator of the intercalated disc in a zebrafish model of arrhythmogenic cardiomyopathy. *Science Translational Medicine*. 2014;6:240ra274

12. Caulfield JB, Borg TK. Collagen network of the heart. *Lab Invest*. 1979;40:364-372

13. Dou JG, Tseng WYI, Reese TG, Wedeen VJ. Combined diffusion and strain mri reveals structure and function of human myocardial laminar sheets in vivo. *Magnet Reson Med*. 2003;50:107-113

14. Legrice IJ, Takayama Y, Covell JW. Transverse-shear along myocardial cleavage planes provides a mechanism for normal systolic wall thickening. *Circ Res*. 1995;77:182-193

15. Costa KD, Takayama Y, McCulloch AD, Covell JW. Laminar fiber architecture and three-dimensional systolic mechanics in canine ventricular myocardium. *Am J Physiol-Heart C*. 1999;276:H595-H607

16. Dvir T, Levy O, Shachar M, Granot Y, Cohen S. Activation of the erk1/2 cascade via pulsatile interstitial fluid flow promotes cardiac tissue assembly. *Tissue Eng*. 2007;13:2185-2193

17. Lorenzen-Schmidt I, Schmid-Schonbein GW, Giles WR, McCulloch AD, Chien S, Omens JH. Chronotropic response of cultured neonatal rat ventricular myocytes to short term fluid shear. *Cell Biochem Biophys*. 2006;46:113-122

18. Deng LH, Trepat X, Butler JP, Millet E, Morgan KG, Weitz DA, Fredberg JJ. Fast and slow dynamics of the cytoskeleton. *Nat Mater*. 2006;5:636-640

19. Hochmuth RM. Micropipette aspiration of living cells. *J Biomech*. 2000;33:15-22

20. Levental I, Levental KR, Klein EA, Assoian R, Miller RT, Wells RG, Janmey PA. A simple indentation device for measuring micrometer-scale tissue stiffness. *J Phys-Condens Mat*. 2010;22

21. Mahaffy RE, Park S, Gerde E, Kas J, Shih CK. Quantitative analysis of the viscoelastic properties of thin regions of fibroblasts using atomic force microscopy. *Biophys J*. 2004;86:1777-1793

22. Radmacher M. Measuring the elastic properties of biological samples with the afm. *Ieee Eng Med Biol*. 1997;16:47-57

23. Yang Z, Bowles NE, Scherer SE, Taylor MD, Kearney DL, Ge SP, Nadvoretskiy VV, DeFreitas G, Carabello B, Brandon LI, Godsel LM, Green KJ, Saffitz JE, Li H, Danieli GA, Calkins H, Marcus F, Towbin JA. Desmosomal dysfunction due to mutations in

desmoplakin causes arrhythmogenic right ventricular dysplasia/cardiomyopathy. *Circ Res*. 2006;99:646-655

24. Li J, Swope D, Raess N, Cheng L, Muller EJ, Radice GL. Cardiac tissue-restricted deletion of plakoglobin results in progressive cardiomyopathy and activation of {beta}-catenin signaling. *Mol Cell Biol*. 2011;31:1134-1144

25. Eldar-Finkelman H, Martinez A. Gsk-3 inhibitors: Preclinical and clinical focus on cns. *Frontiers in Molecular Neuroscience*. 2011;4:1-18

26. Coghlan MP, Culbert AA, Cross DAE, Corcoran SL, Yates JW, Pearce NJ, Rausch OL, Murphy GJ, Carter PS, Cox LR, Mills D, Brown MJ, Haigh D, Ward RW, Smith DG, Murray KJ, Reith AD, Holder JC. Selective small molecule inhibitors of glycogen synthase kinase-3 modulate glycogen metabolism and gene transcription. *Chem Biol*. 2000;7:793-803

27. Kirby LA, Schott JT, Noble BL, Mendez DC, Caseley PS, Peterson SC, Routledge TJ, Patel NV. Glycogen synthase kinase 3 (gsk3) inhibitor, sb-216763, promotes pluripotency in mouse embryonic stem cells. *Plos One*. 2012;7

28. Gross ER, Hsu AK, Gross GJ. Delayed cardioprotection afforded by the glycogen synthase kinase 3 inhibitor sb-216763 occurs via a katp- and mptp-dependent mechanism at reperfusion. *American journal of physiology. Heart and circulatory physiology*. 2008;294:H1497-1500

29. Asimaki A, Tandri H, Duffy ER, Winterfield JR, Mackey-Bojack S, Picken MM, Cooper LT, Wilber DJ, Marcus FI, Basso C, Thiene G, Tsatsopoulou A, Protonotarios N, Stevenson WG, McKenna WJ, Gautam S, Remick DG, Calkins H, Saffitz JE. Altered desmosomal proteins in granulomatous myocarditis and potential pathogenic links to

arrhythmogenic right ventricular cardiomyopathy. *Circ-Arrhythmia Elec*. 2011;4:743-U240

30. Wei Q, Hariharan V, Huang H. Cell-cell contact preserves cell viability via plakoglobin. *Plos One*. 2011;6

31. Elkin BS, Azeloglu EU, Costa KD, Morrison B. Mechanical heterogeneity of the rat hippocampus measured by atomic force microscope indentation. *J Neurotraum*. 2007;24:812-822

32. Lin DC, Dimitriadis EK, Horkay F. Robust strategies for automated afm force curve analysis - i. Non-adhesive indentation of soft, inhomogeneous materials. *J Biomech Eng-T Asme*. 2007;129:430-440

33. Kwong KF, Schuessler RB, Green KG, Laing JG, Beyer EC, Boineau JP, Saffitz JE. Differential expression of gap junction proteins in the canine sinus node. *Circ Res*. 1998;82:604-612

34. Saffitz JE, Green KG, Kraft WJ, Schechtman KB, Yamada KA. Effects of diminished expression of connexin43 on gap junction number and size in ventricular myocardium. *Am J Physiol-Heart C*. 2000;278:H1662-H1670

35. Ingber DE. Tensegrity i. Cell structure and hierarchical systems biology. *J Cell Sci*. 2003;116:1157-1173

36. Valente M, Calabrese F, Thiene G, Angelini A, Basso C, Nava A, Rossi L. In vivo evidence of apoptosis in arrhythmogenic right ventricular cardiomyopathy. *Am J Pathol*. 1998;152:479-484

37. Smith DG, Buffet M, Fenwick AE, Haigh D, Ife RJ, Saunders M, Slingsby BP, Stacey R, Ward RW. 3-anilino-4-arylmaleimides: Potent and selective inhibitors of glycogen synthase kinase-3 (gsk-3). *Bioorg Med Chem Lett*. 2001;11:635-639

38. Gross ER, Hsu AK, Gross GJ. Delayed cardioprotection afforded by the glycogen synthase kinase 3 inhibitor sb-216763 occurs via a k-atp- and mptp-dependent mechanism at reperfusion. *Am J Physiol-Heart C*. 2008;294:H1497-H1500

39. Cross DAE, Culbert AA, Chalmers KA, Facci L, Skaper SD, Reith AD. Selective small-molecule inhibitors of glycogen synthase kinase-3 activity protect primary neurones from death. *J Neurochem*. 2001;77:94-102

40. Deng H, Dokshin GA, Lei J, Goldsmith AM, Bitar KN, Fingar DC, Hershenson MB, Bentley JK. Inhibition of glycogen synthase kinase-3 beta is sufficient for airway smooth muscle hypertrophy. *J Biol Chem*. 2008;283:10198-10207

41. Bierkamp C, McLaughlin KJ, Schwarz H, Huber O, Kemler R. Embryonic heart and skin defects in mice lacking plakoglobin. *Dev Biol*. 1996;180:780-785

42. Ruiz P, Brinkmann V, Ledermann B, Behrend M, Grund C, Thalhammer C, Vogel F, Birchmeier C, Gunthert U, Franke WW, Birchmeier W. Targeted mutation of plakoglobin in mice reveals essential functions of desmosomes in the embryonic heart. *J Cell Biol*. 1996;135:215-225

43. Gallicano GI, Kouklis P, Bauer C, Yin M, Vasioukhin V, Degenstein L, Fuchs E. Desmoplakin is required early in development for assembly of desmosomes and cytoskeletal linkage. *J Cell Biol*. 1998;143:2009-2022

44. Grossmann KS, Grund C, Huelsken J, Behrend M, Erdmann B, Franke WW, Birchmeier W. Requirement of plakophilin 2 for heart morphogenesis and cardiac junction formation. *J Cell Biol*. 2004;167:149-160

45. Wakatsuki T, Schlessinger J, Elson EL. The biochemical response of the heart to hypertension and exercise. *Trends Biochem Sci*. 2004;29:609-617

46. Hausenloy DJ, Yellon DM. Survival kinases in ischemic preconditioning and postconditioning. *Cardiovasc Res*. 2006;70:240-253

47. Sadoshima J, Izumo S. The cellular and molecular response of cardiac myocytes to mechanical stress. *Annu Rev Physiol*. 1997;59:551-571

48. Grossman W, Jones D, Mclaurin LP. Wall stress and patterns of hypertrophy in human left-ventricle. *J Clin Invest*. 1975;56:56-64

49. Lammerding J, Kamm RD, Lee RT. Mechanotransduction in cardiac myocytes. *Ann Ny Acad Sci*. 2004;1015:53-70

50. Garcia-Gras E, Lombardi R, Giocondo MJ, Willerson JT, Schneider MD, Khoury DS, Marian AJ. Suppression of canonical wnt/beta-catenin signaling by nuclear plakoglobin recapitulates phenotype of arrhythmogenic right ventricular cardiomyopathy. *J Clin Invest*. 2006;116:2012-2021

4 Different ARVC-Causing Proteins Produce Similar Changes to Cell Properties

4.1 – Introduction

The identification of defective molecular mechanisms that are common across ARVC-patients remains a strategic area of research. Specifically, recent studies have investigated the mechanistic basis for different ARVC-causing mutations in hopes of identifying common defects in a signaling pathway – information that could be used to develop diagnostic tests or identify therapeutic targets.[1-3] For example, it has been hypothesized that mutations in genes encoding desmosomal proteins could destabilize desmosomal junctions, leading to the hallmark features of ARVC such as arrhythmia (via disruption of gap junctions) or apoptosis (via suppression of Wnt signaling by nuclear plakoglobin).[1, 3] While our findings in chapter 3 support this hypothesis, it remains to be seen if this defective phenotype is also present in cells expressing other, more common disease-causing mutant desmosomal genes (such as plakophilin).

In chapter 3, we showed that the expression of ARVC-causing mutations in plakoglobin can reversibly alter the cell's ability to remodel cell-cell junctions in response to shear stress, without significantly affecting cell-cell adhesion or stiffness. In order to determine if these features are common among cells expressing different mutant desmosomal genes, we investigated the mechanical and signaling properties of cardiac myocytes expressing mutations in plakophilin - the most commonly mutated gene in ARVC patients.[4-6] Key features of mutant plakophilin-2 mediated ARVC pathogenesis include the intrinsic instability of the protein, and resulting disruption of desmosomal formation, but how these features might affect the cell's ability to alter the junctional distribution of plakophilin in response to mechanical loading has not yet been investigated.[7] Furthermore, it is widely believed that the plakoglobin redistribution

is central feature ARVC pathogenesis,[1, 8] but whether mutant plakophilin-2 expression can also alter the cellular distribution of plakoglobin remains to be seen. We hypothesize that the expression of ARVC-linked mutant plakophilin-2 alters the cellular distributions of both plakophilin-2 and plakoglobin, without changes in biomechanical properties.

In order to gain insight into plakophilin-2-mediated ARVC pathogenesis, we characterized biomechanical properties and responses to shear stress in neonatal rat ventricular myocytes expressing a mutant form of plakophilin-2. In studying the response to shear stress, we specifically focused on cell junctions where plakophilin-2 is a binding partner. In addition to repeating key assays performed in chapter 3 in cells expressing mutant plakophilin-2 (i.e. – dispase assays, TUNEL stains, and atomic force microscopy), we also investigate the hierarchical effects of plakoglobin or plakophilin suppression on desmosomal destabilization (i.e. - the ability of mutant plakophilin-2 to regulate junctional plakoglobin localization, and vice versa). Finally, to determine if mutant desmosomal proteins participate in the mechanism by which SB216763 can restore the wild-type phenotype, we compare the effects of mutant protein expression and siRNA-mediated suppression on junctional remodeling in cells treated with SB216763.

Similar to cells expressing ARVC-causing plakoglobin, mutant plakophilin-2 expression altered the cell's ability to remodel plakophilin-2 at cell-cell junctions in response to shear stress, without affecting cell-cell adhesion or stiffness. Interestingly, the expression of mutant plakophilin also altered the junctional localization of plakoglobin as well (a feature not seen in cells expressing mutant plakoglobin). Suppression of plakophilin-2 mimicked the effects of mutant plakophilin-2 expression (i.e. – treated cells were unable to increase the immunoreactive signal for plakoglobin in response to shear stress), although SB216763 treatment did not restore

the wild-type phenotype in these cells. Finally, we show that treatment with SB216763, but not siRNA mediated GSK3 inhibition, was able to restore the wild-type phenotype in cells expressing mutant plakophilin-2.

4.2 – Methods

4.2.1 – Cell Culture and Transfection

Primary cultures of neonatal rat myocyte cultures (NRVM) were prepared from ventricles of 1-day old Wistar rat pups (Charles River, Indianapolis) as previously described.[9] Hearts from 10 neonatal rats were removed and finely minced. The pieces were serially digested in a dissociation solution (Ca^{2+}/Mg^{2+}-free Hanks balanced salt solution, GIBCO) containing 0.1% trypsin, 60 μg/ml pancreatin (Sigma, MO), 20 units/ml penicillin and 20 μg/ml streptomycin. NRVM were cultured on collagen-coated glass slides in M199 media (Life Technologies, NY) supplemented with 5% fetal calf serum (Sigma, MO) and 100 μM BRDU (Sigma, MO). After 2 days in culture (or immediately following isolation for cell aggregate cultures), cells were exposed for 1 hour at 37 ºC to adenoviruses containing wild-type human plakophilin-2, or a plakophilin-2 construct with the 1851del123 mutation (deletion of exon 10 linked to ARVC).

Adenoviral constructs were created using Gateway® Technology with Clonase® II from Invitrogen. The wild-type plakophilin-2, mutant plakophilin-2, and eGFP entry clones were developed by performing a BP recombination reaction between attB-flanked plakophilin-2 or eGFP DNA fragments and an attP-containing pDONR™ 221 vector. The attB-flanked DNA fragments were generated using the following primers (5'→3')_with an attB-KOZAK-overhang:

Forward primer for wild-type and mutant plakophilin-2 -
GGGGACAAGTTTGTACAAAAAAGCAGGCTTAGCCACCATGGCCGTCCCCGGC

Reverse primer for wild-type plakophilin-2 –
GGGGACCACTTTGTACAAGAAAGCTGGGTGGTCTTTAAGAGAGTGGTAGGCTTTGGC

Reverse primer for mutant plakophilin-2 –
GGGGACCACTTTGTACAAGAAAGCTGGGTGTCTTCCTCCCATCGGGCCAG

Forward primer for eGFP –
GGGGACAAGTTTGTACAAAAAAGCAGGCTTAGCCACCATGGTGAGCAAGGGC

Reverse primer for eGFP –
GGGGACCACTTTGTACAAGAAAGCTGGGTGTCTAGATCCGGTGGATCCCGG

Following the BP recombination reaction, the entry clone reaction products were amplified using DH5α chemically competent cells (New England Biolabs) and purified using the Qiaprep Spin Mini-prep kit (Qiagen) according to the manufacturer's recommended protocol. The entry clones were sequenced to verify that the PCR and BP recombination reaction steps had not introduced any point mutations (insert sequences can be found in Appendix 4.6), and an LR recombination reaction was performed to transfer the genes of interest into an attR-containing pAd/CMV/V5/DEST adenoviral destination vector. The destination vectors were subsequently amplified, sequenced, and sent to Vector Biolabs (Philadelphia, PA) for packaging, amplification and titration. The titers for the wild-type plakophilin-2, mutant plakophilin-2 and eGFP adenoviruses were $4.4x10^{10}$, $3.5x10^{10}$, and $3.6x10^{10}$ PFU/mL. Cells transfected with virus containing wild-type plakophilin-2 were used to control for viral transfection and possible effects related to over-expression. Adenovirus containing green fluorescent protein (eGFP) was used to monitor transfection efficiency. The wild-type plakoglobin construct and both mutant forms of plakoglobin included a linker (40 amino acids) and V5 epitope tag to facilitate exogenous protein identification by immunostaining and immunoblotting. Experiments were performed 24 hours after adenoviral transfection. All animal work was performed in accordance with NIH guidelines and the Institutional Animal Care and Use Committee of Columbia University.

4.2.2 – Cell-Cell Adhesion Assays

Cell-cell adhesion strength was measured using dispase assays. Dispase assays were performed using monolayers of transfected NRVM on collagen-coated glass chamber slides. Monolayers were pre-treated with 10 μM blebbistatin for 20 minutes to minimize contractions, followed by a solution containing 2.4 U/mL dispase and 10 μM blebbistatin for 30 minutes at 37 ^{o}C and 1% CO2. Intact cell sheets that had lifted off the culture dish were agitated for 20 min in a rotary shaker at 70 rpm, and the number of fragments was quantified using ImageJ.[10, 11] To further validate the dispase assays, additional studies were performed in non-transfected monolayers exposed to either of two specific siRNAs against plakophilin-2, as previously described,[12] to compare effects on adhesion strength caused by plakoglobin knockdown versus expression of mutant plakoglobin.

4.2.3 – Immunoblotting

Immunoblotting was performed as previously described.[12] Cultured NRVM were lysed in standard RIPA lysis buffer containing 500 nM phenylmethanesulfonyl fluoride, 50 mM sodium fluoride, 1 mM sodium orthovanadate, 10 mM sodium pyrophosphate, and protease inhibitor cocktail. Samples were solubilized in LDS sample buffer supplemented with 5% v/v 2-mercaptoethanol. Total protein concentration was determined by Bradford assay (Sigma). Soluble fractions containing equal amounts of total protein were separated using SDS polyacrylamide gel electrophoresis and transferred onto PVDF membranes (Millipore, MA). Immunoblotting was performed using the following antibodies: mouse anti-V5 (Invitrogen 1:1000), mouse anti-plakophilin-2 (Fitzgerald 1:20), mouse anti-GAPDH (Novus Biologicals

1:2000), rabbit anti-GSK3 (Cell Signalling 1:2000) and horseradish peroxidase-conjugated secondary antibody (Biorad 1:1000). Blots were developed with ECL reagents (Perkin Elmer, MA) and imaged using a FUJI imaging unit (Fujifilm, CT). Relative band intensities were quantified using ImageJ, with values normalized to loading controls.

4.2.4 – Shear Flow

NRVM were sheared under oscillatory flow conditions in a parallel-plate shear chamber at 0.06 Pascal (Pa) for 4 hours at 37^{o}C. Thereafter, the cells were either immunostained for plakoglobin/N-cadherin or lysed for immunoblotting measurements of plakoglobin, V5, and phosphorylated or total ERK. The shear level was estimated by (1) using a parallel plate model to simulate the shear induced by adjacent myocardial sheets,[13] and (2) using a range of shear stresses that have been previously shown to induce ERK phosphorylation without activation of the p38 pathway.[14] The derivation of the formula used to calculate the shear level may be found in the methods of Chapter 3, Section 2.5. To investigate the ability of SB216763 to restore the wild-type phenotype in cells transfected to express mutant plakophilin-2 or treated with specific siRNA against plakoglobin or plakophilin-2, cells were incubated with SB216763 (5 μM) for 24 hours before shearing and throughout the duration of shear. Suppression of GSK3 with siRNA was used to determine if recovery of the wild-type phenotype in cells expressing mutant plakophilin-2 was dependent on SB216763-mediated inhibition of GSK3.

4.2.5 – Immunofluorescence

NRVM were immunostained based on established protocols.[15] Cells were simultaneously blocked and permeabilized for 45 minutes in 3% normal goat serum, 1% w/v BSA, and 0.15%

Triton X-100 in PBS, followed by an overnight incubation at 4°C with either mouse-monoclonal anti-plakophilin-2 (Fitzgerald; 1:20) or anti-plakoglobin (Sigma; 1:1500 in blocking buffer) antibodies. Samples were then incubated with secondary antibody (Invitrogen; 1:1500) for 2 hours at room temperature. The immunostained preparations were imaged at 40x (1.3 NA) using an Olympus IX-81 inverted confocal microscope. Each image was subsequently masked to isolate cell junctions, allowing for discrete quantification of junctional immunoreactive signal. Images were analyzed using quantitative confocal microscopy as previously described.[10, 16] Each image was masked to isolate cell junctions, allowing for discrete quantification of junctional immunoreactive signal. Using ImageJ, the same threshold was applied to each image. The fraction of junctional pixels above threshold was calculated by dividing the number of pixels above threshold by the total number of pixels in the image.

4.2.6 – Apoptosis Assay

Terminal deoxynucleotidyl transferase dUTP nick end labeling (TUNEL) assays were performed using an *in situ* cell death detection kit (Roche Diagnostics, Basel, Switzerland) as previously described.[12] Adherent cells were fixed in 4% paraformaldehyde for 1 hour at room temperature, permeabilized with 0.1% Triton X-100 for 2 minutes on ice, and then incubated in 50μL of TUNEL reaction mixture at 37 °C for one hour in the dark. Samples were analyzed directly using fluorescence microscopy.

4.2.7 – Statistical Analysis

Data sets were analyzed using the non-parametric Kruskal-Wallis analysis of variance (ANOVA) test in Prism. Data showing significance ($p \leq 0.05$) were further analyzed using

Dunn's *post hoc* test for multiple comparisons. Differences were considered to be statistically significant and indicated with * when $p \leq 0.05$ or ** when $p \leq 0.01$. Error bars are plotted as the standard deviation of the data.

4.3 – Results

4.3.1 – Expression of ARVC-Causing Mutant Plakophilin-2 in Cardiac Myocytes

Immunostaining with an antibody against the V5 epitope tag in non-transfected (control), wild-type (WT PKP), and mutant plakophilin-2 (1851del123 PKP) transfected myocytes confirmed the localization of exogenous plakophilin-2 at cell junctions in WT PKP cells, but not 1851del123 PKP cells (Figure 4.1A). Only background levels of signal were seen in non-transfected control cells. Immunostaining with an antibody against a C-terminal epitope in plakophilin-2 confirmed junctional localization of plakophilin-2 in all cases (Figure 4.1B). Immunoblotting of untransfected and transfected cardiac myocyte lysates with an anti-V5 antibody confirmed expression of exogenous plakophilin-2 in both the WT PKP and 1851del123 PKP cells (Figure 4.1C). Immunoblotting with a C-terminal antibody against plakophilin-2 (which tags both the exogenous and endogenous forms), normalized to GAPDH, was used to confirm that transfection did not result in overexpression of the exogenous protein (Figure 4.1C). Due to the relatively similar size of exogenous and endogenous proteins, immunoblotting with the C-terminal plakophilin-2 antibody did not show two discrete bands, although comparison of immunostains using antibodies against C-terminal PKP2 and V5 suggests the exogenous wild-type and mutant proteins are being expressed (but not overexpressed, as evidenced by the relatively similar intensity of bands when immunoblotting with the C-terminal PKP2 antibody). Transfection with a GFP virus exhibited 97.9 ± 0.2 percent viral efficiency, and was used to

determine the multiplicity of infection for the WT PKP and 1851del123 PKP viral constructs (Figure 4.1D).

4.3.2 – Cell-Cell Adhesion Strength and Stiffness Unaffected by Mutant Plakophilin-2 Expression

Dispase assays were used to determine whether expression of mutant plakophilin-2 affected the strength of cell-cell adhesion. As shown in Figure 4.2A, the number of fragments resulting from mechanical agitation of monolayers in the dispase assay was not significantly different among the control myocytes and myocytes expressing mutant plakophilin-2. To determine whether the effects on cell adhesion are different following knockdown of a desmosomal protein versus expression of a disease-causing mutation, we treated non-transfected myocytes with either of two specific siRNAs against plakoglobin. As shown in Figure 4.2B, treated cells exhibited a marked reduction in plakophilin-2 expression. Cells treated with either of two specific siRNAs against plakophilin-2 showed between 1.9- and 3.5-fold increases in monolayer fragmentation relative to time-matched controls after 1 or 3 minutes of agitation (Figure 4.2B, left), whereas treatment with a negative siRNA had no effect on cell-cell adhesion. Taken together, these results indicate that expression of mutant forms of plakophilin-2 does not affect cell-cell adhesion strength, whereas knockdown of the endogenous protein has a marked effect in reducing adhesion. Knockdown efficiency was quantified by western blot (Figure 4.2B, right), and a TUNEL assay was used to exclude reduced cell viability as a possible cause of increased sheet fragmentation (Figure 4.2C).

Previous studies, in addition to our work in chapter 3, have shown that different mutations can exhibit changes in cell stiffness.[10] We next used AFM to measure cell stiffness.[17]

Similar to our results in Chapter 3, we found no changes in stiffness in cardiac myocytes expressing mutant plakophilin-2 (Figure 4.2D).

4.3.3 – Shear Stress Induces Junctional Plakophilin-2 and Plakoglobin Remodeling

In response to oscillatory fluid shear at 0.06 Pa, control and WT PKP transfected myocytes exhibited 2.9- and 3-fold increases in immunoreactive signal for junctional plakophilin-2 (Figure 4.3A and B) compared to unsheared cells. In contrast, myocytes expressing the 1851del123 form of plakophilin-2 failed to increase junctional plakophilin-2 signal following shear. To determine whether SB216763 could restore the control-level response to shear in cells expressing mutant plakophilin-2, we repeated experiments in cultures exposed to SB216763 for 24 hours. As shown in Figure 4.3C, cells expressing the 1851del123 variant of plakophilin-2 exhibited a robust increase in junctional signal for plakophilin-2 in response to oscillatory shear equivalent to the response in controls and WT PKP cells (3.5-fold increase in 1851del123 cells compared with 3.2- and 2.1-fold increases in control and WT PKP cells).

Cells expressing mutant plakophilin-2 did not exhibit significant remodeling of plakoglobin at cell junctions. Control and WT PKP transfected myocytes exhibited 4- and 2-fold increases in immunoreactive signal for junctional plakoglobin (Figure 4.3D) compared to unsheared cells, while 1851del123 PKP cells were unable to increase the immunoreactive signal for junctional plakoglobin. Treatment with SB216763 recovered the wild-type phenotype; cells expressing the 1851del123 variant of plakophilin-2 exhibited 2.7-fold increases in junctional signal for plakoglobin in response to oscillatory shear (Figure 4.3E). Surprisingly, junctional plakophilin expression was unaltered in cells expressing mutant plakoglobin (Figure 4.3F-G).

4.3.4 – Plakophilin Knockdown Alters Plakoglobin Remodeling, But Not Vice Versa

To better understand the mechanism by which mutant desmosomal proteins can alter junctional remodeling, we treated cells with siRNA to suppress either plakoglobin or plakophilin and immunostained for plakophilin or plakoglobin, respectively. In each case, application of shear stress to cells where either plakoglobin or plakophilin was suppressed led to a large number of cells being sheared away (>50%). The remaining cells, dispersed across the slide in small groups (~10-15 cells), maintained enough cell-cell contact for quantification, which was performed following mechanical stimulation. Similar to cells expressing mutant plakoglobin, suppression of plakoglobin did not alter junctional plakophilin remodeling (Figure 4.4A-B). Cells treated with siRNA to suppress plakophilin did not exhibit a significant increase in junctional plakoglobin in response to shear stress, and treatment with SB216763 was unable to recover the wild-type phenotype in these cells (Figure 4.4C-D).

4.3.5 – SB216763, But Not GSK3 Knockdown, Rescues Wild-Type Phenotype

To determine if GSK3 inhibition was the mechanism by which SB216763 restored the wild-type phenotype, cells transfected with WT PKP or 1851del123 PKP were exposed to shear stress following siRNA-mediated suppression of GSK3. In response to shear stress, WT PKP transfected myocytes exhibited 2.2- and 2.3-fold increases in immunoreactive signal for junctional plakoglobin with and without GSK3 siRNA treatment, respectively, compared to unsheared cells (Figure 4.5). In contrast, cells transfected with 1851del123 PKP did not recover the ability to increase junctional immunoreactive signal in response to shear stress following GSK3 inhibition.

4.4 – Discussion

One key finding in this chapter is that cells expressing mutant plakophilin-2 respond abnormally to shear stress without changes in biomechanical properties (i.e. - cell-cell adhesion and stiffness). Another, arguably more significant finding, was that the expression of mutant plakophilin-2 altered the junctional remodeling of both plakophilin-2 as well as plakoglobin in response to shear stress, making defective plakoglobin trafficking a common phenotype in cells expressing different ARVC-causing mutant desmosomal proteins. Interestingly, while the expression of mutant plakophilin was able to alter plakoglobin trafficking, there was asymmetry with respect to the expression of mutant plakoglobin being able to alter the cellular distribution of plakophin-2. Although we show that desmosomal protein suppression can mimic the effects of mutant protein expression in certain aspects (i.e. – junctional remodeling), protein suppression does not fully recapitulate the disease phenotype (i.e. – mutant protein expression is required for SB216763 to restore the wild-type phenotype). Finally, we reaffirm our findings in chapter 3, that GSK3 inhibition does not recapitulate the effects of SB216763, particularly in cells expressing mutant plakophilin-2.

In Chapter 3 we showed, despite the belief that defective intracellular adhesion plays a pathogenic role in ARVC, that the expression of ARVC-causing plakoglobin has no significant effect on cell-cell adhesion strength *in vitro*. Our findings in this chapter, namely that lack of adhesion differences between cells expressing mutant plakophilin-2 and control cells, reinforce our hypothesis that adhesion defects are secondary, if they exist at all, to abnormal cellular response to certain mechanical stresses in ARVC pathogenesis. Consistent with our previous findings, siRNA-mediated suppression of plakophilin-2 significantly decreased cell-cell adhesion strength. These data highlight the differences between suppression of a desmosomal protein

versus expression of a mutant form of a desmosomal protein, where the latter likely reflects the pathophysiology of the disease in patients.

Immunostaining revealed that the expression of mutant plakophilin-2 was able to alter the junctional localization of both plakophilin-2 as well as plakoglobin, while the expression of mutant plakoglobin only altered the cellular distribution of plakoglobin. This is a significant finding as it identifies, for the first time, a shear-stimulated signaling defect common across cells expressing different disease-causing desmosomal proteins. Although follow-up work is necessary to determine if all ARVC-causing mutations alter plakoglobin trafficking, our data suggest that the cellular redistribution of plakoglobin likely plays a critical pathogenic role. To further investigate how plakophilin-2 altered junctional plakoglobin distribution, we treated cells with siRNA to suppress plakophilin-2, and immunostained for plakoglobin. Although suppression of plakophilin-2 altered the junctional localization of plakoglobin in response to a shear stimulus, SB216763 treatment was unable to recover the wild-type phenotype. These data provide further evidence that mutant protein expression, and not suppression, is necessary to recapitulate the disease phenotype.

Treatment with SB216763 was able restore the junctional remodeling of both plakophilin-2 and plakoglobin in cells expressing mutant plakophilin-2. Together with our findings in chapter 3, these data provide supporting evidence for the ‘final common pathway’ hypothesis. Although SB216763 is advertised as a GSK3 inhibitor, siRNA-mediated GSK3 suppression was unable to recapitulate the effects of SB216763. It is likely that in addition to inhibiting GSK3, SB216763 also has secondary effects, which are not recapitulated by siRNA-mediated GSK3 suppression. Further investigation is needed to determine the mechanism of action.

We conclude that ARVC-causing mutations in plakophilin lead to altered cellular distribution of both plakophilin and plakoglobin, without alterations in cell mechanical properties.

4.5 – Figures

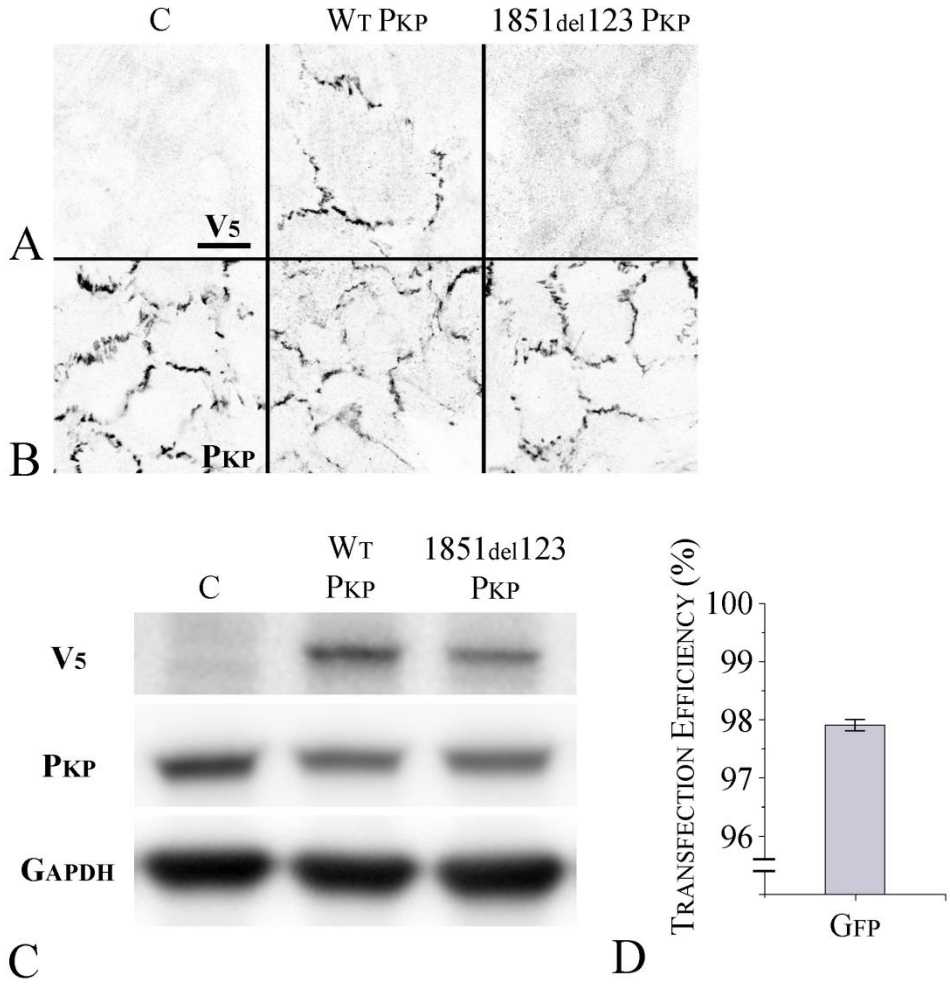

Figure 4.1 – ARVC models express transgenic plakophilin: **(A)** V5 Stain on control (C), wild-type plakophilin (WT PKP), and mutant plakophilin (1851del123 PKP) transfected myocytes. Normal junctional localization is seen in WT PKP transfected cells. No junctional signal is observed in cells expressing 1851del123 PKP. **(B)** Immunostaining with an anti-plakophilin-2 antibody against a C-terminal epitope (which recognizes both endogenous and transfected forms of WT PKP and 1851del123 PKP. **(C)** Immunoblots using anti-V5 (top), anti-C-terminal plakophilin (middle) and anti-GAPDH (bottom) antibodies. V5 bands in the WT PKP and 1851del123 PKP lysates confirm successful transfection. The relatively similar size between

exogenous and endogenous plakophilin prevented detection of discrete bands using the anti-C-terminal plakophilin antibody. **(D)** Quantification of cells transfected with a GFP virus to confirm 97.9 ± 0.2% transfection efficiency (n=3). Scale bars = 20 μm.

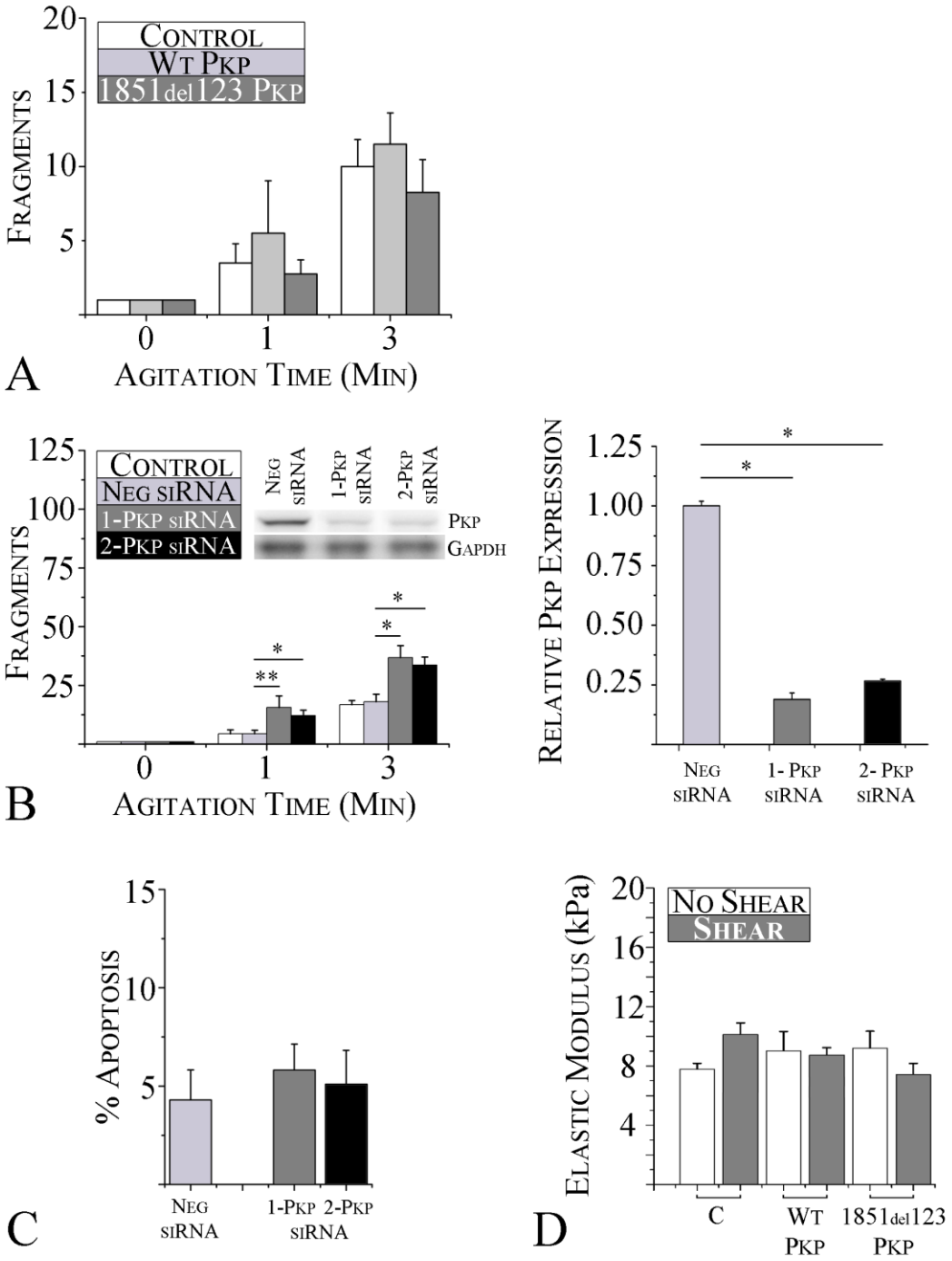

Figure 4.2 - Cell-cell adhesion strength and stiffness are unaffected by mutant plakophilin expression: **(A)** Quantification of control and mutant plakophilin transfected cardiac myocyte monolayer fragmentation in dispase assays before and after 1 or 3 minutes of agitation. Similar

to myocytes expressing mutant plakoglobin, cardiac myocytes expressing mutant plakophilin-2 (n=6) also show no differences in cell-cell adhesion relative to WT PKP (n=4), suggesting the effect does not depend on which desmosomal protein is being mutated. **(B)** Dispase assays in normal (non-transfected) cardiac myocytes showing significant reduction in cell-cell adhesion in cells following siRNA knock-down of endogenous plakophilin-2 (n=5). Plakophilin-2 knock-down was confirmed by immunoblotting (inset), and quantified (right). **(C)** Quantification of apoptosis (percent TUNEL-positive nuclei) in control cells transfected with non-targeting siRNA, or siRNA targeting plakophilin (n=6). **(D)** Cell stiffness measurements in control cells (C) and cells expressing wild type or mutant plakophilin before and after exposure to mechanical shear stress (n=3). Cardiac myocytes expressing mutant plakophilin show no differences in cell stiffness compared to control cells. *$p<0.05$; **$p<0.01$

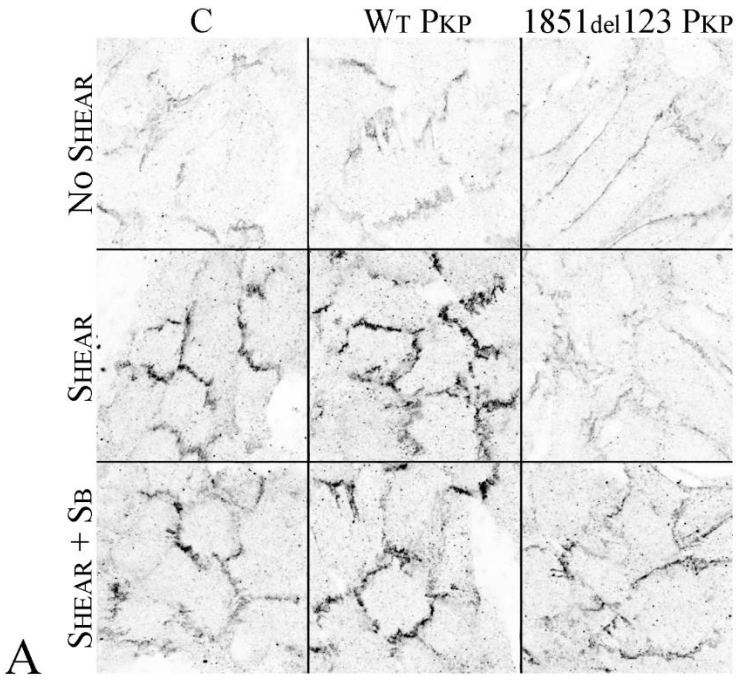
C
WT PKP
1851del123 PKP
NO SHEAR
SHEAR
SHEAR + SB

A

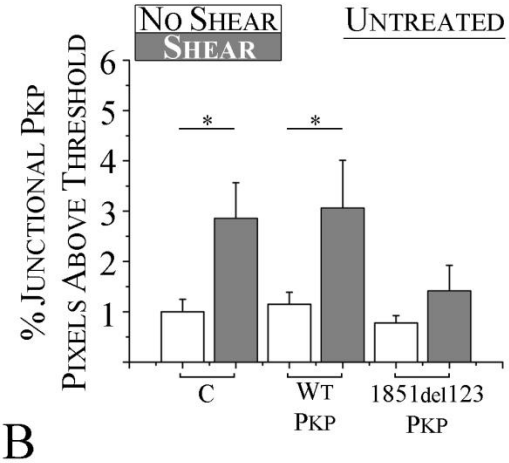
NO SHEAR
SHEAR
UNTREATED
% JUNCTIONAL PKP PIXELS ABOVE THRESHOLD
C
WT PKP
1851del123 PKP

B

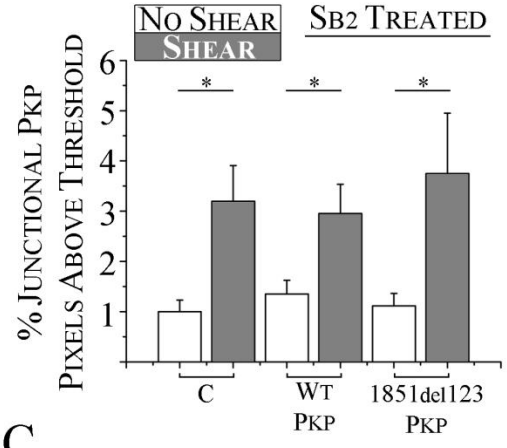
NO SHEAR
SHEAR
SB2 TREATED
% JUNCTIONAL PKP PIXELS ABOVE THRESHOLD
C
WT PKP
1851del123 PKP

C

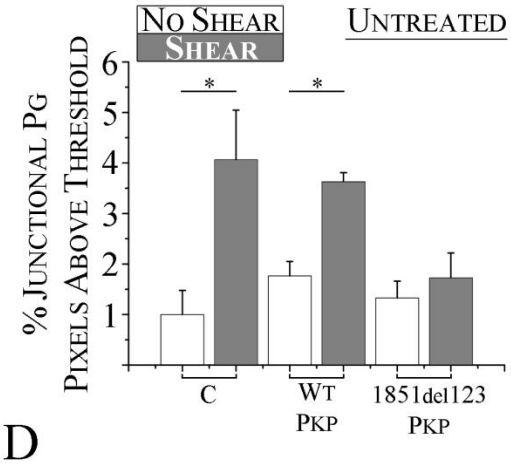
NO SHEAR
SHEAR
UNTREATED
% JUNCTIONAL PG PIXELS ABOVE THRESHOLD
C
WT PKP
1851del123 PKP

D

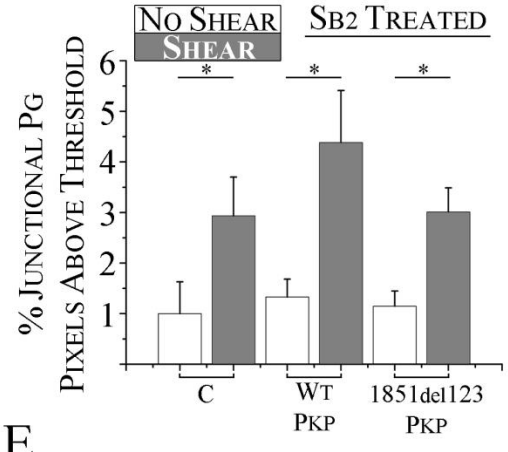
NO SHEAR
SHEAR
SB2 TREATED
% JUNCTIONAL PG PIXELS ABOVE THRESHOLD
C
WT PKP
1851del123 PKP

E

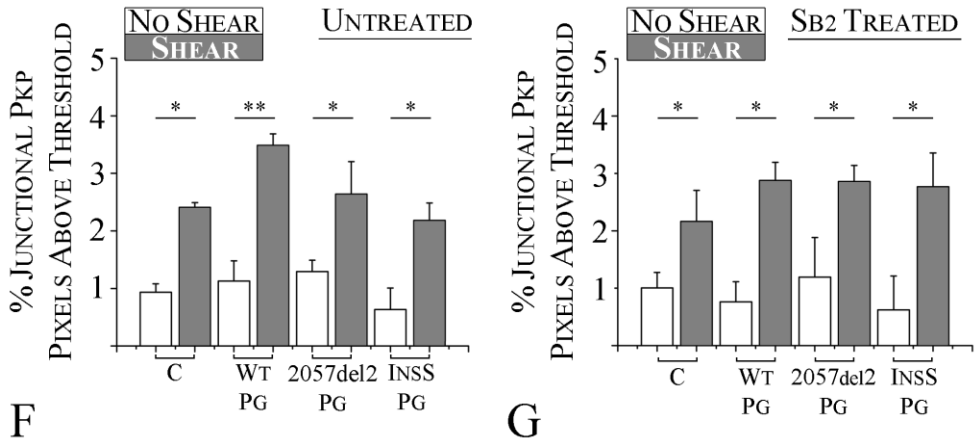

Figure 4.3 – Shear-induced plakoglobin and plakophilin localization are reversibly altered in pkp-model ARVC cells: **(A)** Immunofluorescence images showing the distribution of plakophilin (C-terminal antibody) in control (C) and transfected cardiac myocytes before (top) and after (middle) exposure to shear, and after treatment with SB216763 (SB2; bottom). Control and WT PKP cells show increased immunoreactive signal with junctional localization after shear, whereas cells expressing 1851del123 PKP show no apparent increase in junctional signal after shear. Treatment with the drug restored the normal shear-induced increase of in junctional signal in cells expressing mutant plakophilin. **(B-C)** Quantification of junctional plakophilin signal before and after shear in **(B)** untreated (n=3) or **(C)** SB216763 treated (n=3) cells transfected with wild-type or mutant plakophilin. **(D-E)** Quantification of junctional plakoglobin signal before and after shear in **(D)** untreated (n=4) or **(E)** SB216763 treated (n=4) cells transfected with wild-type or mutant plakophilin. **(F-G)** Quantification of junctional plakophilin signal before and after shear in **(F)** untreated (n=3) or **(G)** SB216763 treated (n=3) cells transfected with wild-type or mutant plakophilin.*p< 0.05; **p<0.01

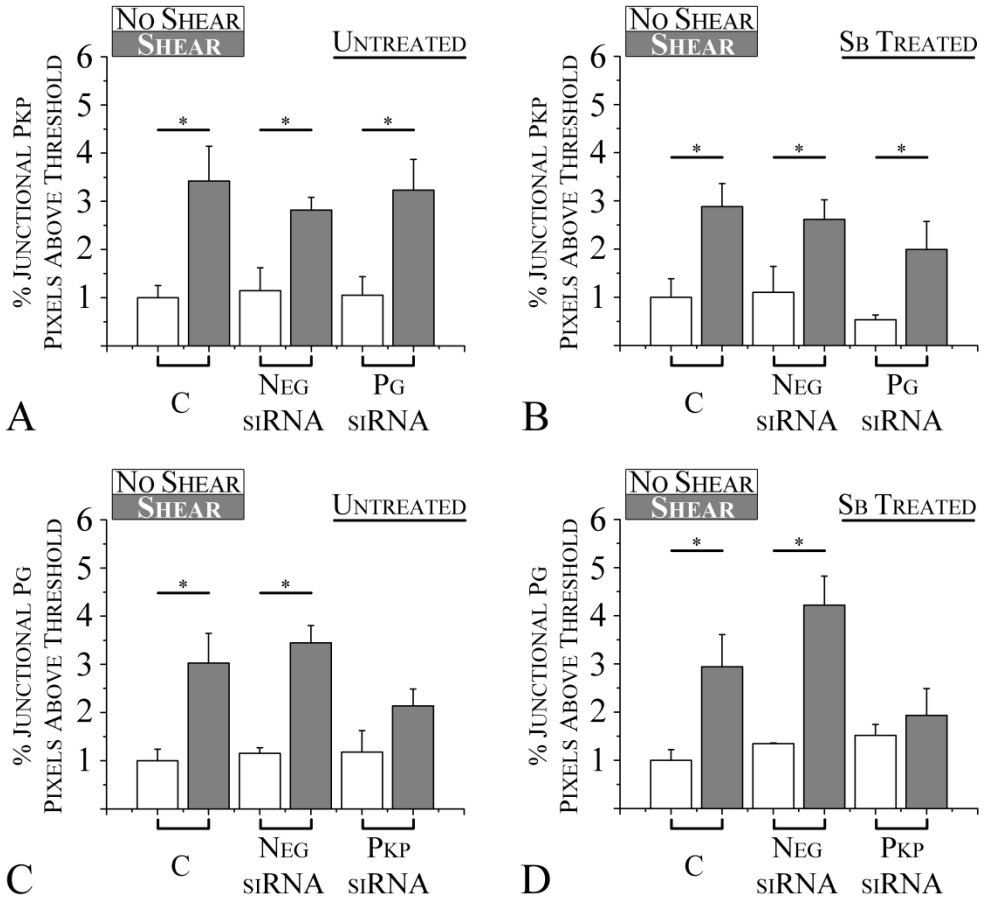

Figure 4.4 – Plakophilin Knockdown Alters Plakoglobin Remodeling, But Not Vice Versa: **(A-B)** Quantification of junctional plakophilin signal before and after shear in **(B)** untreated (n=3) or **(C)** SB216763 treated (n=3) cells where plakoglobin has been suppressed. **(C-D)** Quantification of junctional plakoglobin signal before and after shear in **(B)** untreated (n=3) or **(C)** SB216763 treated (n=3) cells where plakophilin has been suppressed.

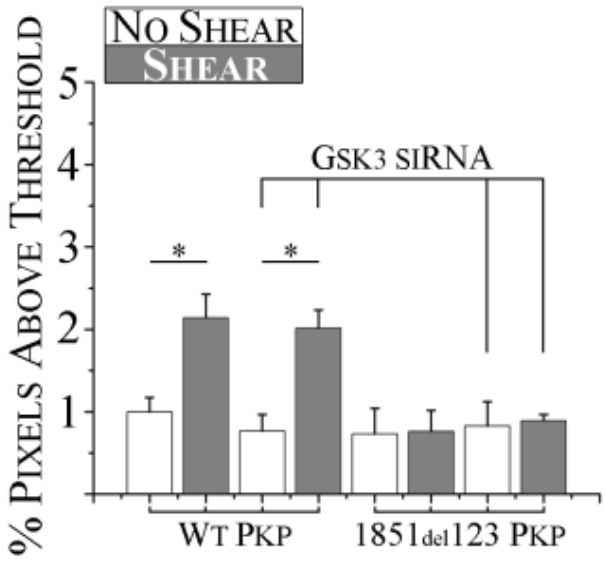

Figure 4.5 - SB216763 treatment, but not GSK3 suppression, rescues wild-type phenotype: Quantification of junctional plakoglobin signal before and after shear in non-targeting siRNA treated (n=3) or GSK3 siRNA treated (n=3) cells transfected with wild-type or mutant plakophilin. Suppression of GSK3 siRNA did not mimic the effects of SB216763. Suppression of GSK3 did not recover junctional remodeling in cells expressing mutant plakoglobin. *$p < 0.05$

4.6 – Appendix

Wild-type plakophilin-2: GTACAAAAAAGCAGGCTTAGCCACCATGGCCGTCCCCGGCTCACTGGC

CGAGTGTGGCTACATCCGGACTGTGCTGGGCCAGCAGATCCTGGGTCACCTGGACAGCTCCAGC

CTGGCCTTGCCCTCCGAGGCCAGACTGAGGCTGGCCGGCAGCAGCGGCCGCGGCGACCCGGCGG

CCCGGAGCCAGCGGATCCAGGAGCAGGTGCAGCAGACCCTGGCCCGCCGGGGCCGGAGCTCTGC

GGTCAGCGGGAACCTTCACCGAACCAGCAGTGTCCCTGAGTATGTCTACAAGCTACACGTGGTT

GAGAATGACTTTGTTGGACGGCAGTCACCTGTCACTAGGGACTATGACATGCTTAAGGCTGGAA

TGACTGCCACTTATGGAAGTCGCTGGGGGAGAGCAGCAGCACAGTACAGTTCCCAGAAGTCAGT

GGAGGAGAGATCCTGGAGGCAGCCTCTGAGGAGACTTGAGATTTCCCCAGATAGCAGCCCGGAG

AGAGCCCACTATGGGCACAGCGAATACCAGTATGCCTGGCGGAGCCACGTGGTGCCTGGTGGGC

GCCTCACCCTGCCACGCTATGCTCGCTCAGAGATCCTGGGCCTACGCCAGGCTGGCACAGCCCG

CAGGCCACCTGGGTGCGGGTCATTCAGCGATGCTGTCTTCGACAATGGCCCACTCAAGCCCACA

ATGCCCACCCACCCTCCTGGCACCAGCCACAGTGCGGGCAGCTTGTTGGAAGAGACCACTGTGC

GCGTGAGCCAGGCTCGGCTTCAAAGCACGCAGAGCAGAACCGCCCGCTCCTCCTGGCCCAGGAG

CTCAGTCCGCAGTAGCCTGCGGGAGCCAGGAAGAATGCTGACCACCGCAGGCCAGGCTGCCGTG

GGCAGCGGGGATGCACATGGGGACAGGAGTGTCTTCGCTGACGCCCAGCTGGGGAATGCAGACA

TCGAAATGACCTTGGAGAGAGCTGTGAATATGCTGGATGCAGACCATGTACCAGTATCCAAGAT

CTCTGCCGCAGCTACCTTCATACAGCATGAGAGCTTCCAAAAATCTGAAGCACGGAAAAGGGTC

AATCAACTTCGAGGCATCCCTAAGCTTCTACAACTGCTCAAACTTCAGAACGAAGATGTTCAAC

GGGCTGCTTGTGGGGCCTTGAGAAACTTGGTATTTGAAGACAATGATAACAAGTTGGAGGTAGC

TGAACTGAATGGAGTGCCTCGGCTACTGCAGGTGCTGAAGCAAACCAGAGACTTGGAGACAAAA

AAGCAAATAACAGGTTTGCTCTGGAACCTGTCCTCTAGTGATAAACTCAAGCATCTCATGATAA

CAGAAGCCTTGCTCACCTTGACAGAGAGTGTCATCATCCCCTTCTCCGGGTGGCCTGAAGGCGA

CTACCCCAAAGCCAATGGCTTGCTTGATTTTGATATATTCTACAATGTCACTGGATGCCTAAGG

AACATGAGCTCTGCTGGCCCCGATGGGAGGAAGATGATGAGAAGGTGTGATGGTCTCATTGACT

CATTGGTCCACTATGTCAGAGGAACTATTGCAGACTACCAGCCAGATGATAAGGCCACAGAGAA

CTGTGTGTGCATTCTTCATAACCTCTCCTACCAGCTGGAGGCAGAGCTCCCAGAGAAATATTCC

CAGAGTATCTACATGCAAAACCGGAATATCCAGACTAACAGTAACAAAAGTATTGGGTGTTTTG

GCAGCCGAAGTAGGAAACTAAAAGAGCAATACCAAGACTTGCAGATGCCAGAGGAAAGGAGCAA

TCCACATGGCATTGAGTGGCTGTGGCATTCCATTGTGATAAGGATGTATTTGTCCTTAATTGCC

AAGAGTACCCGAAACTATACCCAAGAGGCATCACTTGGGGCTCTCCAGAACCTCACAGCAGGAG

GCGGCCCGATACCCACATTGGTGGCTCGAATGGTTGTCCAAAAGGAAAATGGTCTTCAGCATAC

ACGGAAGATGCTGCACGTGGGTGATCCCAGTGTGAAAAAGACTGCGGTCTCCCTGCTGAGGAAT

TTGTCACGGAATCTTTCCCTGCAGAATGAAATTGCTAAAGAAACTCTACCAGATTTGGTTTCTA

TAATTCCTGACACAGTCCCAAGTACTGACCTTCTCATTGAAACCACAGCCTCTGCTTGCTATAC

GTTGAACAATTTAATGCAAAATAGTTACCAGAATGCACGAGACCTTCTGAACACCGGAGGTCTG

CAGAAAATTATGACCATCAGCATAGGGGAAGGCTATGCCCCCAACAAGGCCAGCAAAGCAGCCT

CTGTCCTCCTTTACTCTCTGTGGGCACATACAGAGCTGCATCACGCCTATAAGAAGGCTCAGTT

TAAGAAAACAGACTTTGTCAACAGCCGGACTGCCAAAGCCTACCACTCTCTTAAAGACCACCCA

GCTTT

Mutant plakophilin-2: GTACAAAAAAGCAGGCTTAGCCACCATGGCCGTCCCCGGCTCACTGGCC

GAGTGTGGCTACATCCGGACTGTGCTGGGCCAGCAGATCCTGGGTCACCTGGACAGCTCCAGCC

TGGCCTTGCCCTCCGAGGCCAGACTGAGGCTGGCCGGCAGCAGCGGACGCGGCGACCCGGCGGC

CCGGAGCCAGCGGATCCAGGAGCAGGTGCAGCAGACCCTGGCCCGCCGGGGCCGGAGCTCTGCG

GTCAGCGGGAACCTTCACCGAACCAGCAGTGTCCCTGAGTATGTCTACAAGCTACACGTGGTTG

AGAATGACTTTGTTGGACGGCAGTCACCTGTCACTAGGGACTATGACATGCTTAAGGCTGGAAT

GACTGCCACTTATGGAAGTCGCTGGGGGAGAGCAGCAGCACAGTACAGTTCCCAGAAGTCAGTG

GAGGAGAGATCCTGGAGGCAGCCTCTGAGGAGACTTGAGATTTCCCCAGATAGCAGCCCGGAGA

GAGCCCACTATGGGCACAGCGAATACCAGTATGCCTGGCGGAGCCACGTGGTGCCTGGTGGGCG

CCTCACCCTGCCACGCTATGCTCGCTCAGAGATCCTGGGCCTACGCCAGGCTGGCACAGCCCGC

AGGCCACCTGGGTGCGGGTCATTCAGCGATGCTGTCTTCGACAATGGCCCACTCAAGCCCACAA

TGCCCACCCACCCTCCTGGCACCAGCCACAGTGCGGGCAGCTTGTTGGAAGAGACCACTGTGCG

CGTGAGCCAGGCTCGGCTTCAAAGCACGCAGAGCAGAACCGCCCGCTCCTCCTGGCCCAGGAGC

TCAGTCCGCAGTAGCCTGCGGGAGCCAGGAAGAATGCTGACCACCGCAGGCCAGGCTGCCGTGG

GCAGCGGGGATGCACATGGGGACAGGAGTGTCTTCGCTGACGCCCAGCTGGGGAATGCAGACAT

CGAAATGACCTTGGAGAGAGCTGTGAATATGCTGGATGCAGACCATGTACCAGTATCCAAGATC

TCTGCCGCAGCTACCTTCATACAGCATGAGAGCTTCCAAAAATCTGAAGCACGGAAAAGGGTCA

ATCAACTTCGAGGCATCCCTAAGCTTCTACAACTGCTCAAACTTCAGAACGAAGATGTTCAACG

GGCTGCTTGTGGGGCCTTGAGAAACTTGGTATTTGAAGACAATGATAACAAGTTGGAGGTAGCT

GAACTGAATGGAGTGCCTCGGCTACTGCAGGTGCTGAAGCAAACCAGAGACTTGGAGACAAAAA

AGCAAATAACAGGTTTGCTCTGGAACCTGTCCTCTAGTGATAAACTCAAGCATCTCATGATAAC

AGAAGCCTTGCTCACCTTGACAGAGAGTGTCATCATCCCCTTCTCCGGGTGGCCTGAAGGCGAC

TACCCCAAAGCCAATGGCTTGCTTGATTTTGATATATTCTACAATGTCACTGGATGCCTAAGGA

ACATGAGCTCTGCTGGCCCGATGGGAGGAAGACACCCAGCTTT

eGFP: GTACAAAAAAGCAGGCTTAGCCACCATGGTGAGCAAGGGCGAGGAGCTGTTCACCGGG

GTGGTGCCCATCCTGGTCGAGCTGGACGGCGACGTAAACGGCCACAAGTTCAGCGTGTCCGGCG

AGGGCGAGGGCGATGCCACCTACGGCAAGCTGACCCTGAAGTTCATCTGCACCACCGGCAAGCT

GCCCGTGCCCTGGCCCACCCTCGTGACCACCCTGACCTACGGCGTGCAGTGCTTCAGCCGCTAC

CCCGACCACATGAAGCAGCACGACTTCTTCAAGTCCGCCATGCCCGAAGGCTACGTCCAGGAGC

GCACCATCTTCTTCAAGGACGACGGCAACTACAAGACCCGCGCCGAGGTGAAGTTCGAGGGCGA

CACCCTGGTGAACCGCATCGAGCTGAAGGGCATCGACTTCAAGGAGGACGGCAACATCCTGGGG

CACAAGCTGGAGTACAACTACAACAGCCACAACGTCTATATCATGGCCGACAAGCAGAAGAACG

GCATCAAGGTGAACTTCAAGATCCGCCACAACATCGAGGACGGCAGCGTGCAGCTCGCCGACCA

CTACCAGCAGAACACCCCCATCGGCGACGGCCCCGTGCTGCTGCCCGACAACCACTACCTGAGC

ACCCAGTCCGCCCTGAGCAAAGACCCCAACGAGAAGCGCGATCACATGGTCCTGCTGGAGTTCG

TGACCGCCGCCGGGATCACTCTCGGCATGGACGAGCTGTACAAGTCCGGACTCAGATCTCGAGC

TCAAGCTTCGAATTCTGCAGTCGACGGTACCGCGGGCCCGGGATCCACCGGATCTAGACACCCA

GCTTT

4.7 – References

1. Garcia-Gras E, Lombardi R, Giocondo MJ, Willerson JT, Schneider MD, Khoury DS, Marian AJ. Suppression of canonical wnt/beta-catenin signaling by nuclear plakoglobin recapitulates phenotype of arrhythmogenic right ventricular cardiomyopathy. *J Clin Invest*. 2006;116:2012-2021
2. Asimaki A, Kapoor S, Plovie E, Arndt AK, Adams E, Liu Z, James CA, Judge DP, Calkins H, Churko J, Wu JC, MacRae CA, Kleber AG, Saffitz JE. Identification of a new modulator of the intercalated disc in a zebrafish model of arrhythmogenic cardiomyopathy. *Science Translational Medicine*. 2014;6:240ra274
3. Asimaki A, Tandri H, Huang H, Halushka M, Basso C, Thiene G, Tsatsopoulou A, Protonotarios N, McKenna WJ, Calkins H, Saffitz JE. A new diagnostic test for arrhythmogenic right ventricular cardiomyopathy. *Circulation*. 2008;118:S774-S774
4. Gerull B, Heuser A, Wichter T, Paul M, Basson CT, McDermott DA, Lerman BB, Markowitz SM, Ellinor PT, MacRae CA, Peters S, Grossmann KS, Drenckhahn J, Michely B, Sasse-Klaassen S, Birchmeier W, Dietz R, Breithardt G, Schulze-Bahr E, Thierfelder L. Mutations in the desmosomal protein plakophilin-2 are common in arrhythmogenic right ventricular cardiomyopathy. *Nat Genet*. 2004;36:1162-1164
5. Kapplinger JD, Landstrom AP, Salisbury BA, Callis TE, Pollevick GD, Tester DJ, Cox MGPJ, Bhuiyan Z, Bikker H, Wiesfeld ACP, Hauer RNW, van Tintelen JP, Jongbloed JDH, Calkins H, Judge DP, Wilde AAM, Ackerman MJ. Distinguishing arrhythmogenic right ventricular cardiomyopathy/dysplasia-associated mutations from background genetic noise. *Journal of the American College of Cardiology*. 2011;57:2317-2327

6. den Haan AD, Tan BY, Zikusoka MN, Llado LI, Jain R, Daly A, Tichnell C, James C, Amat-Alarcon N, Abraham T, Russell SD, Bluemke DA, Calkins H, Dalal D, Judge DP. Comprehensive desmosome mutation analysis in north americans with arrhythmogenic right ventricular dysplasia/cardiomyopathy. *Circ-Cardiovasc Gene*. 2009;2:428-U436

7. Kirchner F, Schuetz A, Boldt LH, Martens K, Dittmar G, Haverkamp W, Thierfelder L, Heinemann U, Gerull B. Molecular insights into arrhythmogenic right ventricular cardiomyopathy caused by plakophilin-2 missense mutations. *Circ-Cardiovasc Gene*. 2012;5:400-411

8. Lombardi R, Cabreira-Hansen MD, Bell A, Fromm RR, Willerson JT, Marian AJ. Nuclear plakoglobin is essential for differentiation of cardiac progenitor cells to adipocytes in arrhythmogenic right ventricular cardiomyopathy. *Circ Res*. 2011;109:1342-U1386

9. Asimaki A, Tandri H, Duffy ER, Winterfield JR, Mackey-Bojack S, Picken MM, Cooper LT, Wilber DJ, Marcus FI, Basso C, Thiene G, Tsatsopoulou A, Protonotarios N, Stevenson WG, McKenna WJ, Gautam S, Remick DG, Calkins H, Saffitz JE. Altered desmosomal proteins in granulomatous myocarditis and potential pathogenic links to arrhythmogenic right ventricular cardiomyopathy. *Circ-Arrhythmia Elec*. 2011;4:743-U240

10. Huang H, Asimaki A, Lo D, McKenna W, Saffitz J. Disparate effects of different mutations in plakoglobin on cell mechanical behavior. *Cell Motil Cytoskel*. 2008;65:964-978

11. Sato PY, Coombs W, Lin XM, Nekrasova O, Green KJ, Isom LL, Taffet SM, Delmar M. Interactions between ankyrin-g, plakophilin-2, and connexin43 at the cardiac intercalated disc. *Circ Res*. 2011;109:193-U160

12. Wei Q, Hariharan V, Huang H. Cell-cell contact preserves cell viability via plakoglobin. *PLoS One*. 2011;6

13. Lorenzen-Schmidt I, Schmid-Schonbein GW, Giles WR, McCulloch AD, Chien S, Omens JH. Chronotropic response of cultured neonatal rat ventricular myocytes to short term fluid shear. *Cell Biochemistry and Biophysics*. 2006;46:113-122

14. Dvir T, Levy O, Shachar M, Granot Y, Cohen S. Activation of the erk1/2 cascade via pulsatile interstitial fluid flow promotes cardiac tissue assembly. *Tissue Engineering*. 2007;13:2185-2193

15. Kwong KF, Schuessler RB, Green KG, Laing JG, Beyer EC, Boineau JP, Saffitz JE. Differential expression of gap junction proteins in the canine sinus node. *Circ Res*. 1998;82:604-612

16. Saffitz JE, Green KG, Kraft WJ, Schechtman KB, Yamada KA. Effects of diminished expression of connexin43 on gap junction number and size in ventricular myocardium. *Am J Physiol-Heart C*. 2000;278:H1662-H1670

17. Ingber DE. Tensegrity i. Cell structure and hierarchical systems biology. *Journal of Cell Science*. 2003;116:1157-1173

5 Summary and Future Directions

5.1 – Summary

The goal of this dissertation was to provide insight into the effects of ARVC-causing mutant proteins on the mechanical and signaling properties of cardiac myocytes. To that end, we began by employing histological techniques and elastography to first characterize the structural and mechanical properties of the healthy right ventricular myocardium, in hopes of identifying features that would make the right ventricle susceptible to ARVC pathogenesis. We next moved to an in vitro disease model to investigate the effects of ARVC-causing desmosomal protein expression at the cellular level. Specifically, we used adenoviral infection to express ARVC-causing mutant plakoglobin in neonatal rat ventricular myocytes, and performed a variety of assays to measure changes in cell-cell adhesion, cell stiffness, subcellular protein distribution, apoptosis, and ERK phosphorylation (an upstream marker of cardiac hypertrophy). Finally, to identify common mechanical or signaling defects in cells expressing different mutant desmosomal proteins, we repeated key assays previously performed in cells expressing mutant plakoglobin, but now in cells expressing mutant plakophilin-2. The following is a brief summary of the major findings:

1. The right ventricular apex exhibits cardiac fiber disarray and diminished junctional protein localization.
2. Elastography data revealed persistent, elevated strains in the right ventricle, and heterogeneous strain distributions near the right ventricular apex.

3. Expression of ARVC-linked mutant plakoglobin and plakophilin-2 did not alter cell biomechanical properties, including cell-cell adhesion and cell stiffness
4. Suppression of desmosomal proteins did not recapitulate the ARVC phenotype with respect to changes in cell-cell adhesion strength and junctional protein remodeling, highlighting the differences in the pathophysiological consequences of suppression of a desmosomal protein versus expression of a mutant form of a desmosomal protein.
5. Expression of either mutant plakoglobin or plakophilin reversibly altered the junctional localization of plakoglobin in response to shear stress. Only the mutant plakophilin (not mutant plakoglobin) expression altered the junctional localization of plakophilin. Treatment with SB216763 was able to recover the wild-type phenotype.
6. SiRNA mediated suppression of plakophilin altered the junctional remodeling of plakoglobin, but not vice versa.

5.2 – Limitations

There are several limitations to consider with respect to work presented in this dissertation. Although rats do not naturally suffer from ARVC, we chose to study fiber disarray in this species because their cardiac physiology exhibits a striking similarity to that of humans (i.e. – a four-chambered heart that pumps blood throughout the circulatory system). Several studies have also confirmed that artificial induction of a desmosomal gene mutation thought to cause ARVC in humans can result in an ARVC-like phenotype in rats. The use of Eulerian-based incremental strains was necessitated by the elastography acquisition approach. Further work using multiple angles of approach, in addition to a larger sample size of hearts that are co-analyzed using elastography and processed for staining, will permit the extraction of three-dimensional strain data and allow a more in depth analysis to support these preliminary findings.

Additionally, close examination of the three-dimensional strains around the RVA in particular may be helpful in more precisely characterizing the strain magnitudes and spatial distributions of such strains that may provide more insight into the structure-function relationship of this region.

The cell-cell adhesion data presented in Chapters 3 & 4 do not necessarily represent in vivo tissue cohesion, particularly because neonatal cells do not possess the anisotropic characteristics of adult myocytes, which may affect cell-cell adhesion. However, it was unexpected, given all the previous work, that there was no significant alteration in cell-cell adhesion. While shear responses are consistent with ARVC, we do not claim that ARVC development is attributed primarily to shear response; likely stretch and non-mechanical pathways are also involved.

We note that the use of viral transduction of mutant plakoglobin and plakophilin did not lead to significant overexpression of the exogenous proteins, which increases confidence that our results are due to the effects of the transgene and not protein overexpression. Since Naxos disease is recessive; it is possible that our model cells express sufficient endogeneous plakoglobin to attenuate the effects of the 2057del2 PG mutation. However, plakoglobin re-distribution to nuclear sites and elevated apoptosis suggest this is not the case, and that Naxos disease may be related to the expression of the mutant protein with a gene-dosage effect. Furthermore, the insS PG mutation is dominant and no significant biomechanical changes were observed, while both mutant plakoglobin and plakophilin variants led to molecular changes. Thus we have some confidence that molecular changes likely dominate in the manifestation of ARVC.

Further investigation is required to determine the exact mechanism of action for SB216763. SiRNA-mediated suppression of GSK3 did not recapitulate the effects of SB216763,

suggesting the compound either does not inhibit GSK3 (unlikely considering the reported function for the compound by the manufacturer, and the numerous publications in which the compound is used for GSK3 inhibition), or that the compound has secondary effects. The reported method of inhibition is competitive binding to GSK3's ATP binding site, without altering the expression level of the protein, which prevented the validation of SB216763's function via immunoblotting. Direct validation of GSK3 activity was not feasible as the necessary equipment (scintillation counter) was not readily available. Noting that GSK3 functions in the phosphorylation of β-catenin, GSK3 activity kits typically involve measuring the incorporation of radioactively-labeled phosphate groups into substrates of GSK3 with the use of a scintillation counter. Microarray analysis performed on cells expressing 2057del2 PG further supported the role of SB216763 in having secondary effects on gene expression. Although multiple genes were differentially expressed, immunoblotting did not identify differences between cells expressing either wild-type or mutant plakoglobin. The analysis of this data is admittedly incomplete, requiring further analysis of other gene targets, as well as repeating microarray analysis for wild-type cells for a more robust comparison, as well as performing analysis across multiple time points.

It should also be noted that the 1851del123 PKP mutation has not been identified as an ARVC-causing mutation, per se. Instead, the mutation results in a deletion of exon 10 in the PKP2 gene. Although the sequence to function relationship is not fully understood, the high concentration of ARVC-causing mutations found in this region (9 unique mutations in total) suggests that result in a similar ARVC-phenotype suggest that the disease may be modeled by the deletion of this exon. In fact, cells expressing 1851del123 PKP mimic the effects observed in cells expressing ARVC-causing mutant plakoglobin. Although further investigation is necessary,

our initial findings support the hypothesis that tertiary structure of plakophilin-2 encoded by exon 10 is sensitive to any changes in primary structure. We did not repeat all of the experiments using mutant plakophilin-2, because our previous findings suggested that plakoglobin re-distribution is a key event in the final common disease pathway regardless of the underlying pathogenic mutation, and partially because the 1851del123 PKP mutation is not directly linked to ARVC cases, but rather a deletion of a region that is prone to ARVC mutation.

5.3 – Future Studies

Here we propose several studies that could follow from the findings of this dissertation:

5.3.1 – In Vivo / In Vitro Comparison Study

Preliminary work has shown that healthy rodents can exhibit exercise-induced changes in junctional protein localization (namely plakoglobin). The work in this dissertation has shown that the expression of ARVC-causing mutant proteins can alter the cellular distribution of plakoglobin in response to mechanical stress. Comparison of *in vitro* and *in vivo* data investigating the similar mutations would provide further insight into whether or not defective plakoglobin trafficking is a conserved phenotype that contributes to ARVC pathogenesis at the organism level. Furthermore, these experiments discretely characterize the role of increased mechanical stimulation, one of many exercise-induced changes that occur at the organism level, in ARVC pathogenesis.

5.3.2 – Determining the mechanism of action for SB216763

Further investigation is needed to determine how SB216763 is able to restore the wild-type phenotype in cells expressing mutant desmosomal proteins. SiRNA-mediated protein

expression experiments have confirmed that the mechanism likely includes secondary effects to the inhibition of GSK3, and requires the expression of mutant desmosomal proteins (i.e. – SB216763 is unable to recover the wild-type phenotype in cells where plakoglobin or plakophilin has been suppressed). Preliminary work has shown SB216763 alters the cellular expression of connexin-43. Further investigation is necessary to determine the effects of altered connexin-43 expression on calcium handling the cardiac action potential, particularly in cells expressing arrhythmogenic cardiomyopathy-causing proteins. These experiments would shed light on the final common pathway hypothesis, and whether or not SB216763 treatment would be effective in treating all ARVC resulting from the expression of different disease-causing proteins.

5.3.3 – Mechanical Stimulation of Human iPSC-Derived Models of ARVC

The development of platforms for diagnostic testing and pharmacological interrogation remains a strategic area of research, and could have a clinical benefit for patients diagnosed with ARVC. Specifically, epigenetic modifiers and variable phenotypic expression can often result in a higher rate of misdiagnosis. Furthermore, lethal arrhythmias can form well before a patient progresses to the overt stages of the disease. It would be interesting to see if mechanical stimulation of patient-derived iPSCs could accelerate the disease phenotype in vitro, or mimic the effects presented in this dissertation. Furthermore, investigating the effects of acute vs chronic stimulation (mimicking moderate and strenuous exercise, respectively) could provide inside into the role of exercise in disease pathogenesis. It remains to be seen if modulating the intensity (strain magnitude), duration (acute vs. chronic), and frequency of mechanical loading can recapitulate late stage disease characteristics *in vitro*. As more progress is made towards

identifying final common disease pathways, *in vitro* platforms for pharmacological testing will become a necessity as more drugs targets are identified (similar to the identification of and inhibition of GSK3 using SB216763).

5.4 – Conclusions

The data presented here provide significant insight into the structural and mechanical properties of the native right ventricular myocardium, as well as the underlying defects that contribute to the pathogenesis of ARVC, which is not well understood.

Despite the fact that the right ventricular apex is a key site for the development of arrhythmias, little investigation has been done into this region of the heart. Our detailed characterization of the right ventricular apex revealed key features (i.e. - cardiac fiber disarray, diminished junctional protein expression, and elevated / heterogeneous strain distributions) that implicate this region as a weak spot in the heart, and motivated our study of the effects of ARVC-causing proteins on the redistribution of junctional proteins in response to mechanical stress.

Defective intercellular adhesion is widely believed to be a pathogenic factor in disease progression, but evidence for this hypothesis typically stems from cell and animal models where desmosomal proteins have been suppressed. While it should not be surprising that knockdown of a desmosomal gene leads to loss of cell-cell adhesion, our results show that expression of a mutant desmosomal gene has a different effect which is more likely to reflect the pathophysiology of the disease in patients. In particular, the data presented in this dissertation shows that the expression of ARVC-linked mutant plakoglobin in ventricular myocytes in amounts roughly equivalent to that of the native protein, has no apparent effect on cell

mechanical properties (no change in cell stiffness or cell-cell adhesion strength), but instead has a marked effect on the cellular response to mechanical shear stress.

The identification of defective molecular mechanisms that are common across ARVC-patients remains a strategic area of research, particularly for the development of diagnostic tests or identification of therapeutic targets.[5-7] We identify a common signaling defect in cells expressing different ARVC-linked mutant proteins; the data presented shows that the cells expressing either mutant plakoglobin or mutant plakophilin exhibit an abnormal response to mechanical stress. Furthermore, we show that these defects could be corrected with SB216763, an annotated inhibitor of GSK3β.[25-28]

5.5 – References

1. Marcus FI, Fontaine GH, Guiraudon G, Frank R, Laurenceau JL, Malergue C, Grosgogeat Y. Right ventricular dysplasia - a report of 24 adult cases. *Circulation*. 1982;65:384-398
2. Lobo FV, Heggtveit HA, Butany J, Silver MD, Edwards JE. Right ventricular dysplasia: Morphological findings in 13 cases. *Can J Cardiol*. 1992;8:261-268
3. Thiene G, Nava A, Corrado D, Rossi L, Pennelli N. Right ventricular cardiomyopathy and sudden death in young people. *N Engl J Med*. 1988;318:129-133
4. Hayashi M, Takatsuki S, Maison-Blanche P, Messali A, Haggui A, Milliez P, Leenhardt A, Extramiana F. Ventricular repolarization restitution properties in patients exhibiting type 1 brugada electrocardiogram with and without inducible ventricular fibrillation. *Journal of the American College of Cardiology*. 2008;51:1162-1168

5. Garcia-Gras E, Lombardi R, Giocondo MJ, Willerson JT, Schneider MD, Khoury DS, Marian AJ. Suppression of canonical wnt/beta-catenin signaling by nuclear plakoglobin recapitulates phenotype of arrhythmogenic right ventricular cardiomyopathy. *J Clin Invest*. 2006;116:2012-2021

6. Asimaki A, Kapoor S, Plovie E, Arndt AK, Adams E, Liu Z, James CA, Judge DP, Calkins H, Churko J, Wu JC, MacRae CA, Kleber AG, Saffitz JE. Identification of a new modulator of the intercalated disc in a zebrafish model of arrhythmogenic cardiomyopathy. *Science Translational Medicine*. 2014;6:240ra274

7. Asimaki A, Tandri H, Huang H, Halushka M, Basso C, Thiene G, Tsatsopoulou A, Protonotarios N, McKenna WJ, Calkins H, Saffitz JE. A new diagnostic test for arrhythmogenic right ventricular cardiomyopathy. *Circulation*. 2008;118:S774-S774